Double-Walled Carbon Nanotube Processing

*Katherine E. Moore, Daniel D. Tune, and Benjamin S. Flavel**

Single-walled carbon nanotubes (SWCNTs) have been the focus of intense research, and the body of literature continues to grow exponentially, despite more than two decades having passed since the first reports. As well as extensive studies of the fundamental properties, this has seen SWCNTs used in a plethora of applications as far ranging as microelectronics, energy storage, solar cells, and sensors, to cancer treatment, drug delivery, and neuronal interfaces. On the other hand, the properties and applications of double-walled carbon nanotubes (DWCNTs) have remained relatively underexplored. This is despite DWCNTs not only sharing many of the same unique characteristics of their single-walled counterparts, but also possessing an additional suite of potentially advantageous properties arising due to the presence of the second wall and the often complex inter-wall interactions that arise. For example, it is envisaged that the outer wall can be selectively functionalized whilst still leaving the inner wall in its pristine state and available for signal transduction. A similar situation arises in DWCNT field effect transistors (FETs), where the outer wall can provide a convenient degree of chemical shielding of the inner wall from the external environment, allowing the excellent transconductance properties of the pristine nanotubes to be more fully exploited. Additionally, DWCNTs should also offer unique opportunities to further the fundamental understanding of the inter-wall interactions within and between carbon nanotubes. However, the realization of these goals has so far been limited by the same challenge experienced by the SWCNT field until recent years, namely, the inherent heterogeneity of raw, as-produced DWCNT material. As such, there is now an emerging field of research regarding DWCNT processing that focuses on the preparation of material of defined length, diameter and electronic type, and which is rapidly building upon the experience gained by the broader SWCNT community. This review describes the background of the field, summarizing some relevant theory and the available synthesis and purification routes; then provides a thorough synopsis of the current state-of-the-art in DWCNT sorting methodologies, outlines contemporary challenges in the field, and discusses the outlook for various potential applications of the resulting material.

1. Background

Carbon nanotubes are an allotrope of carbon having the form of hollow cylinders composed of rolled-up sheets of graphene, which is itself an extended hexagonal lattice of purely sp^2-bonded carbons. Strictly speaking, carbon nanotubes are either single-walled (SWCNTs) or multi-walled (MWCNTs), but for many reasons double-walled carbon nanotubes (DWCNTs) are prominent in the literature. A single carbon cylinder, be it an SWCNT or a component wall of a DWCNT or MWCNT, can be completely described, except for its length, by an intrinsic geometric property, $\mathbf{C}_h$, known as the chiral vector.[1,2] The chiral vector is defined by the equation $\mathbf{C}_h = n\mathbf{a}_1 + m\mathbf{a}_2$ where the integers (n,m) are the number of steps along the zig-zag carbon bonds and $\mathbf{a}_1$, $\mathbf{a}_2$ are the graphene lattice basis vectors in real space (**Figure 1**a). The chiral vector makes an angle, θ, known as the chiral angle, with the zig-zag or $\mathbf{a}_1$ direction. This angle determines the amount of "twist" in the nanotube and two limiting cases exist where the chiral angle is at 0° and 30°. These are known as zig-zag (0°) and armchair (30°) based on the geometry of the carbon bonds around the circumference of the nanotube (Figure 1b,c). All other conformations in which the C–C bonds lie at angles $0° < \theta < 30°$ are known as chiral (Figure 1d).

Because the n,m integers completely describe nanotube chirality, they also determine the electronic band structure. Thus, it is the chirality that has the most impact on the optical and electronic properties of carbon nanotubes. In particular, a slight change of the chiral angle yields nanotubes that are metallic conductors, low bandgap or high bandgap semiconductors. In the case of semiconductors, the bandgap energy is inversely dependent on the nanotube diameter. The armchair nanotubes are the only type that are intrinsically metallic (zero bandgap), although approximately a third of the zig-zag nanotubes also exhibit metallic properties at room temperature because the bandgap is smaller than the thermal energy, k_BT, allowing thermal excitation of carriers into

Dr. K. E. Moore, Dr. D. D. Tune
Centre for Nanoscale Science and Technology
School of Chemical and Physical Sciences
Flinders University
Adelaide 5042, Australia

Dr. K. E. Moore, Dr. D. D. Tune, Dr. B. S. Flavel
Institute of Nanotechnology
Karlsruhe Institute of Technology
76021 Karlsruhe, Germany
E-mail: benjamin.flavel@kit.edu

DOI: 10.1002/adma.201405686

the conduction band. All chiral nanotubes and the remaining two thirds of zig-zag nanotubes are therefore semiconducting at room temperature. This leads to the observation that approximately 60% of all nanotube chiralities are semiconducting with the remaining 40% metallic.[3]

Carbon nanotubes are so small that they exhibit quasi-1D properties, with the confinement of electrons into allowed momentum states giving rise to van Hove singularities in their electronic density of states (DOS) (Figure 1e,f). In bulk semiconducting materials, the energy gap between the valance and conduction bands defines the absorption onset wavelength of the optical spectra, but in the case of carbon nanotubes the discrete electronic transitions in their DOS produce a series of characteristic peaks in the optical absorption spectra at correlated energies (Figure 1g). In the case of bulk semiconducting materials, the single-particle model (an electron absorbs a photon and thus moves from a lower energy level to a higher one) provides a reasonably close approximation of empirical observations. However, the 1D confinement of electrons in carbon nanotubes causes a significantly higher electron–hole binding energy (*eh*) and electron–electron repulsion (*ee*), meaning that true consideration of the optical absorption spectra of nanotubes must be entirely excitonic in nature (light energy is absorbed by the material creating excited states a.k.a. bound electron–hole pairs) with the many-body effects (*eh* and *ee*) included for an accurate description.[4] This means that the actual light energy required to produce a "v_i–c_i" transition is ($Ec_i - Ev_i$) + binding energy (*eh*) − self energy (*ee*), and leads to the experimental finding that E_{22}/E_{11} tends to a value of 1.8 with decreasing tube diameter, rather than the value of 2 as would be expected from density functional theory (DFT) calculations alone.[5] The excitonic nature of the optical properties is an important consideration for specialists however, in the interests of simplicity, we present only the single-particle approximation throughout this review as this is sufficient to appreciate the concepts. There are two other important processes in nanotubes which, in addition to optical absorption spectroscopy, provide vital information regarding nanotube type and character. These are photoluminescence (PL), in which semiconducting nanotubes are excited by an S_{22} photon which then decays emitting a detectable S_{11} photon and allowing chiral identification, and Raman spectroscopy, in which the magnitude of the shift in Raman scattered light, which is exquisitely sensitive to the strong vibrational phonon modes present in the lattice of carbon nanotubes, is plotted to yield a rich variety of structural information. Detailed treatments of these phenomena are readily available in the literature and, in the case of DWCNTs, we refer the reader to Pfeiffer et al.,[6] Shen et al.[7] and Kim et al.[8]

DWCNTs consist of two coaxially aligned SWCNTs and, as such, they share many of the attractive properties of SWCNTs,[9,10] but, owing to the presence of a second wall, are more physically robust and electronically more complex.[11] Similar to SWCNTs, DWCNTs are uniquely characterized by the chiral indices of the constituent inner and outer walls (n_i,m_i)@(n_o,m_o), where each wall can be either semiconducting (S) or metallic (M) depending on its chiral index (Figure 1h).[12] This gives rise to four possible combinations of inner@outer wall; namely, M@M, M@S, S@M, and S@S. This is in contrast to MWCNTs, which are all metallic due to the complex inter-wall coupling. Because DWCNTs represent the simplest form of a MWCNT, they are interesting for investigation of inter-wall coupling, which has a significant influence on the electronic states of the nanotubes and is highly dependent on

Katherine E. Moore has a B.Sc. with First Class Honors and a Ph.D. in Nanotechnology from the Flinders University of South Australia. During her postgraduate degree she received many prestigious awards and grants and her work has been featured in several nanotechnology news platforms. Her research interests include the separation of carbon nanotubes, nanotube sensors, and single nanotube electronic devices.

Daniel D. Tune holds a B.Sc. and Ph.D. in Nanotechnology from the Flinders University of South Australia and is the 2014 recipient of the South Australian Science Excellence Award (PhD category). Daniel is currently working as a postdoctoral researcher in the Carbon Nanotube Solar Cells and Sensors group at the Institute of Nanotechnology, Karlsruhe Institute of Technology. His interests are in renewable energy, nanoelectronics, and composite nanostructures, with a focus on the understanding of carbon nanotubes, fullerenes and graphene, and the application of this in the development of new and improved devices and materials.

Benjamin S. Flavel obtained both a B.Sc. (Hons) and Ph.D. in Nanotechnology at the Flinders University of South Australia. He has since received research fellowships from the Australian Government's Endeavour Program, the Alexander von Humboldt Foundation and is currently a Junior Research Group Leader at the Institute of Nanotechnology, Karlsruhe Institute of Technology under the German Research Foundation's Emmy Noether Program. His research interests include the separation of carbon nanotubes and their integration into devices for optics, sensing, and energy.

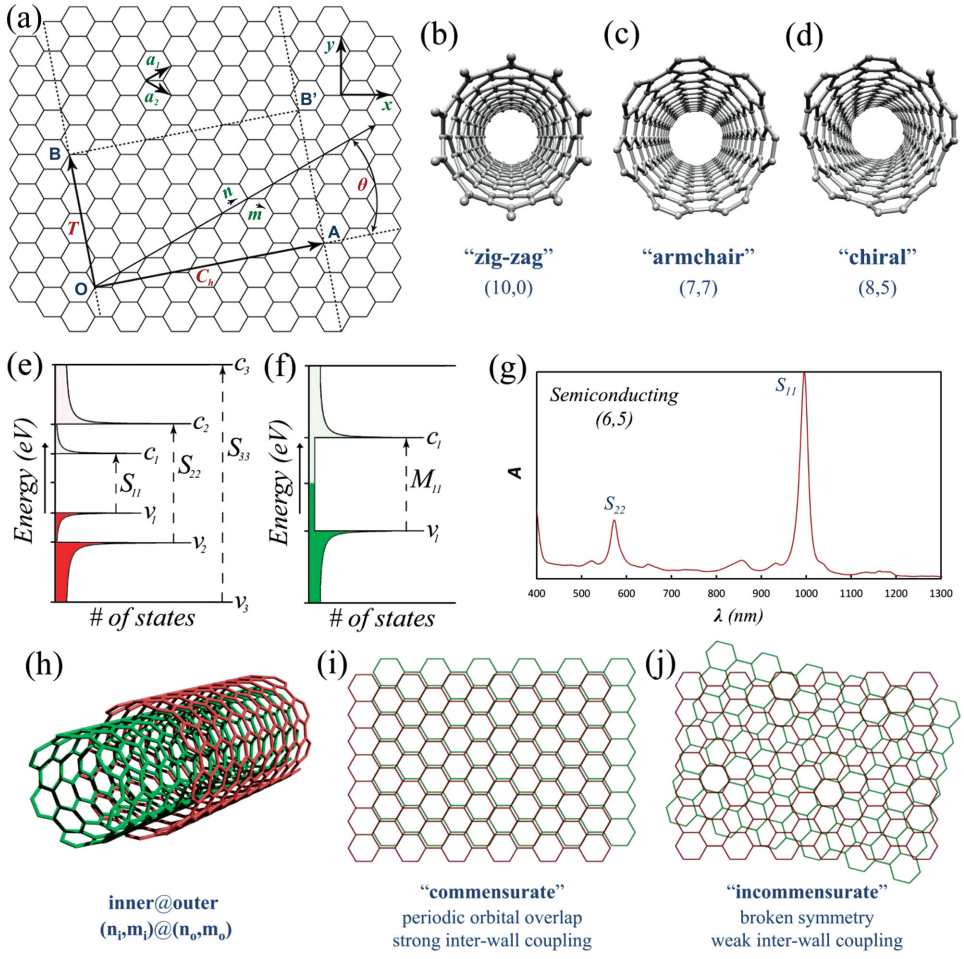

Figure 1. a) Unrolled graphene sheet showing the geometry of the (6,3) nanotube where the vectors OA and OB define the chiral and translational vectors C_h and T, respectively, and the rectangle OAB'B defines the nanotube's unit cell. O, A, B, and B' are reference atoms, a_1 and a_2 are the graphene lattice basis vectors and θ is the chiral angle. b–d) Examples of the three classes of nanotube sidewall; zig-zag, armchair, and chiral. e,f) Schematics of the electronic density of states of semiconducting and metallic (zig-zag) nanotubes showing the valence and conduction states, v_i and c_i, and optically active electronic transitions, S_{ii} and M_{ii}. g) Optical absorption spectrum of the (6,5) semiconducting nanotube showing the S_{11} and S_{22} absorption features. h) Schematic of a double-walled carbon nanotube. i,j) Representations of commensurate and incommensurate lattice stacking.

whether the lattice stacking of the two walls is commensurate or incommensurate.[10,13–18] A DWCNT is commensurate if the ratio between the unit cell lengths of the two walls is a rational number and, as a result, the DWCNT has a periodic lattice structure (Figure 1i). In an incommensurate DWCNT, the ratio is an irrational number and the nanotube experiences broken symmetry (Figure 1j). This causes reduced inter-wall coupling because the inter-wall transfer at each lattice site oscillates around zero in a quasiperiodic manner, resulting in a net interference that is destructive.[19] In general, the extra Coulomb interaction due to inter-wall coupling reduces the electron–hole binding energy and thus lowers the optical bandgap (red shifting the absorption features) relative to the same (n,m) isolated tube; however, as discussed later, there are some wall configurations in which inter-wall coupling interactions increase the bandgap (blue shifting the absorption features).

An important characteristic of DWCNTs is that their concentric structure allows for the opportunity to simultaneously exploit the chemical reactivity of the outer wall as well as the excellent conductance of the unfunctionalized inner wall, making them ideal candidates for nanotube-based sensor devices. During reactions, only the outer wall is exposed to the chemical environment and can be decorated with a high density of chemical moieties.[20,21] As a result of such shielding by the outer wall, the inner wall does not suffer the drawbacks associated with functionalization, such as reduced conductivity due to degradation of the pristine sp^2 hybridized framework.[22]

DWCNTs exhibit great potential from both an applications-based and a fundamental viewpoint; however, their use has remained quite limited. This is in large part due to the lack of a method to synthesize pure, electronically well-defined raw material. While several synthesis methods, including arc discharge,[23–25] peapod growth[26,27] and catalytic chemical vapor deposition,[28] can be optimized to produce high-purity DWCNTs (up to 90%),[29] each method inevitably produces a myriad of contaminants including SWCNTs and MWCNTs, residual catalyst, amorphous carbon, and fullerenes. Purification methods exist to remove some of the unwanted

contaminants and increase the DWCNT purity,[24,30] but they are unable to overcome the inherent dispersion of DWCNT lengths, diameters, and inner@outer wall electronic combinations. Like SWCNTs, such inhomogeneity imposes many limitations on potential applications and has spurred the development of new research focused on the preparation of DWCNT material sorted by diameter, length, and/or electronic character. This emerging field has seen the recent implementation of several strategies previously successful for SWCNT processing, such as reversible covalent modification,[31] biofunctionalization,[32] molecular nanocalipers,[33] density-gradient ultracentrifugation,[34,35] and gel permeation[36,37] with several other potential methods looking promising, such as polymer wrapping[38,39] and aqueous two-phase extraction.[40,41] As a result, well defined DWCNT material can now be used to further our fundamental knowledge of inter-wall interactions, to finally begin to realize their potential in advanced electronics and sensor applications, and to explore the rich new physics they possess.

In light of this, we present a review of DWCNT processing techniques and the significance they each pose in this developing field. This review complements others in the literature that are more focused on growth mechanisms, the origin of Raman modes, the effects of temperature, pressure, and doping, the thermal and mechanical properties, photoluminescence, and outer wall selective functionalization, for which we again refer the reader to Pfeiffer et al.,[6] Shen et al.[7] and Kim et al.[8]

2. DWCNTs: Metallic or Semiconducting?

Despite the ability to classify the individual electronic types of the inner and outer walls, identifying the overall electronic nature of a DWCNT is more complicated; being highly dependent on inter-wall interactions, which in turn depend on the inter-wall distance and whether the constituent nanotubes are commensurate or not.[17,42,43] Despite the fact that commensurate DWCNTs are rarely observed experimentally because it is unlikely to have two commensurate SWCNTs with the appropriate radius difference (ca. 0.33–0.41 nm[1,44] for the formation of a DWCNT,[10,13,45] they are commonly employed in theoretical studies. This is due to their defined unit cell lengths, which allow for the use of far simpler computational models and also result in very strong inter-wall coupling.[17,42,43] Indeed, theoretical calculations of commensurate DWCNTs have yielded some unexpected results, for example; a DWCNT in which both walls are semiconducting, but which exhibits overall metallic character.[17,42] Liang found that in the case of a commensurate S@S DWCNT, the energy gap scales inversely with the inter-wall coupling, which in turn is inversely proportional to the inter-wall distance.[14] Thus, as the inter-wall distance decreases, stronger inter-wall coupling causes the bandgap to vanish and the S@S DWCNT behaves as a metal.[14,17]

Okada and Oshiyama used DFT to further investigate the curious behavior of S@S DWCNTs.[42] For a (7,0)@(16,0) DWCNT, it was calculated that the conduction band of the inner wall and valance band of the outer wall merge, forming a finite density of states at the Fermi level. However, as the outer wall diameter is increased, and thereby also the inter-wall spacing, as seen in the case of (7,0)@(17,0) and (7,0)@(19,0), the electronic structure changes to yield semi-metallic behavior. DWCNTs of increasing inner wall diameter (with respect to a constant outer wall) were also investigated using the (8,0)@(19,0) and the (10,0)@(19,0), and both were determined to be semiconducting with finite bandgaps. Interestingly, the semiconducting (10,0)@(19,0) shares the same inter-wall spacing as the smaller (7,0)@(16,0); however, the latter is found to be metallic, highlighting the importance of the inner wall diameter and nanotube curvature on the overall electronic character of a DWCNT. Very small nanotube diameters (0.4–0.6 nm), with their greater curvature, exhibit increased σ–π rehybridization, leading to metallization.[42,46] From the work of Okada and Oshiyama,[42] it is therefore theorized that the metallization of S@S DWCNTs arises due to a combination of curvature differences between the inner and outer walls, rehybridization of the inner wall, and the inter-wall distance.[42]

Likewise, Moradian et al. used DFT calculations to investigate the cases of M@S and S@M DWCNTs and found equally surprising results.[17] For a (6,0)@(20,0) M@S DWCNT, the constituent nanotubes were found to maintain their individual electronic character; however, as a whole, and in agreement with Okada and Oshiyama,[42] the DWCNT behaves as a metal due to overlap of the valence and conduction states of the component walls. Decreasing the inter-wall distance was found to cause a semiconductor-to-metal phase transition in the outer wall. Thus, both constituent walls and the overall DWCNT exhibit metallic behavior. For S@M DWCNTs, all the nanotubes investigated were determined to be metallic and, once again, the inter-wall distance was found to have an effect on the electronic character of the constituent nanotubes. For example, in (10,0)@(21,0) and (14,0)@(21,0) DWCNTs, the semiconducting inner wall becomes metallic, but in the (8,0)@(21,0) DWCNT, where the inter-wall distance is larger, the two nanotubes exchange electronic type. Moradian et al. concluded that as the inter-wall distance is decreased, the semiconducting inner wall becomes metallic, whereas as the inter-wall distance is increased, an exchange of metallicity of the constituent nanotubes occurs.[17]

Despite the increased complexity, some theoretical studies have been performed on incommensurate DWCNTs.[15,19,47,48] These show that the type of conductance is dependent upon the position of the Fermi level and on the length of the nanotubes.[47,49,50] When the Fermi energy is close to the charge neutral point, the energy levels of the constituent nanotubes are uncorrelated and coupling is weak.[49] Thus, in this energy regime, conduction is confined to one nanotube and is expected to be ballistic, as seen in the work of Ahn et al.,[49] who observed that conductance was confined to the inner wall of the (9,1)@(17,2) DWCNT. As the Fermi energy was increased, conduction shifted from ballistic to diffusive and was distributed evenly among the inner and outer walls.

While the number of experimental investigations into the transfer of charge between the constituent walls of incommensurate DWCNTs has remained small, significant insights have been gained through the work of Kalbac et al.[51] and Liu et al.[18] In the work of Kalbac et al.,[51] in situ Raman spectroelectrochemical measurements were used to observe doping behavior and the effects of charge transfer between the inner

and outer walls for different incommensurate M/S combinations. The results were obtained using DWCNTs with a defined outer wall electronic character, but with both metallic and semiconducting inner walls. By selecting appropriate laser excitation energies, Raman spectra of each of the four electronic combinations could be observed while the electrochemical potential (and thus Fermi level) was shifted in the positive or negative direction. When this change in Fermi level resulted in filling or depleting of an electronic state, bleaching of the Raman signal was observed.[52] As the inner wall is protected from the surrounding environment by the outer wall, it is neither in direct contact with a working electrode nor with compensating electrolyte counterions.[53] Thus, the origin of inner wall doping could only stem from transfer from its surrounding outer wall.[51] Through the use of this technique, Kalbac et al. determined that the potential required to observe charge transfer increased in the order of M@M < S@M < M@S < S@S. In each case, charge transfer was dependent upon the identity of both the outer and inner walls. For metallic outer walls, charge transfer to the inner wall could occur at small potentials close to the undoped state, whereas semiconducting outer walls required the first van Hove singularity to be filled. A similar observation was made for inner walls, with metallic nanotubes readily accepting charge from either outer wall type. Semiconducting inner walls accepted charge only when the filled states of the outer wall were higher than their first van Hove singularity. This means that for both the S@M and S@S DWCNTs, the inner wall only becomes doped when the electrochemical potential reaches that of the first van Hove singularity of the inner semiconducting wall. **Figure 2** shows a diagram of the respective DOS of each of the four electronic combinations of DWCNTs in the case of shifting the electrochemical potential in the negative direction. The position of the Fermi level required for electron transfer from the outer wall to the inner wall is indicated.

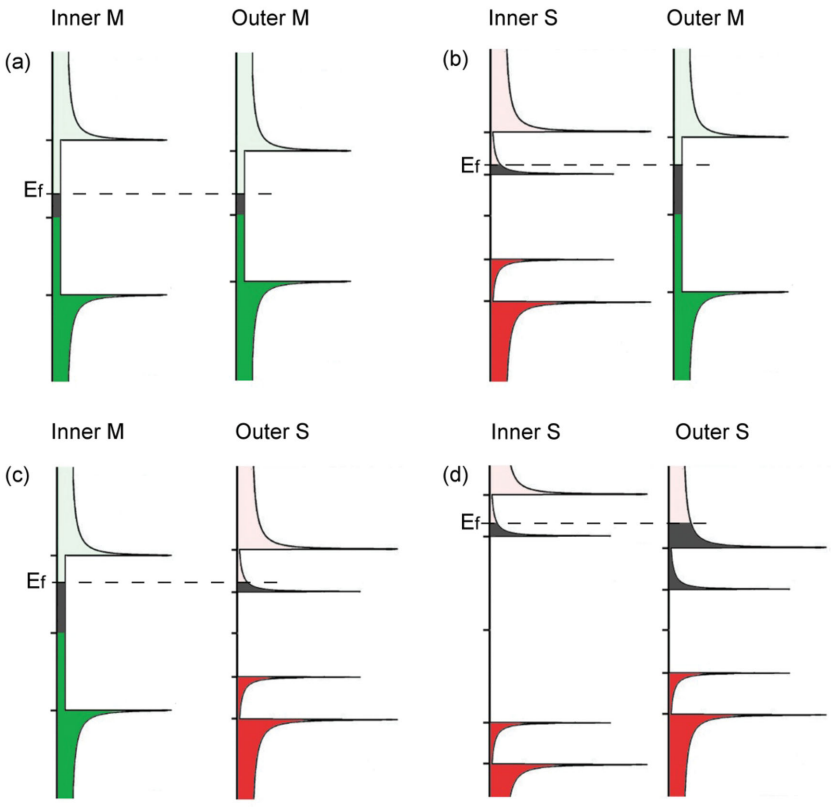

Figure 2. Schematic of the electronic structures of: a) M@M, b) S@M, c) M@S and d) S@S DWCNTs showing the Fermi level position at the point where electron transfer from the outer wall to the inner wall occurs, as described in ref. [51]. Adapted with permission.[51] Copyright 2011, Wiley-VCH.

Liu et al. also investigated incommensurate DWCNTs and have shown that under certain conditions coupling can be quite strong and can influence the electronic states of the nanotube.[18] In that work, optical transitions were observed between 480–750 nm (1.45–2.55 eV) for various suspended incommensurate $(n_i,m_i)@(n_o,m_o)$ combinations and the peak positions were compared to that of the individually suspended SWCNTs.[54] Significant shifts (–50 to 200 meV) were observed across 99 different $(n_i,m_i)@(n_o,m_o)$ combinations. While a redshift of ca. 50 meV can be attributed to the environmental effects seen previously for SWCNTs,[55] such effects cannot account for some of the very large and transition-dependent variations observed, especially the significant blue shifts for certain transitions. Therefore, such strong variations must be attributed to intrinsic effects, such as orbital hybridization between the inner and outer walls. Through the use of perturbation theory, the authors determined that any observed shift is reliant upon several factors including; the inner wall diameter and chiral angle, the outer wall diameter and chiral angle, and the energy level of the excitation. While these works provide insight into the complex and relatively unknown interactions between the constituent walls of incommensurate DWCNTs, there is still much that is yet to be understood.

3. The Characterization Problem

Absorption, PL, and Raman spectroscopy are the most commonly employed characterization techniques for SWCNTs and rely on an assumed relationship between structure and properties.[56] This relationship has afforded a well-documented library of nanotube optical and Raman transitions that allow for the easy identification of SWCNT species.[5,56–62] As DWCNTs are a coaxial arrangement of two SWCNTs, they exhibit similar optical and Raman features to the individual constituent nanotubes. The commonality of transitions often results in the application of the SWCNT library to DWCNTs; however, this can be problematic. One reason is that, in the case of DWCNTs, convolution of the inner and outer wall optical transitions occurs, which, in combination with the presence of additional SWCNTs, makes the identification of the

constituent wall type difficult. Unfortunately there is no clear optical absorption feature exclusively indicative of DWCNTs. This problem can be demonstrated using material that consists of DWCNTs (1.5–2 nm) as well as small- (0.8–1 nm) and large-diameter (1.5–1.8 nm) SWCNTs as impurities.[21,34,35,63] In such material, the outer wall of a DWCNT has first-, second-, and third-order semiconducting transitions (S_{11}, S_{22} and S_{33}) at ca. 2000, ca. 1150, and ca. 600 nm and inner wall transitions at ca. 1050, ca. 650, and ca. 350 nm. It is clear that the S_{22} of the outer wall and S_{11} of the inner wall overlap, and likewise the S_{33} of the outer wall with the S_{22} of the inner wall. Further complicating the absorption measurements is the presence of the metallic M_{11} transitions of the inner and outer walls at ca. 550 and ca. 800 nm. The optical transitions of large-diameter SWCNT contaminants also share the same region as those of the DWCNT outer walls; whilst the optical transitions of the small-diameter SWCNTs share the same region as those of the DWCNT inner walls. **Figure 3** shows an example of the absorption spectra of small-diameter SWCNTs, large-diameter SWCNTs, sorted SWCNTs, and sorted DWCNTs, where the overlap of transitions between the small- and large-diameter nanotubes can be clearly seen.

Additionally, owing to strong absorption by water above 1400 nm, the S_{11} of the outer wall cannot be seen in a typical solution absorption measurement without the use of D_2O to extend the solvent window.[64] Consequently, without the corresponding S_{11} transition, interpretation of S_{22} and S_{33} transitions for (*n*,*m*) identification is difficult. This issue can be resolved with the use of thin films, as seen in Figure 3. However, the spectra can differ significantly from solution measurements, where the nanotubes are present in the isolated/individualized state. This is because the excitonic properties of the nanotubes are highly sensitive to many-body interactions, Coulomb interactions, and charge transfer between adjacent nanotubes in bundles.[65] Indeed there are many examples in the literature of discrepancies between solution and substrate-bound nanotube peak positions of up to ca. 50 meV.[55]

For DWCNTs, shifts in peak position are also seen on the individual nanotube level due to the effects of strong inter-wall coupling between the constituent walls.[19] Unlike SWCNTs, the optical spectra of DWCNTs are also affected by the relative

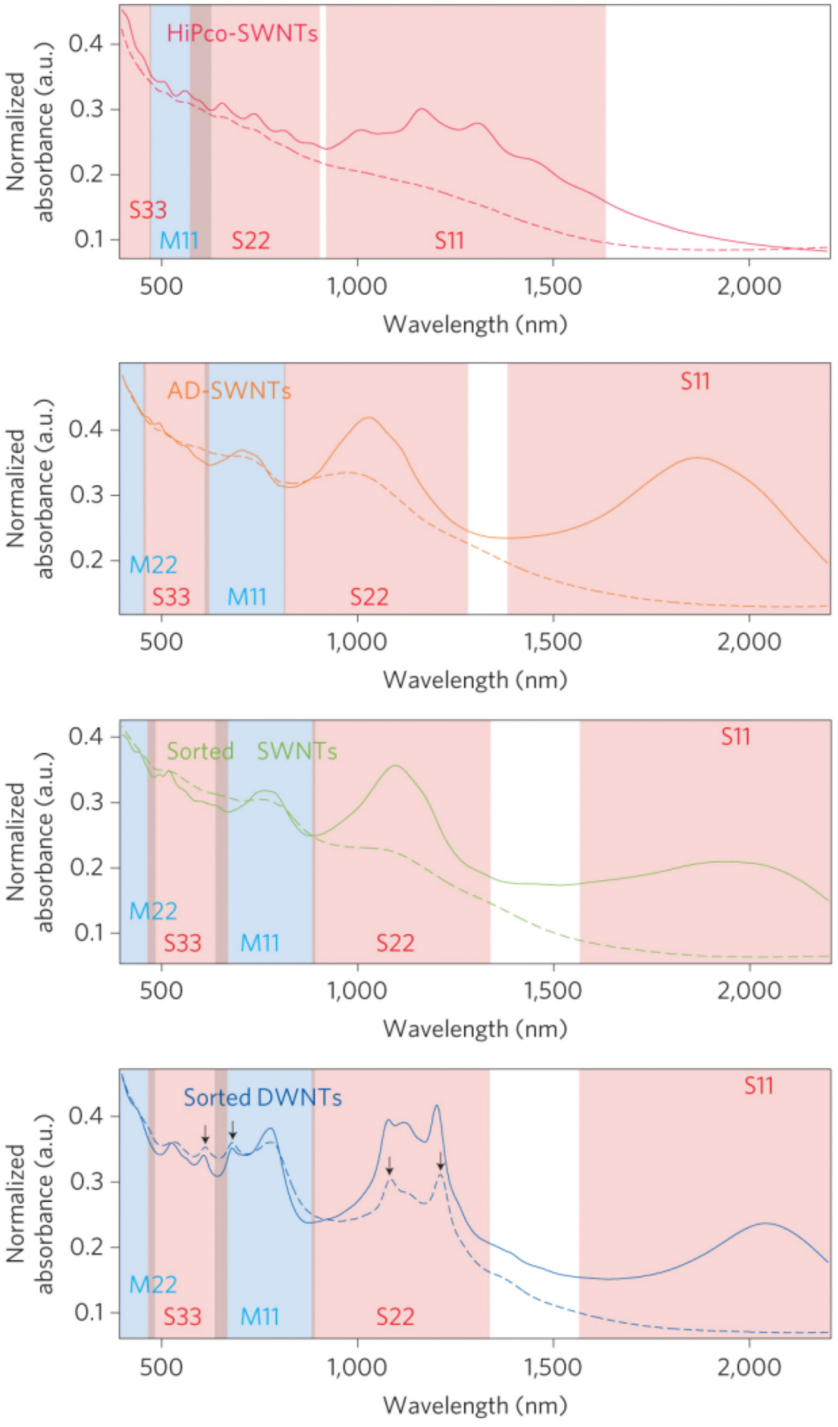

Figure 3. The absorbance spectra of films of HiPco SWCNTs (small diameter), arc-discharge (AD) SWCNTs (large diameter), sorted AD SWCNTs, and sorted DWCNTs before (solid curves) and after (dashed curves) doping with thionyl chloride. The first-, second- and third-order semiconducting optical transitions of the SWCNTs and the DWCNT outer wall (shaded red) are labelled S_{11}, S_{22}, and S_{33}, and the first- and second-order metallic transitions (shaded blue) are labeled M_{11} and M_{22}. For SWCNT materials, thionyl chloride doping completely suppresses the S_{11} transitions and significantly attenuates the S_{22} and M_{11} peaks. The sorted DWCNT film maintains several strong peaks (indicated by the arrows) in the S_{22}, S_{33}, and M_{11} regions that are attributed to inner walls of DWCNTs. Reproduced with permission.[34] Copyright 2009, Nature Publishing Group.

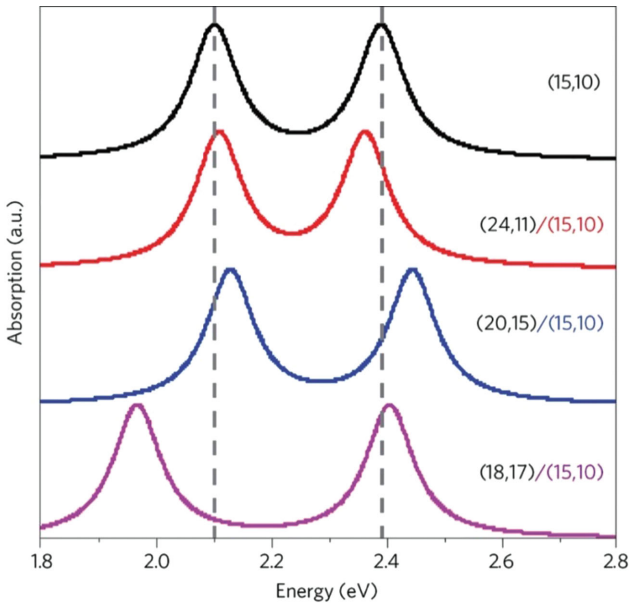

Figure 4. The effect of inter-wall coupling on the optical transitions of DWCNTs. Optical resonances (S_{33} and S_{44}) from the (15,10) nanotube show a significant energy shift. The amplitude of the energy shift depends sensitively on the specific optical transition and the outer nanotube species, and can be either positive or negative, with a magnitude as large as 150 meV. Reproduced with permission.[18] Copyright 2014, Nature Publishing Group.

handedness of the constituent walls i.e., the S- or R- stereoisomers.[18] This arises due to obvious differences in inter-wall coupling experienced by DWCNTs of different relative handedness. Overall, the effects of inter-wall coupling can produce unusual variations in the optical spectra, making chirality assignment based on the known optical properties of SWCNTs problematic. An example of this is given in **Figure 4**, which shows the third- and fourth-order optical transitions (S_{33} and S_{44}) of the (15,10) nanotube, both on its own (i.e., as an SWCNT) and when contained within the outer walls of various (n,m) indices. The different inter-wall coupling within the various (15,10)@(n_o,m_o) combinations significantly alters the peak position.

Notwithstanding the variance in peak position from the expected SWCNT transitions, it is possible to perform doping experiments wherein the origin of the transitions, whether from the inner or outer wall, can be elucidated by observing the effect of the doping on the optical transitions.[34–36] In theory, only the inner wall transitions should remain active due to shielding by the outer wall, and comparison between spectra before and after doping should allow for inner and outer wall identification. However, in practice such shielding is incomplete[66] and can often introduce a new level of uncertainty. The data in Figure 3 also show the optical absorption spectra of different DWCNTs before and after chemical doping with thionyl chloride. For each nanotube of different diameter, the S_{11} transition is completely depleted by the doping due to a shift of the nanotube Fermi level into the highest occupied molecular orbital (HOMO) as a result of the withdrawal of electrons by the powerful oxidizer.[34–36] In the case of the large-diameter nanotubes (denoted "AD" for the arc-discharge method of synthesis), significant attenuation of the S_{22} transition also occurs, and in the case of DWCNTs, this attenuation of S_{22} reveals the underlying S_{11} transitions corresponding to the inner walls. Whilst this cannot be used for chirality assignment, subtraction of the inner wall spectra obtained after doping from the convolution spectra of both inner and outer walls measured before doping has been used for determination of the electronic purity.[35] In a similar manner, doping/oxidation experiments can also be used in conjunction with Raman measurements.[34–36,67]

In Raman spectroscopy, the effect of inter-wall coupling can be clearly seen when comparing the SWCNT radial breathing modes (RBMs), which have a well-established relationship with the nanotube diameter, to those of DWCNTs. For a specific (n_i,m_i) inner wall nanotube, a cluster of RBMs with almost the same resonance energy is observed,[6] spanning an 18 cm^{-1} frequency range.[68] This cluster arises from the same (n_i,m_i) nanotube residing within multiple (n_o,m_o) outer walls, with the RBM shift dependent upon the strength of the inter-wall interaction.[69] This makes chirality assignment based on RBM frequency unreliable. Furthermore, the RBMs of DWCNT inner walls can have significantly narrower line widths than those usually observed for similar diameter SWCNTs (typically 12 cm^{-1}), with some DWCNT RBM line widths being as small as 0.4 cm^{-1}.[70] This is because the inner walls can be remarkably defect-free owing to the protective nature of the outer wall, and thus exhibit very long phonon lifetimes.[6]

Circumventing the aforementioned difficulties in exact chirality assignment using optical absorption or standard Raman spectroscopy, a new approach has been presented by Kalbac and co-workers to discern the ratio of single- to double-walled nanotubes using Raman spectro-electrochemistry.[71] This technique exploits the diameter dependence of the high frequency, two-phonon mode (G′), which is an overtone of the disorder-induced mode (D band).[72] While both modes demonstrate a dependence on diameter, the dependence is stronger for the G′, as is its intensity arises due to different selection rules.[73] This diameter dependence results in a DWCNT-specific doublet where the higher-frequency component corresponds to larger-diameter outer walls and the lower frequency component to smaller-diameter inner walls. Upon electrochemical doping, nanotubes in direct contact with a working electrode or with compensating electrolyte counterions (SWCNTs or DWCNT outer walls) experience an upshift in frequency as well as peak broadening. In the case of SWCNTs, all nanotubes are doped and the observed peaks are upshifted. In DWCNTs however, the inner walls are protected and only the outer-wall G' peak is upshifted. Thus, the electrochemical doping accentuates the splitting and enables distinction of SWCNTs/outer walls from inner walls.[71] By comparing ratios of pure SWCNTs and DWCNTs and employing a model relating the peak area to the nominal composition, it is therefore possible to determine the contaminating SWCNT percentage. This technique offers the advantage of reproducible and precisely controlled doping compared with traditional chemical doping strategies[71] and, furthermore, results in a clear difference between the contribution of DWCNT inner walls and SWCNTs.

In terms of obtaining structural information, scanning tunneling microscopy (STM)[74] and transmission electron microscopy (TEM) are obvious choices as they can overcome the limitations of optical and Raman spectroscopy; however,

TEM is considered the definitive tool for DWCNT measurement. TEM can achieve quantitative characterization of the real mean diameter of both the inner and outer walls, indications of the relative concentration of DWCNTs within a mixed sample containing single- and/or multi-walled contaminants, and the real diameter distribution and its standard deviation.[75] Additionally, by combining TEM with electron diffraction it is possible to determine the (*n*,*m*) type of the two constituent nanotubes in a DWCNT.[10] Unfortunately, TEM is time consuming and does not give a complete overview of the entire nanotube population under investigation nor does it provide any electronic information. The preparation of uniform samples that accurately represent the population can be difficult; surfactants are usually required to individualized nanotubes, but the presence of surfactant can introduce sample bias due to differences in surfactant wrapping of tubes and resultant interactions with the substrate during sample preparation. Therefore, unless the prepared DWCNT sample can be reliably assumed to be extremely uniform and fully representative, calculated (*n*,*m*) indices for individual nanotubes cannot be conclusively extrapolated to the entire ensemble. It is reasonable to assume that cryoTEM,[76] in which thin slices taken directly from the frozen nanotube suspension are analyzed, may circumvent this difficulty, but the technique has not yet been widely applied to DWCNTs. Thus, as a compromise, a combination of absorption techniques in conjunction with TEM is typically used to characterize DWCNT samples.

4. Synthesis Methods

4.1. Arc Discharge

The arc-discharge method was first used to prepare carbon nanotubes in 1991 by Iijima whilst attempting to synthesize C_{60}.[77] The synthesis technique involves applying a voltage and current between two closely spaced (typically 1–2 mm), highly pure graphite electrodes in an inert atmosphere. Typically, the anode is partially hollowed and filled with carbon feedstock (usually graphitic powder) and a catalyst/promoter, of which there are many combinations depending upon the desired product. Upon application of a current (steady state or pulsed), a plasma forms between the electrodes. Random collisions between the carbon atoms, catalyst particles, and gas then result in the formation of carbonaceous material as a macroscopic deposit on the cathode, as well as the reactor walls. Fullerenes and carbon nanotubes of varying types can be found within this carbonaceous soot.[78] The type of carbon nanotube produced can be tailored to be single-, double- or multi-walled through careful control of catalyst composition, atmosphere, current/voltage conditions, and carbon feedstock. This field is vast, but some significant reports on the optimization of these growth conditions to yield DWCNTs are now discussed.

Hutchison et al.[23] were the first to selectively synthesize DWCNTs with the steady-state arc-discharge method in 2001. They used a mixture of Ni, Co, and Fe catalyst within the graphite anode in an Ar/H_2 atmosphere with varying amounts of S included as a growth promoter. The resultant DWCNTs had a purity varying from ca. 10% to 70% and at the end of their study the authors concluded that the presence of S in the catalyst was not critical to the formation of DWCNTs. However, in later work by Saito et al., the presence of S as a growth promoter was concluded to be indispensable for the production of DWCNTs.[29] They also concluded that the catalyst must contain Fe and that H_2 was of vital importance for DWCNT production. Upon optimizing the catalyst (FeS:NiS:CoS = 1:1:1) and the atmosphere composition, the highest purity achieved was ca. 90% DWCNTs with the average outer diameter ranging from 2 to 5 nm. The presence of halides can also improve the yield of DWCNTs, as demonstrated by Qiu et al. using steady-state arc discharge in a hydrogen atmosphere.[25] Through the introduction of chloride (specifically KCl) to the catalyst mix, they achieved an increased yield of DWCNTs (10 wt% without KCl to 50 wt% with KCl) with a purity of 90%.

While an atmosphere containing H_2 is now commonly employed, it is possible to achieve DWCNT growth without the presence of reactive gases. Huang et al.[79] prepared DWCNTs without H_2 by customizing the shape of the cathode to a bowl-like structure. Using the now well-established catalysts of Ni, Co, Fe, and S, they demonstrated the growth of DWCNTs with a purity of ca. 80%. The DWCNTs possessed improved oxidation resistance compared to conventionally prepared arc-discharge- or catalytic chemical-vapor-deposition-produced DWCNTs, owing to the large hot region within the bowl-like cathode. This hot region allowed for in situ annealing or "defect-healing" of the DWCNTs. A report of DWCNT synthesis by Sugai et al. demonstrated the first use of high-temperature pulsed arc discharge without H_2.[24] Contrary to the steady-state methods, pulsed arc discharge also allows for DWCNT production without the presence of Fe and S. In this case, an Y/Ni catalyst commonly used in the formation of SWCNTs was used,[30,80] however a change from preferential formation of SWCNTs to DWCNTs occurred due to the increased temperature. It has been shown that the SWCNT diameter increases with increased temperature until 1200 °C, at which point the nanotube reaches a critical diameter and DWCNTs become the favored product. Owing to the highly controlled arc conditions (600 µs pulse at 50 Hz), small-diameter DWCNTs (1.6–2.0 nm) could be produced. Similarly, Zhao et al. also demonstrated the growth of DWCNTs without the presence of H_2 (or any expensive high-purity gases) with a steady-state arc-discharge approach.[81] In that work, Fe was used to catalyze the growth reaction with S present as a promoter, while dry air flowed throughout the reaction at reduced pressure. The authors showed that DWCNTs were the dominant product with diameters ranging between 3 and 7 nm, but that SWCNTs and triple-walled carbon nanotubes (TWCNTs) were also present, as well as a considerable amount of other carbonaceous material. Whilst the gross DWCNT purity is significantly reduced without the presence of H_2 (only 20% was reported by Sugai et al.[24] and no purity was estimated by Zhao et al.,[81] such a route offers the advantages of reduced cost and a simpler growth process, and minimizes the dangers associated with large-scale application of H_2 gas. In the future, the issue of low purity may be addressed through further optimization or post-growth purification strategies.

Although catalyst composition and reaction atmosphere are critically important for DWCNT growth and much work to date has been focused on these aspects, the literature also

contains studies into the effect of the composition of the carbon feedstock. Li et al. demonstrated that MWCNTs/CNF (carbon nanofibers) can be successfully used to grow high-purity DWCNTs by steady-state arc discharge in a H_2 atmosphere.[82] The anodic carbon feedstock (usually high-purity graphite >99%) was substituted with the MWCNT/CNF mixture, which had a diameter range of 40–220 nm. The authors found that DWCNTs produced from MWCNTs/CNFs were of higher quality than those prepared by graphite powder using the same process and they determined the DWCNT purity to be 83% with the outer diameter ranging from 1.75 to 4.87 nm. Recently, Xu et al. demonstrated that asphalt[83] and petroleum coke[84] could also be used as the carbon feedstock in lieu of high-quality (and very expensive) graphitic powders. In both of those cases, Fe was used as the catalyst and, in the case of petroleum coke, an Ar atmosphere was shown to lead exclusively to the production of DWCNTs with diameters of 3–4.4 nm.

While arc-discharge methods can produce high-purity DWCNTs (up to 90%[29]) with few structural defects, it is limited to large diameters and provides low yield. For instance, arc-discharge methods generally produce nanotubes with diameters >2 nm. Although these may be desirable for some applications, large diameters are not easily characterized using Raman or absorption spectroscopy owing to limitations in the spectral windows, and very large diameters (>4 nm) can easily collapse.[85] Currently, the mean diameter distribution can be reduced through the use of pulsed arc-discharge methods to give nanotubes with diameters of 1.6–2 nm; however, this comes at great expense to the yield, which is significantly reduced to only 10%.[30] This is quite low compared to the yields of steady-state methods employing H_2, Fe, S, and halides, which produce large-diameter DWCNTs of up to 50%.[25] While the arc-discharge method may be limited to large diameters currently, future investigation into the thermodynamics and kinetics of growth, as well as the role of growth promoters, may lead to a higher level of control over the diameter.

4.2. Peapod Growth

DWCNTs can be grown by the so-called "peapod" method by first encapsulating a precursor material within an SWCNT and subsequently treating it to induce coalescence and thereby form an inner wall. The first report of this technique was by Smith et al.,[86] who observed that during the pulsed vaporization of graphite, a technique previously reported to synthesize SWCNTs and fullerenes,[87] C_{60} and C_{70} can become trapped inside appropriately sized SWCNTs. In situ TEM revealed that the fullerenes were deposited on the surfaces of the nanotubes from the gas phase and were seen to enter the nanotubes via the uncapped ends or through defect sites. Once inside the nanotubes, the fullerenes self-assembled into chains, called "bucky-peapods" with uniform center-to-center distances. After extended exposure to a 100 kV electron beam or, as later discovered, temperatures above 1100 °C,[26] the fullerenes coalesced to form the inner wall of a DWCNT with a nearly uniform inter-wall spacing of 0.3 nm. An in-depth investigation into the temperature dependence of the DWCNT formation conducted by Bandow et al. determined that the process of coalescence only occurs at temperatures above ca. 800 °C, becomes better with increasing temperature, and is complete at ca. 1200 °C.[88] The authors further report that other fullerenes, such as C_{76}, C_{78}, and C_{80}, can be used as a precursor material and that the diameter of the resultant inner tube is determined solely by the diameter of the parent wall, irrespective of the fullerene size. Thus, other carbon-containing aromatic precursor materials could very well be used for DWCNT formation, provided that they can be encapsulated by the parent nanotube. Indeed, there are several reports of SWCNT encapsulation of ferrocene[89] which further enables the introduction of a metal catalyst.[90]

Recently, peapod growth has been demonstrated by photon-induced decomposition of fullerenes.[27,91] With the use of a UV laser, Berd et al.[92] irradiated C_{60} peapods with photons of energy higher than that of the fullerene bandgap (1.7 eV for C_{60}) resulting in C_{60} fragmentation.[93] Berd et al.[92] determined the optimum laser excitation was 3.7 eV, which effectively achieved coalescence of the encapsulated C_{60} molecules while maintaining the structural integrity of the parent nanotube. This technique was claimed to be advantageous for nanoelectronic applications as it allows for in situ growth of DWCNTs at room temperature and in ambient conditions,[27,91] but, of course, most conceivable nanoelectronics applications will be exquisitely sensitive to the type of inner wall that is grown. This means that this technique has questionable real-world applicability unless the type of nanotube that is grown can be finely controlled.

The peapod growth method affords very high quality DWCNTs[70] that are clean of residual catalyst and enable the production of very thin DWCNTs (theory predicts diameters as small as 1.174 nm can be filled with C_{60}.[94] Purities of ca. 90% can be achieved, with the only source of contaminant being SWCNTs.[92] However, the method still requires small-diameter SWCNTs to first be synthesized, purified, and carefully processed to allow for the introduction of the precursor material.[95] There is also the issue of unfilled SWCNT contamination, which must currently be addressed post synthesis (although process refinements could likely address this issue in full). Such costly, time consuming, and inherently wasteful steps add significantly to manufacturing complexity, reducing the viability of commercial application and meaning that peapod growth will likely remain limited to small-scale research applications for the foreseeable future. Furthermore, poor filling of the parent outer wall with the coalesced inner wall remains an issue in that theoretical calculations predict that when the fully packed C_{60} molecules inside the parent nanotube have completely transformed, only ca. 2/3 of the parent nanotube has been filled, leaving empty space.[88] However, it is conceivable that this could be a distinct advantage in certain applications requiring non-standard on-tube changes in electronic properties, which could in theory be moved back and forth along the outer wall through control of the position of the inner wall, or similarly in nano-electromechanical systems (NEMS).

4.3. Catalytic Chemical Vapor Deposition

In catalytic chemical vapor deposition (CCVD) growth, a volatile gaseous carbon source (typically CH_4, CO, or C_2H_2) is

decomposed at high temperature over metallic nanoparticles. The decomposed carbon atoms diffuse into the metal nanoparticles and, upon saturation, precipitate at the surface and initiate nanotube growth directly from the nanoparticle. Thus, the catalyst particles simultaneously act as nucleation points for nanotube growth and provide catalytic enhancement. The earliest report of CCVD growth was in 1976 by Oberlin et al., who decomposed benzene in a H_2 atmosphere at 1100 °C to produce nanotubes with diameters ranging from 2–50 nm, although these were not recognized as such at the time.[96] Later, Dai et al. used catalytic decomposition of CO over nanometer-sized Mo particles at 1200 °C to form individual SWCNTs with diameters ranging between 1 and 5 nm and realized that the diameter of the catalytic particles closely correlated to the diameter of the resultant nanotubes.[97] This correlation was further investigated by Cheung et al., who synthesized nanotubes using 3, 9, and 13 nm catalyst particles with C_2H_2 or CH_4 as the carbon source at a temperature of 800–1000 °C.[98] It was found that when the catalyst particles were small, the resultant nanotubes were primarily SWCNTs with ca. 30% DWCNTs. By increasing the size to 9 nm, SWCNTs, DWCNTs, and MWCNTs were produced. Finally when the catalyst particles were large (13 nm), only MWCNTs were produced. The shape of the catalyst is also important, as shown by Liu et al., who grew DWCNTs from CH_3 decomposition over porous Fe/MgO.[99] Through application of external pressure, the pore size was varied and the growth of the DWCNTs was found to be highly dependent on the pore size of the catalyst, with pores less than 30–50 nm producing only MWCNTs. It was proposed that the compression and small pore size resulted in deformation and agglomeration of the metal nanoparticles, yielding MWCNTs and carbon capsules. Furthermore, the pore size can physically hinder the growth of DWCNTs when the length of the DWCNTs reaches the depth of the pore. At this point growth can be terminated, extend into the catalyst structure, or buckle and change direction. Thus, large pore size or a loose stacked structure is best when using porous catalyst. However, the deliberate growth of high-purity DWCNTs is not as straightforward as simply controlling the catalyst size or shape and other factors such as catalyst composition,[100,101] temperature,[102,103] atmosphere,[104] and growth templates[105,106] also play pivotal roles.

The importance of catalyst composition was investigated by Hafner et al., who synthesized SWCNTs and DWCNTs from the catalytic decomposition of both CO and C_2H_4 using nanometer-sized alumina and Mo as the catalyst.[102] Only SWCNTs of monodisperse diameter were produced; however, when Fe was introduced into the catalyst mixture, the reaction also produced DWCNTs, highlighting the effectiveness of Fe for catalyzing DWCNT growth. Currently, Fe remains the most commonly used catalyst owing to its catalytic activity for the decomposition and formation of metastable carbides and because carbon is able to rapidly diffuse through and over the metal surface.[107] However, there are examples of other transition metal catalysts producing DWCNTs, such as by Flahaut et al. who used MgCoO catalyst.[108] They demonstrated gram-scale growth of DWCNTs (up to 1.3 g from 10 g of catalyst) using CH_4 as the feedstock by the inclusion of Mo in the catalyst mixture, which had already been shown to increase the yield of nanotube production.[109] It was later demonstrated that the preparation route for the catalyst was of equal importance as the catalyst composition itself.[101] By altering the synthesis route of MgCoMoO from urea-based combustion to citric-acid-based combustion (a milder combustion process) the catalyst had a higher specific surface area and improved homogeneity, resulting in almost 80% DWCNT growth. Similar to the arc-discharge method, the addition of S as a growth promoter can also change the reaction preference from SWCNTs to DWCNTs. This was investigated by Ci et al. for CCVD growth from C_2H_2 decomposition at 900–1100 °C.[110] It was reported that the growth of DWCNTs was strongly dependent on S addition and, without its inclusion in the catalyst material (ferrocene), only SWCNTs were produced. This was also the first report of CCVD synthesis of DWCNTs using a "floating catalyst", a popular variation of CCVD used for SWCNT growth, which involves subliming the catalyst into the gas phase rather than using substrate-bound form and offers the advantage of producing very long nanotube ropes.[111] Further improvements in DWCNT purity can be achieved through temperature control.[102] It is found that by simply increasing the growth temperature from 700 °C to 850 °C, the production of DWCNTs increased from a composition of only 30% to 70%.

CCVD can be used as a means to grow DWCNTs in vertically aligned forests, which allows for their direct integration into applications such as sensors[112] and field emitters.[113–116] The first demonstration of vertically aligned DWCNTs grown on flat substrates was by Yamada et al. using water-assisted CCVD.[117] This was achieved using Fe-Al_2O_3 (30 nm)/SiO_2 (600nm)/Si, with C_2H_4 as the carbon feedstock, and a DWCNT purity of 85% was produced. The high purity was attributed to enacting precise control over the Fe catalyst film thickness, which largely determines the size of the catalyst particles formed upon heating. This was further investigated by Ci et al. who produced high-purity DWCNTs (88%) using Fe films on an Al support layer with C_2H_4 feedstock at 700–850 °C.[118] It was determined that an Fe film thickness of 1.5 nm deposited onto 10 nm of Al provided the greatest selectivity towards DWCNT growth. The optimized growth conditions resulted in ultra-low-density arrays due to the very large diameter of the resultant DWCNTs (7.9 nm) and the low catalyst particle density. Ultra-long, super-aligned DWCNT forests have been reported by Kim et al. with lengths of 9 mm in 10 h of growth time.[119] This was achieved by first reducing the catalyst (Fe film (1 nm)/Al_2O_3 (30 nm)) by exposure to a He/H_2 atmosphere at 750 °C. The reduction time had a significant effect on the density and size of the catalyst particles and ultimately changed the quality and alignment of the nanotubes forests, where, at 5 min of reduction time, the catalyst formed the smallest grain size, leading to the highest-quality growth.

Due to CCVD's compatibility with a wide variety of substrates, researchers are also focused on preparing aligned DWCNT arrays on substrates more easily integrated into electronics, such as silicon or gold. For instance, Chen et al. produced vertically aligned DWCNT arrays using point-arc microwave plasma CCVD to allow for direct measurement of field-emission properties.[114] In that work, a three-layered catalyst of Al_2O_3/Fe/Al_2O_3 (0.5 nm/0.8–1 nm/5 nm) was deposited onto both Cr (100 nm)/Si and SiO_2 (200 nm)/Si. The trilayer catalyst provides two functions: the thicker, bottom Al_2O_3 layer acts as a barrier, preventing the Fe catalyst from reacting with

the underlying substrate; the thin, top Al_2O_3 layer serves to increase the surface diffusion barrier of the Fe atoms so as to suppress aggregation. Growth of the DWCNTs occurs via the decomposition of CH_4 in a hydrogen atmosphere at 600 °C, yielding outer diameters of 2.5–3.8 nm. It was determined that the Cr/Si substrate achieved a higher nanotube density, but had a lower growth rate than the SiO_2/Si substrate. This was attributed to the SiO_2 accumulating heat during the plasma radiation exposure. Importantly, when growing DWCNTs for direct integration into electronic applications, good contact between the DWCNTs and underlying substrate is essential. Chen et al. determined that the presence of Cr provided less resistance (compared to the SiO_2) and the DWCNT/Cr/Si surface demonstrated superior field emission. Liu et al. later showed that SiO_x (30 nm) deposited onto SiO_2 (100 nm)/Si surfaces could be directly used to catalyze DWCNT growth.[120] It was determined that the critical factors for growth were the thickness of the deposited SiO_2 layer and pre-growth heat treatment, which both affect the size of the resultant SiO_x catalyst particles and, in turn, the number of walls. Nanoparticles in the range of 3–5 nm (annealed for 10 min at 850 °C in Ar atmosphere) were found to be the most effective for DWCNT growth, achieving a purity of 70%. Growth directly on conducting metal foils has been reported by Iijima and co-workers, with Ni-based alloys containing Cr or Fe found to be best for DWCNT and SWCNT growth.[106] In that work, an Al_2O_3 (30 nm)/Fe (1 nm) catalyst layer was deposited onto various metal foils and then exposed to C_2H_4 in a H_2O/He atmosphere at 750 °C. By selectively tuning the catalyst thickness to 1.8 nm, DWCNTs were produced and measurement of the field-emission properties confirmed that good electrical contact had been established. As well, Fu et al. demonstrated that DWCNTs could be grown on catalyst (Fe/Al_2O_3)-coated Au films for use as field-effect emitters.[121] This was done by first reducing the catalyst in a H_2 atmosphere before introducing C_2H_4 at 700 °C.

CCVD is the most commonly used growth method to produce DWCNTs as it offers high yields, is cost effective and controllable, and is appropriate for industrial-scale production. Furthermore, the ability to grow nanotubes on a substrate enables direct integration into some applications, as well as ease of collection. However, despite considerable advances in favoring the growth of DWCNTs over other species, CCVD growth cannot yet be tuned to generate a specific DWCNT type and instead produces a heterogeneous mixture of DWCNTs with small- and large-diameter SWCNTs and even triple- and multi-walled contaminants, as well as amorphous carbon and remnants of metal catalyst. The slow development is in part due to the time-consuming nature of the experiments, where each CCVD run can take an entire day to complete and characterize, as well as the large parameter space of the CCVD process itself. Recently, Nikoleav et al. reported the use of automated experimentation as a means to overcome this cumbersome approach and conduct over 100 water-assisted CCVD growth cycles in a single day.[122] The adaptive and rapid experimentation system, equipped with in situ Raman spectroscopy, is capable of mapping regions of selectivity toward SWCNT and MWCNT nucleation and growth in a four-dimensional parameter space from only a limited number of input experiments. From this, the authors conclude that "perfect" selectivity does not exist because the probability of growing either SWCNTs or MWCNTs is never zero when the parameters are optimized to maximize growth of the other; therefore, the typical product is always a mixture of nanotube types.

5. Processing and Sorting

The field of DWCNT processing is still in relative infancy compared to the more extensively investigated field of SWCNTs. In some ways, the sorting of DWCNTs could be viewed as an extension of already-established SWCNT sorting techniques; however, even at this early stage of development, important differences are apparent and these will only become more prominent as researchers refine the specificity of their methodologies toward the ultimate goal of sorting by inner wall character. The discussion that follows is thus necessarily dominated in some parts by the descriptions of progress in SWCNT sorting. Where SWCNT sorting techniques have been utilized for DWCNTs, some notable results are presented, and in all cases the applicability and potential benefits in relation to DWCNT sorting are analyzed. Unless new techniques are developed that provide for targeted growth of highly pure DWCNTs of desired type, there is a clear need to improve the purity of as-produced DWCNT material in order to unlock their potential in useful applications. This can be achieved through several different approaches, where each approach targets certain contaminants. These approaches can be broadly grouped into two categories: purification, which involves the crude removal of amorphous carbon, fullerenes, SWCNTs, MWCNTs, and any remaining catalyst through chemical or thermal treatment; and sorting, where molecular control is enacted to finely refine the desired product according to requirements e.g., the preparation of material with exclusively semiconducting outer walls.

5.1. Purification

Several treatments can be applied post-synthesis to improve the purity of raw DWCNT material by selective removal of contaminants. For example, the pulsed arc-discharge method of Sugai et al. reported only 20% DWCNT purity due to the presence of fullerenes, SWCNTs, and amorphous carbon contamination.[24] Following purification, they were able to dramatically increase the DWCNT purity to ca. 90%. In their purification strategy, the as-prepared material is first washed with CS_2, a solvent known to selectively solubilize fullerenes, allowing their removal by standard laboratory separation techniques.[123] Residual catalyst particles are then dissolved via sonication in concentrated acid; in this case HCl. Treatment with various acids has been used extensively to purify SWCNTs and has been shown to effectively remove metal particles from as-grown nanotubes.[124] However, the process inevitably results in functionalization of the nanotubes to some degree, depending on the temperature and length of exposure. The amorphous carbon and SWCNT material were then removed via subsequent high temperature air oxidation at 500 °C for 1 h. As the SWCNTs have the same average diameter as the DWCNTs (ca. 2 nm), the authors conclude that the greater thermal stability of the DWCNTs originates from a

higher degree of graphitization (with fewer defects) and from interactions between the inner and outer walls. The same group later quantified this effect by determining that under optimized conditions the oxidation rate of DWCNTs is half that of SWCNTs of the same diameter (1.6 nm); hence, SWCNTs are preferentially oxidized and removed.[30] Purities can be greatly improved (from 10% up to 90%) however some hollow and metal-filled carbon capsules remain even after HCl treatment and cannot be removed. Furthermore, it has been reported that hot air oxidation exhibits a selectivity toward metallic SWCNTs, with semiconducting species still remaining after 4 h at 420 °C, highlighting the need for the correct oxidation temperature in DWCNT purification.[125] However, no reports of air oxidation of DWCNTs specifically measure the electronic properties of the remaining SWCNTs; thus, it is unclear how the preference for metallic oxidation affects the remaining SWCNT population. While air oxidation can effectively remove amorphous carbon and SWCNTs in optimized conditions, and offers the advantage of oxidation without the introduction of sidewall defects, it can result in destruction of the nanotubes at temperatures above 750 °C.[126] Alternatively, refluxing in H_2O_2 for 12 h can also be used to oxidize unwanted SWCNTs, as demonstrated by Yoshida et al., who saw a dramatic improvement in DWCNT purity from only 10% initially to 95% after refluxing.[30] As with acid treatment, some oxygen-containing moieties are introduced at defect sites within the lattice,[127] but to a much lesser extent, and Raman studies show a dramatic decrease in the amount of amorphous carbon present.[128] Similar to hot air oxidation, the H_2O_2 also exhibits a preference to attack nanotubes of specific electronic character; however, in this case it is toward semiconducting character. This is evidenced by the H_2O_2 treatment of SWCNTs resulting in a population of ca. 80% metallic composition after ca. 1 h.[125] In the DWCNT case, refluxing in H_2O_2 is for a significantly increased duration and it is unclear whether or not metallic SWCNTs remain after such an extended time. However, one can conclude that, since air oxidation and H_2O_2 exhibit a preference toward metallic and semiconducting SWCNTs, respectively, a combination of the two may prove to be an efficient purification strategy.

5.2. Suspension

All sorting strategies share one commonality, namely the requirement for the production of suspensions of individualized carbon nanotubes in either water[58,61,129,130] or organic solvents.[131,132] This is achieved through either covalent[20,31,133] or non-covalent methods.[76,129,134–136] Covalent chemistry routes involve the introduction of functional groups to the nanotube ends and sidewalls, rendering them soluble.[31,137] Such processes are extremely good at producing well-dispersed, individualized nanotube suspensions, and often also exhibit some selectivity toward certain diameters[31,138] or electronic types,[139] which can provide useful routes toward separation based on these characteristics. However, covalent functionalization is often disadvantageous as it causes disruption of the conjugated π system of the nanotube by introducing sp^3 hybridization into the pristine sp^2 network.[22] Non-covalent approaches include the use of surfactants such as sodium cholate (SC) or sodium dodecyl sulphate (SDS),[60–62,130,140–143] or dispersing agents such as DNA[58,144–146] and organic polymers.[131,132,147,148] Dispersion of the nanotubes in these stabilizing agents is achieved via ultrasonication and often followed by centrifugation to remove remaining bundles and residual catalyst particles.[136]

For surfactant-stabilized dispersions, the surface concentration and orientation of surfactant molecules on the nanotube sidewalls is highly dependent upon the type of surfactant, the concentration in solution, and the diameter and electronic type of the nanotube.[60,62,140,149–153] Generally, the surfactant first forms a random layer and, as more surfactant molecules bind to the surface, begins to form hemimicelles. Further addition of surfactant can cause the formation of a highly packed cylindrical micelle.[154] However, this varies for different diameters, with smaller nanotube diameters exhibiting less-ordered surfactant structures.[149] For example, SDS wrapping of small-diameter nanotubes (<1 nm) tends to result in highly disordered, random configurations at low SDS concentrations (packing densities of ca. 1.0 molecules nm^{-2})[155,156] and more-ordered, cylindrical wrapping at high SDS concentrations (2.8 molecules nm^{-2}).[155] The wrapping of large-diameter nanotubes (>1 nm) is also disordered at low concentration but forms hemimicelles at high SDS concentration.[155,156] Experiments suggest that the correlation between nanotube structure and wrapping is due to differences in the surface π-electron states of the various SWCNT curvatures, which affect the SDS/nanotube interaction.[60] When an SDS molecule wraps around a small-diameter nanotube with a large bond curvature, it encounters a larger energetic barrier due to bending.[156] Therefore, it is energetically more favorable for the SDS to adsorb to larger-diameter nanotubes with smaller curvatures, which is an underlying principle of several of the sorting methodologies described later.[140,155,157] The extent of SDS encapsulation is also dependent upon the electronic character, with metallic nanotubes having a higher degree of SDS wrapping than semiconducting nanotubes, owing to their higher polarizability.[61,140,152,158] Co-surfactant wrapping, which relies upon competitive non-specific binding between different surfactants e.g., SC and SDS, provides a further parameter that can be exploited for nanotube separation according to electronic character.[58,130,142,143]

Suspension of nanotubes with DNA[159–161] and proteins[32,162–165] relies primarily on strong π-stacking onto the nanotube sidewalls. This effectively individualizes the nanotubes and at the same time provides a negative surface charge density due to close proximity of the phosphate backbone to the nanotube.[159] As such, DNA is particularly suitable for solubilization of DWCNTs, with several examples seen in the literature.[135,160,161,166] Using DNA, SWCNTs have been sorted by electronic type[144,159] and (n,m) species[145] through the use of ion-exchange gels. Because they contain biological elements, such suspensions are highly dependent on the pH of the solution, which must be optimized to achieve well-dispersed nanotube suspensions of high concentration. Suspension in organic solvents is used in polymer separation and will be discussed in Section 5.9. Once a good suspension of purified nanotubes has been obtained, there are several techniques that have been developed to sort them using a number of different strategies with varying degrees of complexity, specificity, and success.

5.3. Reversible Covalent Chemistry

Because various covalent modification schemes are selective to nanotube diameter, such inherently scalable approaches are highly attractive for the purification and separation of DWCNTs. One such approach demonstrated by Deng et al.[31] involves the Billups–Birch reductive alkylcarboxylation reaction. That work involved covalently functionalizing CNTs with alkylcarboxylic acids groups progressively from smaller-diameter nanotubes towards larger diameters. Addition of these groups rendered the nanotubes water soluble and the diameter-dependent nature of the reaction allowed for standard phase separation in water–hexane. This resulted in partitioning of functionalized samples into different aqueous extracts of decreasing functionalization and solubility, commensurate with increasing diameter. As well as providing such diameter-selective separation, a further advantage of this kind of approach is the reversible nature of the reactions. In the case of alkylcarboxylation, the sorted nanotubes can be returned to their pristine state through simple annealing. Because wall number is closely correlated with diameter, reductive alkylcarboxylation can also be used to selectively remove single- and multi-walled nanotubes, as well as carbonaceous by-products, from as-synthesized DWCNT material.[167]

In the reductive-alkylcarboxylation method, raw DWCNT material is added to liquid NH_3 containing Na to individualize the nanotubes and enable homogeneity of the subsequent reaction. When Na is added to NH_3, it dissolves completely, with nitrogen lone pairs coordinating to the metal, yielding an electronic liquid comprising $[Na(NH_3)_x]^+$ complexes and free electrons. When nanotubes are added to the solution, the solvated electrons are transferred to the various nanotubes and (aromatic) carbonaceous material, providing a negative surface charge and producing "nanotubide" radical anions. In this way, the van der Waals forces holding the nanotubes in bundles are gently overcome by strong Coulombic repulsion, thus individualizing them.[31] Upon addition of 6-bromohexanoic acid, as in the work of Deng et al.,[31] (or any molecule with a halogen-terminated alkyl chain) a reduction reaction occurs adding alkylcarboxylic acid groups to the nanotube sidewalls. The diameter selectivity arises due to the difference in the Fermi levels of the nanotubes, wherein smaller-diameter nanotubes (with higher Fermi levels)[168] exhibit a greater reduction potential than larger ones. Hence, the reduction by solvated electrons occurs preferentially on the smaller-diameter nanotubes and, with careful control of the reaction stoichiometry, this can then lead to preferential addition of alkylcarboxylic acid groups to the smaller nanotubes.

In the work of Deng et al.,[31] three reaction cycles were completed, each starting with further addition of Na and alkylcarboxylate source, before phase separation in a water/hexane mixture. The more easily functionalized SWCNTs and amorphous carbon were separated into the aqueous fraction, while the less-functionalized DWCNTs and MWCNTs were enriched in the insoluble solid. Deng et al. also demonstrated that the reduction occurs by defect activation and propagates exclusively from sp^3-hybridized sites, giving rise to clusters of functional groups, and thus explaining why the amorphous carbon, which primarily consists of sp^3-hybridized carbon atoms, can be eliminated so easily.[133] By further performing a subsequent 3-cycle alkylcarboxylation on the insoluble solid, the DWCNTs and MWCNTs were then selectively functionalized and water solubilized, leaving the remaining MWCNTs in the insoluble solid. A schematic illustration of the two-step diameter-dependent reaction can be seen in **Figure 5**. After the successful enrichment of DWCNTs, the alkyl functional groups were then removed by thermal annealing of the filtered and washed product in H_2/Ar. High-resolution TEM revealed that while the final sorted product did still contain some MWCNTs (likely resulting from their very high initial composition), the carbonaceous material and SWCNTs had been successfully removed, leading to DWCNT enrichment in the sample. This work not only demonstrates the applicability of covalent chemistry to enrich DWCNTs, but does so using a straightforward and highly scalable technique, which further allows the nanotubes to regain their pristine structure. Although no enrichment by electronic character was observed, the reduction potential of nanotubes does exhibit dependence on electronic character, and even on chirality. In theory it should therefore be possible to use a stoichiometric deficiency of Na to selectively functionalize only those nanotubes with the smallest reduction potential and thus facilitate some degree of sorting.

5.4. Biofunctionalization

An example of the use of biological elements to suspend and sort DWCNTs is seen in the 2011 work of Nie et al. in which DWCNTs were non-covalently biofunctionalized with the protein, lysozyme.[32] Lysozyme is particularly desirable for this purpose as it primarily consists of amine groups, which provide the nanotube with adequate water solubility,[165] and has hydrophobic residues within its core that readily interact with

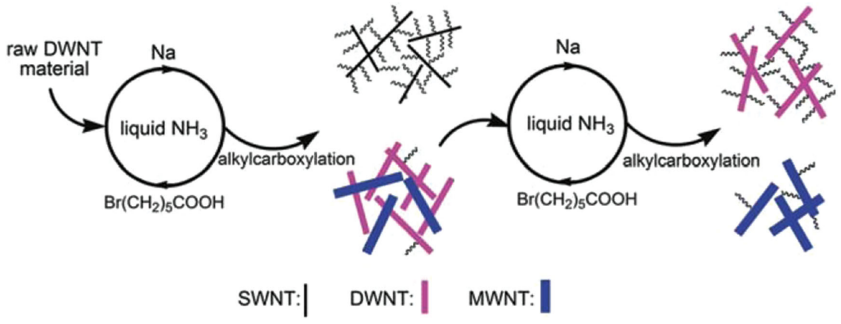

Figure 5. Schematic illustration of the two-stage enrichment of DWCNTs using diameter- and defect-selective alkylcarboxylation. By exploiting the diameter dependence of the reductive alkylcarboxylation of carbon nanotubes, the degree of functionalization and water solubility of the SWCNTs were selectively enhanced, allowing for their removal in aqueous extracts by water–hexane-phase extraction. Additional reaction cycles were performed on the insoluble solid, in which DWCNTs were enriched. Reproduced with permission.[167] Copyright 2011, Royal Society of Chemistry.

nanotubes through π–π stacking.[162] At low pH, protonated amines also interact with the defect sites of the nanotubes and at high pH, through amine adsorption.[162] It was observed that lysozyme selectively suspended large-diameter DWCNTs[32] and this is in agreement with computational studies where MWCNTs of larger diameter (40 nm) consistently showed stronger protein binding than those with a smaller diameter (10 nm).[164] This is also in agreement with studies of protein interactions with nanoparticles.[169] Nie et al. suggest that the stronger bundles formed by smaller-diameter nanotubes[32] may also contribute to their reduced solubilization via protein binding.[32] Because the large-diameter DWCNTs are selectively functionalized, centrifugation provides separation of the larger- and smaller-diameter DWCNTs into supernatant and pellet, respectively. TEM of the respective DWCNT samples reveals two distinct ranges of diameter, of 3–5 nm (Gaussian average of 4.0 nm) and 1–4 nm (Gaussian average of 2.7 nm). As diameter is strongly correlated with wall number, DWCNTs can also be separated from smaller-diameter SWCNTs, providing a convenient method for DWCNT enrichment of such samples. This was shown by adding a 4:1 mixture of pure DWCNTs and SWCNTs to a solution of lysozyme. The mixture was sonicated to aid solubilization and then centrifuged, yielding sediment and a lysozyme-biofunctionalized supernatant. Only large-diameter DWCNTs were found in the supernatant (as determined from TEM), highlighting the applicability of this approach to selectively produce fractions of large-diameter DWCNTs from such mixtures.

In the work of Dresselhaus and co-workers, long and random single-stranded (ss-) DNA was employed to individualize DWCNTs, forming suspensions stable at high pH (>6.8–12.4).[160] As the pH becomes more acidic, the DNA begins to destabilize and then agglomerate due to protonation of the backbone phosphate groups. It is hypothesized that, as the larger-diameter nanotubes are more susceptible to bundling due to increased van der Waals forces, they agglomerate preferentially and can be separated through centrifugation from the suspended small-diameter DWCNTs. However, this is so far based solely on PL and optical absorption, which, as previously discussed, provide less certainty in the case of DWCNTs without corroboration from the more-conclusive TEM analysis.

5.5. Molecular Nanocalipers

The use of chiral diporphyrin nanotweezers and nanocalipers can achieve simultaneous discrimination of nanotube diameter, metallicity, and handedness in SWCNTs.[171,172] This technique involves tailoring of the diporphyrin structure to yield one that is sterically compatible with a nanotube of specific diameter and chiral angle. Such diporphyrins form stable host–guest complexes with the target nanotube through π–π and CH–π interactions, which can be separated from the remaining

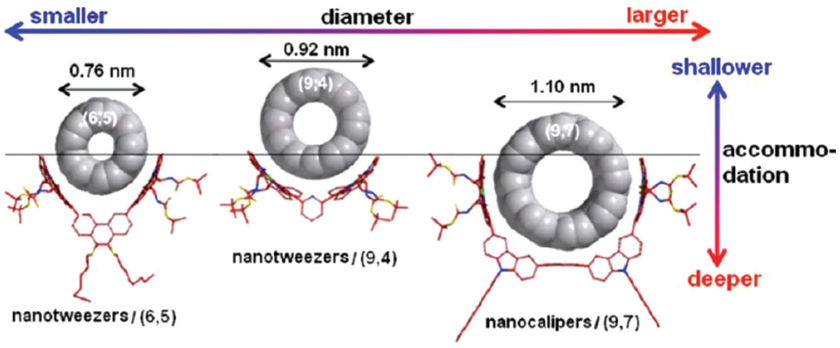

Figure 6. Computer-generated molecular modeling of the interactions between nanotweezers and nanocalipers and appropriately sized SWCNTs. By tailoring the chiral diporphyrin structure to a specific size and depth, the (6,5), (9,4) and (9,7) SWCNTs can be isolated. Reproduced with permission.[172] Copyright 2013, American Chemical Society.

nanotubes via centrifugation. Specificity arises from careful selection of the spacing between the calipers, which affects the width of the host molecule and the depth at which the nanotube sits within the host.[171] These physical parameters become very important when targeting a specific nanotube, with larger nanotubes requiring a deeper position within the host.

Figure 6 shows an example of directly engineered diporphyrins and their complimentary nanotube types. For example, the (6,5) nanotube (diameter of 0.76 nm) can be accommodated by a nanotweezer structure. By altering the structure of the diporphyrin to have a slightly larger spacing, the (9,4) nanotube (diameter of 0.92 nm) can be accommodated. In order to accommodate nanotubes >1 nm, a nanocaliper structure can be used, which possesses arms that extend out to capture the target nanotube. Such tailored host structures not only allow for diameter sorting, but also for enantiomeric separation according to the handedness of the specific nanotube.[171,172] By inclusion of a chiral center within the diporphyrin, two mirror-image (*S*) and (*R*) hosts can be created for each target nanotube diameter, resulting in separation of left-handed (LH) and right-handed (RH) nanotube enantiomers. Initially, the enthalpies of association of the LH and RH nanotubes with an (*S*)-diporphyrin are approximately equal.[171] However, as the number of diporphyrin molecules bound to the nanotube surface increases, the formation of the RH:(*S*) complex becomes more energetically favorable than the LH:(*S*) complex. This means that RH:(*S*) becomes more stable and therefore, more soluble, than LH:(*S*). The opposite can be expected for the mirror-image host, with LH:(*R*) becoming more stable.

DWCNT sorting via the use of chiral diporphyrins was reported by Liu et al., wherein DWCNTs were successfully sorted from MWCNTs and, to a lesser extent, SWCNTs.[33] This was made possible by tailoring a chiral diporphyrin into a nanocaliper structure with a spacer of 1.9 nm between porphyrins. Extraction with the nanocaliper yielded significantly improved DWCNT purity (from 77% up to 90%) and narrower diameter distribution (from 1.23–3.23 nm to 1.25–2.75 nm). After removal of the nanocalipers via repeated washing of the centrifuged solid with tetrahydrofuran (THF) and pyridine, circular dichroism (CD) measurements were performed, where the presence of LH and RH DWCNTs species were confirmed. The authors thus concluded that the DWCNT enantiomers are most

probably obtained through molecular recognition by the chiral diporphyrin nanocalipers.

5.6. Density-Gradient Ultracentrifugation

Density-gradient ultracentrifugation (DGU) is a technique originally designed for separating and isolating biological elements (such as macromolecules or viruses)[173] and was first used to separate SWCNTs by Hersam and co-workers in 2005.[58] This separation method involves taking individualized nanotubes suspended in surfactant and placing them into a graded fluid medium (usually iodixanol owing to its high viscosity and tunable density[142]) of varying density within a centrifuge tube.[58,130,140,143] The various nanotube species are then moved by centripetal forces until they reach their respective isopycnic points (the point where the nanotube's buoyant density matches that of the surrounding fluid medium). The key to the separation lies in the different buoyant densities of each nanotube species, which is a feature that is heavily reliant upon the physical structure of the nanotube itself, as well as the encapsulating surfactant and solvent molecules.

In the case of a binary surfactant, the structure of the surfactant shell is strongly influenced by the nanotube diameter.[140,157] Alternatively, in co-surfactant mixtures the polarizability of the SWCNT plays an important role and leads to non-equivalent wrapping of the two surfactants around different nanotubes.[158] This is especially true for surfactant mixtures with SDS, which is highly sensitive to electronic type[140,158] and results in the encapsulated nanotubes having a strong contrast in density. For example, the addition of SDS to SC-wrapped SWCNTs significantly increases the density of nanotubes with diameters of 0.83 nm and 0.98/1.03 nm, and facilitates their separation from smaller nanotubes (ca. 0.76 nm).[140] Therefore, by employing the appropriate conditions, SWCNT fractions with a narrow diameter distribution, or of defined semiconducting and metallic type, or even of enantiomerically pure single chirality can be produced by DGU.[130,140,143]

Due to the great success of DGU for SWCNTs, it was a natural step to extend the method to DWCNTs. In particular because the inclusion of an inner wall significantly alters the buoyant density and thus offers a convenient method to deal with unwanted SWCNT impurities. This was first achieved by Green and Hersam in 2009 using a two-step DGU process.[34] In the first step, raw material (DWCNT composition of 70%) is suspended in 1 wt% SC. The authors speculate that, due to the anionic planar structure of SC, its encapsulation layers are highly sensitive to nanotube diameter and therefore, its use affords fractions of SWCNTs, DWCNTs, and MWCNTs of very different densities.[34] Furthermore it is speculated that another advantage of SC is its limited sensitivity to the electronic character of the nanotubes, which means that any electronic perturbations of the outer wall by the inner wall will not have an impact on the surrounding surfactant layer. Therefore, for similar diameters, SC encapsulation does not vary between SWCNTs and DWCNTs, and the only difference is a much larger density for DWCNTs due to the inner wall. **Figure 7**a shows a schematic of the SC encapsulation of small- and large-diameter SWCNTs and DWCNTs, as well as its effect on their buoyant densities.

The density gradient consisted of 1.5 mL of 60 wt% iodixanol on the bottom, followed by 5 mL of a linear gradient varying from 32.5 to 17.5 wt% iodixanol with 1.5 mL of 15 wt% iodixanol on top, in which the DWCNTs initially resided. The remaining volume was filled with 0 wt% iodixanol and the linear density was then centrifuged at 41 000 rpm (207 570*g*) for 12 h. In this process the nanotubes are forced to sediment from their initial starting position of low density to a higher density. The advantage of top addition is that lower-density SWCNTs are prevented from reaching the isopycnic point of the much denser DWCNTs. As seen in Figure 7b, this results in 4 bands corresponding to small-diameter SWCNTs (ca. 0.7–1.1 nm),

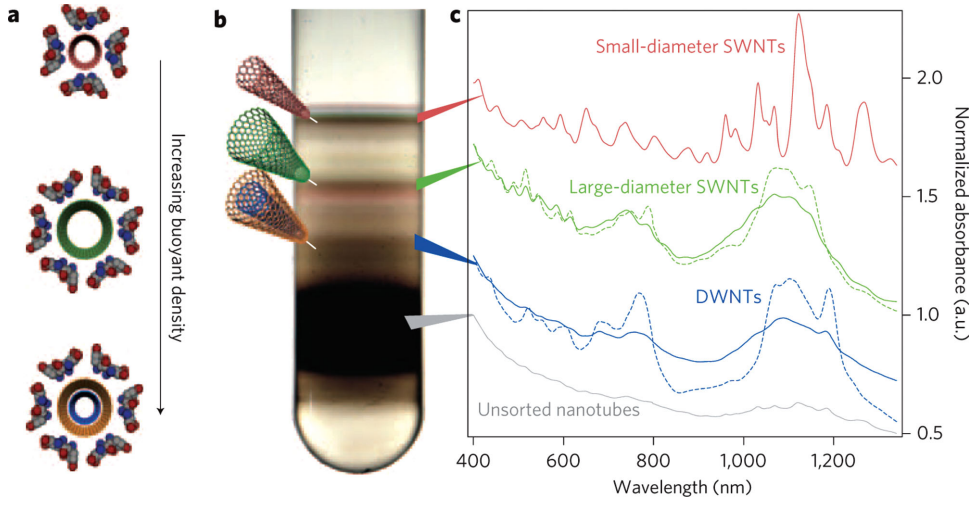

Figure 7. Separation of DWCNTs by the number of walls via DGU. a) Schematic illustration of nanotube encapsulation by SC and its effect on the resultant buoyant density. b) Photograph of a centrifuge tube following the first iteration of the separation showing four bands, corresponding to small-diameter SWCNTs, large-diameter SWCNTs, DWCNTs, and MWCNTs/carbonaceous impurities/bundles. c) Absorption spectra of each band following the initial separation and, in the case of large-diameter SWCNTs and DWCNTs, the first iteration. The absorbance is normalized and offset in each case. Reproduced with permission.[34] Copyright 2009, Nature Publishing Group.

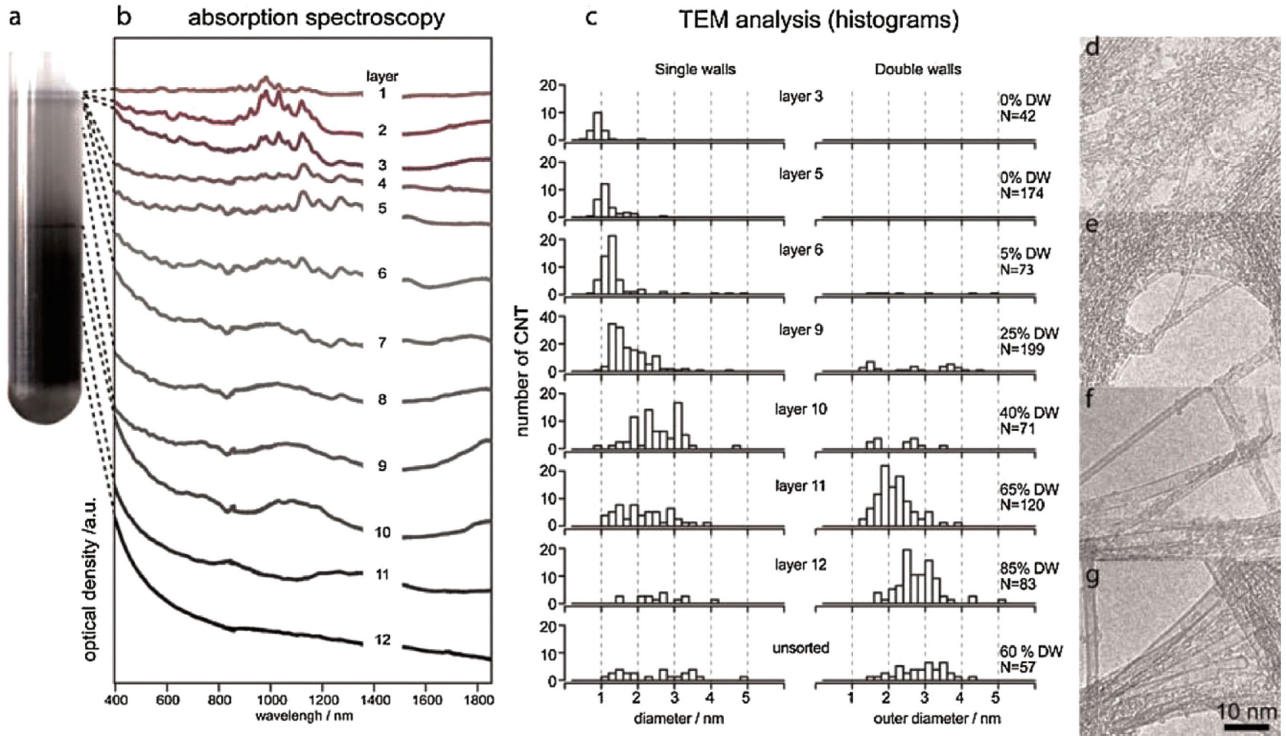

Figure 8. Analysis of the sorting efficiency of the DGU technique by TEM. a) Centrifuge tube of the DGU sorted DWCNT material showing several bands within the linear gradient. b) Absorption spectra of each layer. c) TEM analysis of the different bands showing an increase in mean diameter with increasing density, change in relative concentration of SWCNTs and DWCNTs and the change in distribution shape. d–g) TEM images of SWCNTs and DWCNTs from layers 3, 6, 10 and 12, respectively. Reproduced with permission.[174] Copyright 2008, Wiley-VCH.

large-diameter SWCNTs (ca. 1.6 nm), DWCNTs (ca. 1.6 nm), and MWCNTs, bundles, and carbonaceous impurities. The coarsely refined DWCNTs and large-diameter SWCNTs were then subjected to a second DGU step. In that step the material was now inserted into the bottom of the density gradient, which forced the nanotubes to move from high to low density with the goal of removing any slow-moving, dense species that did not reach their isopycnic points the first step. The second density gradient consisted of 1.5 mL of 60 wt% iodixanol on the bottom, 1 mL of coarsely refined DWCNTs in 33.5 wt% iodixanol, then 5 mL of density gradient ranging from 31 to 16 wt% iodixanol with the remaining space filled with 0 wt% iodixanol. The effect of a subsequent DGU step is clearly visible in the absorption spectra in Figure 7c (dashed lines), where a significant improvement in the purity of the large-diameter SWCNT and DWCNT fractions is seen, as evidenced by the sharper peaks and reduced scattering background.

In an investigation of the sorting efficiency of DGU, Loiseau and co-workers conducted a layer-by-layer analysis of nanotube content by TEM.[174] As seen in **Figure 8**a, twelve bands were taken from the centrifuge tube and characterized by TEM (over 100 nanotubes per band) and absorption spectroscopy (Figure 8b,c). As discussed,[34] the SWCNTs are found in the lower-density top half of the centrifuge tube with a trend of increasing diameter seen with increasing density (layers 1–5), whereas the highest-purity DWCNTs (85%) are found in layer 12. Between layers 6 and 12, a mixture of SWCNTs and DWCNTs were found with increasing DWCNT purity.

Extending the DGU method to sort DWCNTs according to electronic character was a seminal advancement toward the realization of high-technology DWCNT devices, and was achieved by Green and Hersam in 2011.[35] In that work, DWCNTs coarsely purified via their original method[34] were separated by outer wall electronic type using subsequent DGU iterations. However, in the subsequent DGU steps, co-surfactant mixtures of SC and SDS were used. Due to the very different surfactant wrapping of metallic and semiconducting nanotubes,[158] the difference in density between the two electronic types in co-surfactant mixtures is even greater than in the single surfactant case and this can be optimized for a particular metallic/semiconducting separation.[130,140,142] For instance, ratios of 1:4 SDS/SC and 3:2 SDS/SC have been found to be optimal for targeting large-diameter semiconducting and metallic SWCNTs, respectively.[140]

For semiconducting DWCNT enrichment, three iterations followed the initial coarse DGU step. In the first iteration, the DWCNTs were placed at the bottom of a 1 wt% 1:4 SDS/SC density gradient from 25 to 40 wt% iodixanol. The gradient was centrifuged (41 000 rpm or ca. 208 000*g* for 14 h) and resulted in further separation of DWCNTs and SWCNTs. However, separation according to electronic character was also seen owing to the introduction of SDS. The semiconducting outer wall enriched (s-) DWCNT layer was then isolated and used in the second iteration, which was a repetition of the first, but with the s-DWCNTs added to the top of the gradient. In the third iteration, a 3:2 SDS/SC ratio was used with the DWCNTs

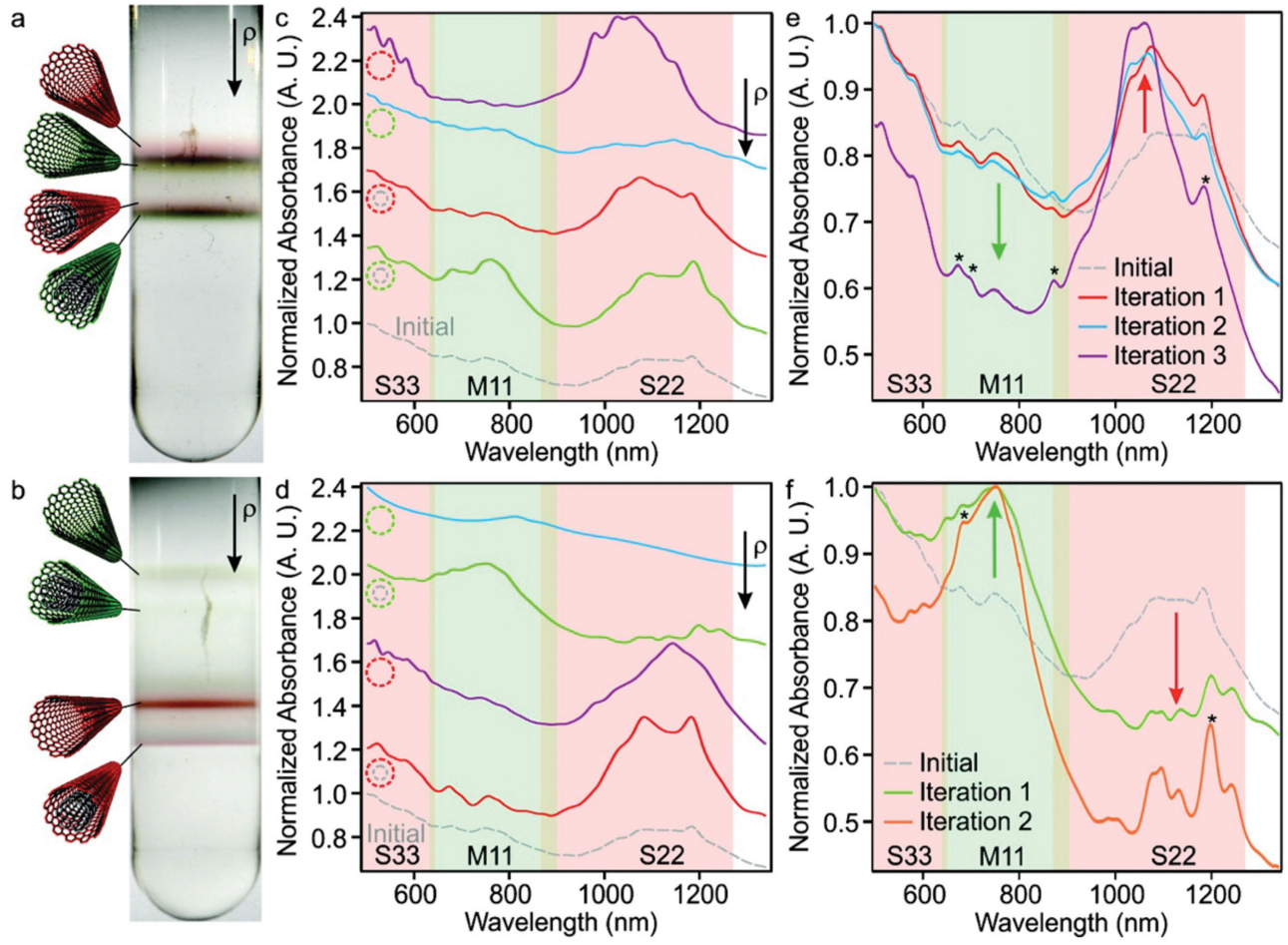

Figure 9. Separation of DWCNTs by outer wall electronic type. a–b) Photographs of centrifuge tubes following DGU separation of SWCNTs/DWCNTs targeted for semiconducting and metallic DWCNTs, respectively. c–d) Absorbance spectra of each band during the first-iteration separations targeting semiconducting and metallic DWCNTs, respectively. Metallic DWCNTs, semiconducting DWCNTs, metallic SWCNTs, semiconducting SWCNTs, and then coarsely enriched input DWCNT material are shown by the red, green, purple, blue, and dashed grey curves, respectively. The spectra are offset for clarity. e–f) Absorbance spectra obtained during successive DGU iterations to produce semiconducting and metallic DWCNTs, respectively. The asterisks mark the absorption peaks attributed to inner-DWCNT-wall transitions. S*ii* (M*ii*) label the *i*th order semiconducting (metallic) optical transitions of the SWCNTs and the outer walls of DWCNTs. Wavelength regions associated with semiconducting and metallic SWCNTs and outer wall DWCNTs transitions are shaded red and green, respectively. Reproduced with permission.[35] Copyright 2011, American Chemical Society.

moving from low to high density to remove any remaining metallic species. For metallic DWCNT enrichment, only two iterations followed the initial coarse DGU step and both used a 1 wt% 3:2 SDS/SC ratio, but differed in initial DWCNT placement.

Figure 9a shows the resultant layer structure for a co-surfactant ratio of 1:4 SDS/SC. Separation occurs primarily by diameter, however red and green fringes corresponding to metallic and semiconducting character, can also been seen. The absorption measurements of each fringe (seen in Figure 9c) also show signs of electronic sorting for both SWCNTs and DWCNTs, with enhanced S_{22} and M_{11} transitions. Alternatively, the separation with a co-surfactant mixture of 3:2 SDS/SC can be seen in Figure 9b, where the increased relative concentration of SDS has significantly changed the resultant band structure. Separation is now dominated by electronic character and occurs concomitantly with diameter, with the four bands visible corresponding to m-SWCNTs, m-DWCNTs, s-SWCNTs, and s-DWCNTs (absorption measurements shown in Figure 9d). As the m-CNTs are coated with an increased surface concentration of SDS compared to that of s-CNTs, their isopycnic points are at lower densities.[175,176] Figure 9e shows absorption spectra after the initial DGU step and the three subsequent iterations for s-DWCNT enrichment. While each DGU step yields enhancement of the S_{22} and reduction in M_{11} features, the most significant enrichment is seen in the final step, which employs the 3:2 SDS/SC co-surfactant mixture. Additionally, there is also a peak at ca. 1200 nm corresponding to the S_{11} transition of an inner wall. Figure 9f shows absorption spectra for each DGU step, targeting m-DWCNTs. Each separation sees the enhancement of the M_{11} transitions with S_{22} contributions from s-DWCNTs removed, revealing inner wall S_{11} peaks in the same region. In each case, very high purities were achieved with final fractions containing 96% and 98% semiconducting and metallic

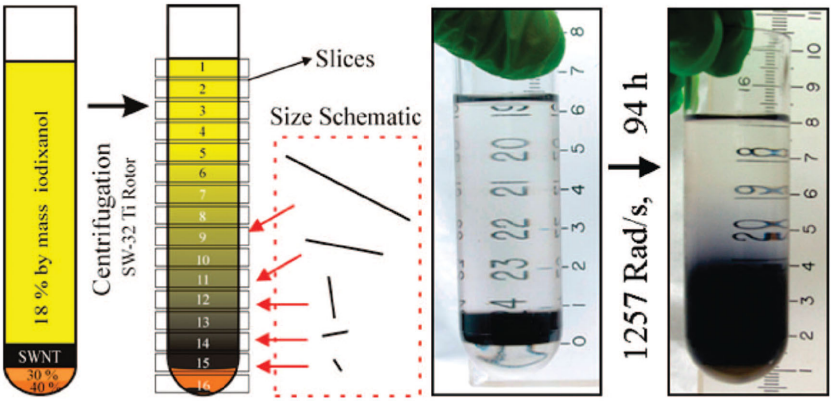

Figure 10. Schematic and photographs of the process of length separation by centrifugation for SWCNTs. An injection layer containing the SWCNTs, modified to the appropriate liquid density, is placed near the bottom of the tube to maximize the separation. Longer nanotubes move further in response to the applied centrifugation, and thus separate up the tube; any high-density impurities move in the opposite direction. Reproduced with permission.[141] Copyright 2008, American Chemical Society.

DWCNTs, respectively. This clearly demonstrates the effectiveness of the DGU technique.

5.7. Centrifugal Length Separation

In addition to the separation of carbon nanotubes by diameter and electronic type, centrifugation has also been used to prepare nanotubes with a narrow length distribution.[141,177] This length-dependent separation technique has previously been reported for the fractionation of SWCNTs with lengths in excess of 1 µm and is achieved by exploitation of the length-dependent friction coefficient through a dense liquid under centrifugation.[141,177] While this technique is very similar to DGU, it employs a fluid medium much denser than the nanotubes such that they can never reach their isopycnic points, and, rather, exploits transient motion, where longer nanotubes travel with greater velocity in opposition to the applied acceleration. This occurs because the rate of nanotube flow through the fluid has a non-linear dependence on length.[177] Separation occurs (with minimal chirality differentiation), provided that $\Delta\rho = \rho_S - \rho_{SWCNT} >> \Delta\rho_{SWCNT} = \rho_{SWCNT} - \rho_{SWCNT,i}$ where $\Delta\rho$ is the difference in density, ρ_S is the density of solution, ρ_{SWCNT} is the average density of all the SWCNT chiralities and $\rho_{SWCNT,i}$ is the density of an individual SWCNT chirality.[177] Thus, the key to length separation is to choose the linear density such that $\Delta\rho >> \Delta\rho_{SWCNT,}$ thus exploiting the transient motion regime and not the regime in which buoyancy equilibrium is reached. **Figure 10** shows a schematic representation and photographs of SWCNT length separation by centrifugation, where longer SWCNTs travel further from the injection layer.

In 2010, Fagan and co-workers separated DWCNTs according to length in a two-step method.[178] Firstly, the DWCNTs were coarsely enriched using the pre-established DGU method.[34] The enriched DWCNT material was then inserted into a centrifuge tube with a specially designed gradient derived from SWCNT length separations.[141,177] Then, 1 mL of high-density (40%, 1.21 g mL^{-1}) iodixanol was added, followed by 1 mL of slightly lower density (30%, 1.16 g mL^{-1}) containing the DWCNTs. Finally, 20 mL of 26% (1.14 g mL^{-1}) solution was added (the race layer in which fractionation occurs), with the concentration of surfactant remaining constant throughout, at 1 wt% deoxycholate (DOC). Importantly, the density of the surrounding medium is greater than the average density of the DWCNTs (ca. 1.11 g mL^{-1}), thus enabling transient motion and not buoyant density. The gradient was then centrifuged at 34 000*g* (16 640 rpm) for 49 h. The top-most layer (containing nanotubes that had travelled the furthest from the DWCNT injection layer), contained nanotubes with a length of 2.2 µm. As expected, the average length decreased for fractions closer to the injection layer, with the shortest average length reported as 0.6 µm, with each layer having a relatively narrow length distribution (distribution of layer 4 was ±0.18–0.3 µm).

Fagan and co-workers also report partial enrichment by electronic character using co-surfactants.[178] In that case, a slightly denser gradient was employed with an additional co-surfactant gradient; however, evidence of electronic enrichment was limited.

5.8. Gel Permeation

The use of Sephacryl gel permeation, first demonstrated by Moshammer et al.,[59] has been shown to be extremely successful in the preparation of (*n*,*m*)-purified SWCNT suspensions. For SWCNTs, this technique has allowed for the high-throughput separation of metallic species from semiconducting species,[59,152,153] the isolation of specific (*n*,*m*) species,[60–62] and, most recently, the separation of optical isomers.[179]

In general, the gel-permeation method involves passing SDS-suspended nanotubes through a stationary phase gel bed contained within a column, at which point semiconducting nanotubes with the highest affinity for the gel (an interaction determined by the SDS wrapping, and hence, the individual nanotube structure) are selectively removed from the bulk solution and retained on the gel matrix.[61] The metallic nanotubes, which exhibit no interaction with the gel,[60,61,152,153] as well as other semiconducting nanotubes with no affinity to the gel (determined by surfactant concentration), continue to flow through the gel and can be collected. The gel is then washed with SDS of either increased concentration[60,61,152] or lower pH,[153,180] or alternatively SC,[59,152] which disrupts the interaction between the adsorbed semiconducting nanotubes and the gel and thus elutes them from the column for collection. This process can be repeated sequentially with the nanotubes that have the highest affinity for the gel becoming preferentially adsorbed each time.

While the exact mechanism of gel-based separation remains speculative owing to the difficulties associated with determining the molecular dynamics on the nanoscale, evidence suggests that it is a kinetically driven selective adsorption

process,[61] highly dependent on the SDS wrapping of the nanotubes.[151] This is evidenced by the clear relationship between SDS concentration and gel adsorptivity,[60,61,151,152] where an increase in the SDS concentration allows additional SDS molecules onto the nanotube surface,[176] reducing its interaction with the gel. In addition to the SDS concentration, pH[62,153] and temperature[151] have also been shown to play important roles, giving rise to a number of separation strategies. While SDS-based separation is successful for small-diameter SWCNTs (0.77–1 nm), adsorption of large-diameter nanotubes (greater than ca. 1.2 nm) to the gel is quite limited.[37] Instead, a co-surfactant separation method can be used, where either the large-diameter material is suspended in a co-surfactant solution and applied to a column, as demonstrated by Miyata et al.[181] and Wu et al.,[182] or where they are suspended in SC and applied to a column in SDS, as demonstrated by Zhang et al.[183] While all of these co-surfactant methods produced highly pure, semiconducting solutions (99%, 98%, and 98%, respectively), none report the purity of the metallic fraction, which is washed off of the gel in the flow-through.

Application of the gel-permeation technique to DWCNTs was first reported by Moore et al. in 2014,[36] wherein the separation of DWCNTs from SWCNTs was demonstrated, producing highly enriched fractions with mean diameters of 1.64 ± 0.15 and 0.93 ± 0.03 nm, respectively. In that work, DWCNT raw material was suspended in 2 wt% SDS by sonication for 8 h, and this was then added to a 25 cm Sephacryl S-200 gel column, also at 2 wt% SDS. While the bulk of the nanotubes passed through the gel, a small amount remained adsorbed to the top of the column. This is in agreement with previous work by Blanch et al.[152] and Flavel et al.[62] where it has been demonstrated that, at a relatively high SDS concentration (1.6–2 wt%), only a very small portion of the overall nanotube population is adsorbed in a competitive process, compared to that for low SDS concentrations (0.4–0.8 wt%).

Addition of 0.5 wt% SC resulted in the desorption of the nanotube material and two distinct bands formed in the column, the first of which was fast moving and dispersed while the second was slower moving and more tightly confined. This can be seen in **Figure 11**a, which shows time-lapse photographs of the initial adsorption and subsequent elution with SC. Extensive atomic force microscopy (AFM), absorption spectroscopy, TEM, and Raman spectroscopy revealed that those bands corresponded to DWCNTs and SWCNT, respectively. One explanation for the significant difference in elution rates is that the nanotubes undergo a size-exclusion process in which the retention time is dependent on the size. Indeed, extensive AFM revealed that there was a significant size difference between the two nanotubes types, which is summarized in Figure 11b. On average, the DWCNTs (ca. 700 nm) are twice as long as the SWCNTs (ca. 300 nm), which may be attributed to the increased structural stability of the DWCNTs during extensive sonication. This is in agreement with Green and Hersam who also observed that DWCNT lengths were ca. 40% longer than SWCNTs after 1.5 h of sonication.[34] However, a true size-exclusion process would also occur in SC, which the authors confirm is not the case. The mechanism is therefore likely a combination of two competing factors: diameter-dependent solvation by the surfactant and length-dependent size exclusion.

Analogous to the evolution of DWCNT sorting by the DGU method, the gel-permeation technique was then extended to the electronic sorting of DWCNTs.[37] In that work, a DWCNT suspension in 1 wt% SC was added to a 20 cm long gel column in 1 wt% SDS. Upon addition of the SC-encapsulated nanotubes to the column, they immediately underwent surfactant exchange, resulting in various ratios of SDS/SC wrapping, depending on the diameter and electronic character.[130,142,143] Owing to this difference in wrapping, nanotubes of different electronic types moved through the column at different rates, forming four bands, which were eluted from the column after different retention times. The four bands were shown to correspond to defected m-DWCNTs, m-DWCNTs, s-DWCNTs, and s-SWCNTs, respectively, with the elution order in excellent agreement with data from the separation of AD and HiPco SWCNTs of a similar electronic type. Thus, it is clear that the separation process is highly sensitive to the surface properties of each nanotube type, with the presence of the inner wall having little effect on the separation. The authors suggest that the mechanism is similar to that observed previously for SWCNT separation, where SDS is sensitive to electronic character and diameter.[60,61,152] Metallic nanotubes, which are known to have a stronger interaction with SDS compared to semiconducting nanotubes,[175] become more fully wrapped and experience limited interaction with the gel as they traverse the column. Thus, they elute first, followed by large- and small-diameter semiconducting nanotubes. **Figure 12**a shows the elution profile of DWCNTs, large-diameter AD SWCNTs and small-diameter HiPco SWCNTs. An excellent agreement between elution times is observed for metallic (Band 2) and semiconducting (Band 3) fractions of DWCNTs and AD SWCNTs, as well as between HiPco SWCNTs and SWCNTs within the DW sample. Absorption spectra of the enriched m- and s- DWCNT fractions are shown in Figure 12b,c, demonstrating clear enhancement of the M_{11} (600–800 nm) and S_{22}

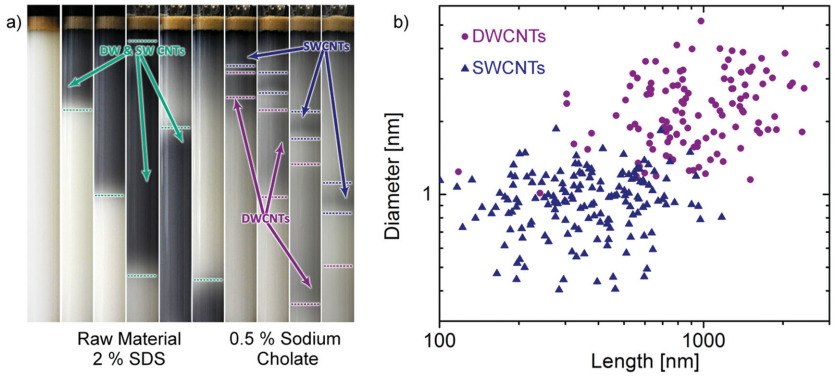

Figure 11. Separation of DWCNTs by gel permeation. a) Time-lapse photography (1 h) showing the introduction of raw, unsorted DWCNT material to the S-200 gel column for the separation of SWCNTs from DWCNTs and b) diameter vs length of SWCNTs and DWCNTs, as determined by AFM. Reproduced with permission.[36] Copyright 2013, American Chemical Society.

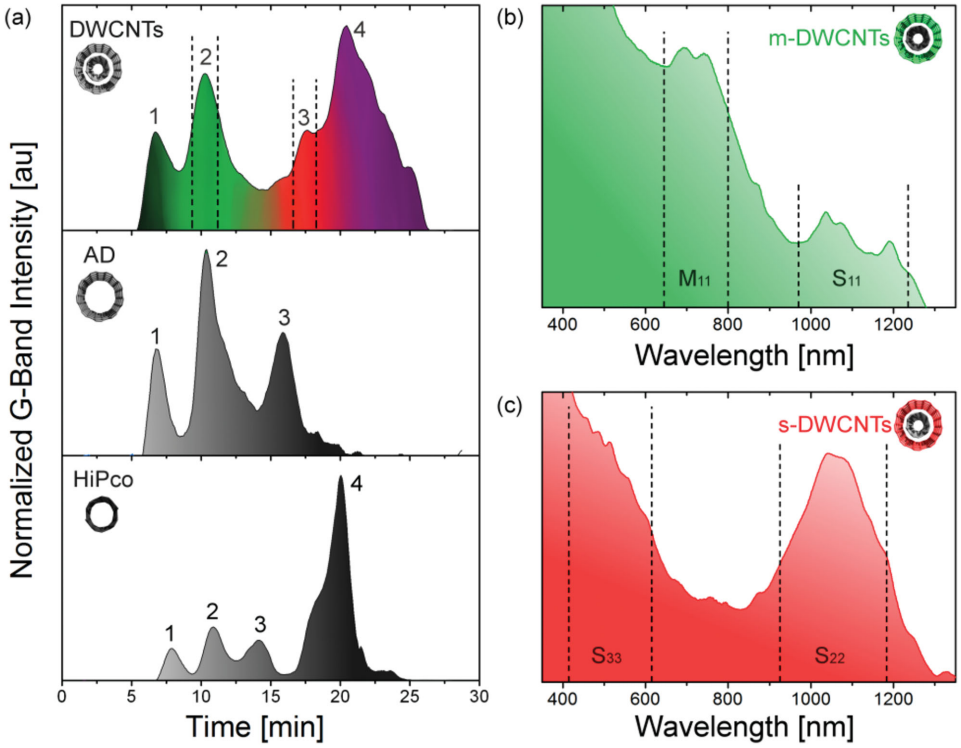

Figure 12. The co-surfactant separation of DWCNTs via gel permeation. a) Elution profiles of the normalized G-Band Raman mode intensity for DWCNTs, AD SWCNTs and HiPco SWCNTs. The dashed lines in the DWCNT elution profile highlight Band 2 and Band 3, which, from the absorption spectra seen in (b) and (c), correspond to DWCNTs with metallic and semiconducting outer walls. Regions of S_{ii} and M_{ii} transitions are highlighted in each spectrum. Reproduced with permission.[37] Copyright 2015, American Chemical Society.

(900–1200 nm) transitions with calculated purities of ca. 70% and ca. 90%, respectively.

5.9. Polymer Wrapping

The dispersion and separation of SWCNTs with aromatic polymers in organic solvents is receiving ever-increasing attention in the research community due to the ability of polymer wrapping to prepare suspensions with a highly pure semiconducting content (>99%).[184–186] In this one-pot approach, raw carbon nanotube material is typically dispersed by ultrasonication in the presence of a chosen polymer followed by ultracentrifugation. Consequently, only those nanotubes with a preferential interaction with the polymer and those that have become individualized during ultrasonication remain suspended in the organic solvent. In pioneering works by Nish et al.,[147] Chen et al.,[148] and Hwang et al.,[132] organic polymers with the fluorene structure as part of their repeat unit were used, such as poly(9,9-dioctylfluorene-2,7-diyl) (PFO), poly[9,9-dihexylfluorenyl-2,7-diyl)-*co*-(9,10-anthracene)] (PFH-A) and poly[(9,9-dioctylfluorenyl-2,7-diyl)-*co*-1,4-benzo-[2,1'-3]-thiadiazole)] (PFO-BT). After almost 10 years of development, the polymer library has grown dramatically to now include polythiophenes, polycarbazoles, and copolymers thereof,[39,187–192] alongside research to develop new polymers via click chemistry in an effort to avoid the strict synthetic conditions associated with Suzuki polycondensation or Yamamoto coupling.[193] Using the currently available polymer library, mixtures of semiconducting SWCNTs through to near-monochiral and monochiral suspensions and most recently even optical isomers thereof[194] have been demonstrated. For example, poly(9,9-dialkyl-2,7-fluorene) has been shown to be sensitive to large chiral angles (close to armchair: $\theta \geq 25°$)[132,148,195] and poly(*N*-decyl-2,7-carbazole) to lower chiral angles (typically $10° \leq \theta \leq 20°$).[191]

Despite the wide-spread application of polymer wrapping, the exact mechanism responsible for separation remains poorly understood and is the subject of current discussion.[185,186,193,196] Nevertheless, it is commonly agreed upon that the polymer interacts by aligning its aromatic backbone along the surface of a carbon nanotube so as to maximize π–π stacking.[38,39,185,188,190] Peripheral groups are then believed to branch away from the nanotube into the solvent and facilitate solubility.[186,196] Berton et al.[187] have developed a hybrid coarse-grain model to describe this interaction by treating the nanotube and polymer as geometrical objects and assuming maximal (attractive) π–π interactions can be reached by maximizing the contact area. In this way, a set of solutions for which the polymer lies flat on the surface of the nanotube were calculated as shown in **Figure 13** for poly(fluorene-*alt*-pyridine) around a 1.2 nm-diameter SWCNT. Intuitively, and also in agreement with Berton's model, the number of favorable wrapping solutions increase with diameter, which may explain why certain polymers are highly (*n*,*m*) specific in the small-diameter regime (i.e., due to other species having limited possible wrapping solutions).

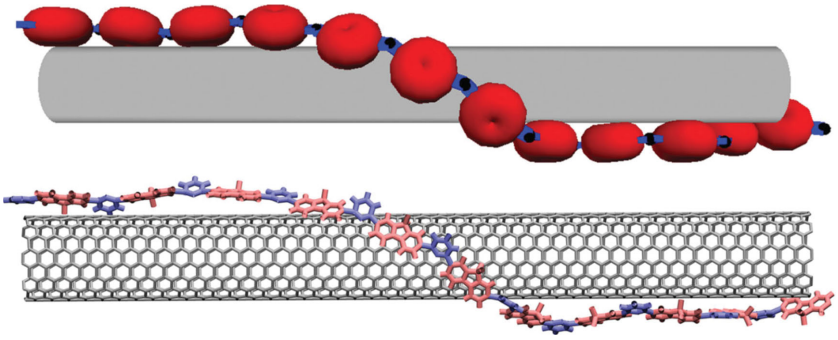

Figure 13. One of the geometric solutions for poly(fluorene-*alt*-pyridine) wrapped around a 1.2 nm-diameter SWCNT and the corresponding molecular model. Alkyl chains are simplified as methyl groups. The red discs and black dots represent the fluorene and pyridine moieties, and these two objects are connected by sticks whose lengths reflect the bonds between the fluorene moiety and the center of the pyridine ring. Adapted with permission.[187] Copyright 2014, Wiley-VCH.

The observed high selectivity of polymer systems to semiconducting SWCNTs is much less understood and experimental evidence suggests that it is dependent upon a number of factors, such as polymer concentration,[186] ultrasonication temperature,[185] and solvent choice.[132,147,185,196] Changes in any one of these parameters have been shown to influence not only the concentration of metallic SWCNTs in solution but also the polydispersity of the semiconducting species. For example Shea et al.[186] showed that for high starting concentrations of PFO in toluene (5 mg mL^{-1}) the polydispersity of s-SWCNT (*n*,*m*) species increased from 5 to 8 and m-SWCNTs became visible in optical absorption measurements. Conversely, at polymer concentrations below 1 mg mL^{-1}, no m-SWCNTs were suspended. As stated by the authors, the increased polydispersity and metallic content is likely to be a result of high PFO concentrations suspending not only individualized SWCNTs but also polydisperse bundles. Likewise, Han et al.[185] dispersed carbon nanotubes with PFO in cyclohexane at increasing temperature (5–55 °C) and found that increased ultrasonication temperature led to an overall higher concentration of s- and m- SWCNTs.

However, it is the choice of solvent that has captured the attention of many in the research community,[132,147,185,196] as it has dramatic effects on the semiconducting purity. As outlined by Wang et al.,[196] upon selecting a solvent, several rules are typically adhered to; namely, the solvent must solubilize the polymer, the SWCNTs must have a low intrinsic solubility in the solvent so that only polymer-wrapped nanotubes are dispersed, and the solvent must have a lower density than the SWCNTs so that the unwrapped SWCNT will sediment after centrifugation. Additionally, Wang et al.[196] go further to state that nonpolar solvents are necessary to prevent solvent interactions with polarized polymer-wrapped m-SWCNTs and allow for better selective sorting of s-SWCNTs. As an example, the use of conjugated polymers in polar solvents such as THF, typically have a higher dispersive yield (i.e., a higher final suspended mass of CNTs) but suspend both m- and s- SWCNT, whereas nonpolar solvents such as toluene, o-xylene, and m-xylene, whilst having a lower dispersive yield, have been shown to afford semiconducting purities of >99%.[184–186]

In the past, research efforts focused mainly on the dispersion of small-diameter (0.8–1.2 nm) carbon nanotubes from the CoMoCat or HiPco processes, and selectivity was shown to be poor for larger diameters.[38,187,197] As the research community now turns to larger-diameter nanotubes due to their potential application in telecommunications[198] and FETs,[199] new polymer systems are also beginning to appear in the literature. Initially it was believed that the poor selectivity to large diameters could be ascribed to the nature of the polymer backbone; however, recent studies point to side chains as playing an important role.[38,192,197,200] Gomulya and co-workers[38,39] investigated the effect of using polyfluorene derivatives with different-length alkyl side chains from C_6H_{13} up to $C_{18}H_{37}$, and found that an alkyl chain length of 8 carbons favored dispersion of diameters of 0.8–1.2 nm, whereas longer alkyls with 12–15 carbons can efficiently interact with nanotubes with diameters up to 1.5 nm. Unfortunately, in spite of improved sensitivity to large diameters, the longer alkyl chains also had the effect of increasing the interaction strength with the nanotubes, and thereby decreased the selectivity. In other work, Berton et al.[188] reported the dispersion of 1.3 nm-diameter SWCNTs using poly(9,9-didodecylfluorene-2,7-diyl-*alt*-anthracene-1,5-diyl); Tange et al.[201] dispersed 1.3 to 1.4 nm diameters with poly(9,9-dioctylfluorene-*alt*-benzothiadiazole) (F8BT), and Wang et al.[197] dispersed AD carbon nanotubes with poly(dithiafulvalene-fluorene-*co*-*m*-thiophene). To date, polymer wrapping has yet to be applied to DWCNTs, but, considering that the outer wall of a DWCNT has a diameter of greater than ca. 1.5 nm, these newly developed polymers look highly promising for the future of DWCNT processing. However, as several researchers point out, the polymer wrapping of a carbon nanotube is also associated with a charge transfer,[190,196,197] and what effect the presence of an electronically coupled inner wall may have on the sorting efficiency remains to be seen.

5.10. Aqueous Two-Phase Extraction

Another separation method that looks promising for the separation of DWCNTs is an adaptation of standard liquid-phase separation, recently applied to the separation of carbon nanotubes by Zheng and co-workers.[40] In this first report, SC-dispersed nanotubes (and an appropriate amount of SDS) were added to a mixture of two water-soluble polymers; polyethylene glycol (PEG) and dextran. Spontaneous and robust separation of the polymer phases occurred with the more-hydrophobic PEG-rich phase on top and the more-hydrophilic dextran-rich phase on the bottom. The nanotubes quickly and spontaneously separated into the two polymer phases with thermodynamic analysis revealing two distinct regimes. First, in the small-diameter regime (0.6–1.0 nm), curvature dominates the solvation free energy with smaller-diameter nanotubes such as (6,4) in the more-hydrophilic dextran-rich phase, and larger-diameter

Table 1. Comparison of the advantages and disadvantages of all current DWCNT-sorting methods with a focus toward commercial application.

Technique	Advantages	Disadvantages
Reversible covalent chemistry	✓ Diameter selective	× Cannot distinguish between number of walls
	✓ Easily scalable	× Currently insensitive to electronic character
	✓ Pristine structure can be recovered	× Multiple steps; time consuming
	✓ Scalable	
Biofunctionalization	✓ Diameter selective	× Cannot distinguish between SWCNTs/MWCNTs and DWCNTs
	✓ Easily scalable	× Not sensitive to electronic character
Molecular nanocalipers	✓ Diameter selective	× Requires complex chemical engineering to make hosts
	✓ Sensitive to handedness	× Requires expensive reagents
	✓ Pristine nanotubes can be recovered	× Limited evidence of electronic sensitivity
	✓ Host can be reused	
DGU	✓ Diameter selective	× Requires expensive ultracentrifuge
	✓ Sensitive to electronic character	× Requires expensive density gradient medium
	✓ Can distinguish between number of walls	× Requires technical expertise to make intricate density gradients
		× Multiple steps; time consuming
Centrifugal separation	✓ Length selective	× Requires pre-sorted DWCNT material
		× Limited evidence of electronic sensitivity
		× Requires expensive density gradient medium
Gel Permeation	✓ Diameter selective	× Requires expensive gel
	✓ Sensitive to electronic character	
Polymer wrapping	✓ Diameter selective	× Requires centrifuge
	✓ Sensitive to electronic character	× Requires expensive polymers
	✓ Scalable	
Aqueous two-phase extraction	✓ Diameter selective	× Diameter selectivity currently limited to small diameter regime < 1.2 nm
	✓ Sensitive to electronic character	
	✓ Easily scalable	
	✓ Inexpensive, readily available reagents	
	✓ True "one-pot" method	

nanotubes such as (7,5) and (8,4) in the more-hydrophobic PEG-rich phase. The second, larger-diameter regime (1.2–1.5 nm), is governed by the degree of nanotube polarizability, and a clean metallic/semiconductor separation can be achieved, with metallic nanotubes found in the more-hydrophilic dextran-rich phase and semiconducting nanotubes in the more-hydrophobic PEG-rich phase.[40] Investigation by Subbaiyan et al. determined that aqueous two-phase separation was driven by the hydrophobicity of the surfactant composition on the nanotube surface rather than the inherent hydrophobicity of the nanotube itself,[41] therefore allowing the surfactant identity and ratio to be tuned to target specific chiralities in a similar manner to gel permeation and DGU. By doing so, it is possible to enrich (6,5), (6,4)/(7,3) and (7,5) species. Since then, several advances have been made through variation of the surfactant concentration[202] and the type of polymer,[203] addition of salts[202] or DNA,[203] and the use of countercurrent chromatography.[204] Single-chirality nanotube suspensions can now be prepared for a number of species, and the use of countercurrent chromatography enables total fractionation with a recovery close to 90% of the starting material.[204] While this rapidly developing technique has made extraordinary advances for small-diameter (<1.2 nm) SWCNTs through elegant refinement, what is of most interest from the DWCNT perspective is the elementary separation of large-diameter nanotubes according to polarizability.[40] The ease with which clean metallic/semiconducting separation can be scaled up (Zheng and co-workers demonstrated separation on the liter scale) provides an obvious opportunity for DWCNT sorting and will most likely be capitalized upon in the near future.[40]

5.11. Analysis and Future Directions

While each of the previously discussed processing techniques led to enrichment of DWCNT material in some respect, each have their advantages and disadvantages, as summarized in **Table 1**. Some are inherent to the techniques themselves and others are simply a result of the current stage of development of the techniques, or of their application to DWCNTs.

As in the case of SWCNTs, an appropriate sorting method should be selected in accordance with the desired application. For instance, applications requiring DWCNTs to be free of SWCNT or MWCNT contaminants may find a number of techniques suitable, and the decision may ultimately depend on the availability of equipment, the cost, and the complexity. Where high-purity DWCNT enrichment is required, DGU and gel permeation may be more appropriate. However, both require specialist equipment and technical expertise, though gel permeation may be a more appropriate technique for those without an ultracentrifuge. While the purities achieved for DGU are currently higher than that achieved for gel permeation, future research may see the gel method further optimized, as has been demonstrated for SWCNTs.[59–61,151,179] Looking forward, it is inevitable that polymer wrapping and aqueous two-phase extraction will be successfully applied to DWCNTs; however, DGU is so far the only technique capable of distinguishing intrinsic differences between DWCNTs and SWCNTs, which are otherwise identical, except for the presence of the inner wall (with the added advantage of also offering sensitivity to electronic character).

Owing to the progress in DWCNT sorting, particularly for metallic/semiconducting separation, the sorted material can now be used to shed light on the intriguing properties of DWCNTs. For instance, Weisman and co-workers took DGU-purified fractions of DWCNTs to determine whether or not the inner walls of DWCNTs fluoresce.[205] Up until that point, there had been many reports of PL from the inner walls of DWCNTs.[160,206] However, considerable uncertainly surrounded the work due to the possibility of emission from SWCNT contamination.[205] High-resolution TEM was used to definitively characterize fractions of DWCNTs and SWCNTs, and to help identify the source of emission in each PL measurement. The results revealed that whilst PL was measurable from small- and **large-diameter** SWCNTs, it was not observed for fractions containing DWCNTs (10 000 times lower than for SWCNTs of similar diameter). The authors therefore suggest that, in previous reports, it was residual SWCNTs trapped within bundles or exposed inner walls, released during extensive chemical or physical treatment, that were responsible for the observed PL.

A similar investigation conducted by Yang et al. also used sorted, high-purity DWCNTs for PL measurements.[207] In that work, the authors showed that both sides of the debate are correct; the inner walls of DWCNTs do fluoresce for a narrow range of diameters (at a significantly reduced intensity than SWCNTs), but for all other diameters, complete quenching occurs. This was shown through extensive optical analyses that revealed that the only inner walls to exhibit PL were (9,4), (9,5), (8,6), (10,3), (7,6), and (10,2). The (9,4) nanotube showed significantly higher intensity than the other chiralities, but despite the DWCNTs being present in higher concentration, this intensity was still much less than that of the SWCNT sample, clearly indicating PL quenching of DWCNTs. The chiralities that were photoluminescent were found to share similar diameters with an average of ca. 0.929 nm, and they all had relatively large chiral angles. As a diameter of 0.930 nm is predicted to have the highest possible PL intensity,[5] this work suggests that only those with the highest theoretical PL intensity could overcome the quenching effect from the outer walls.

While these examples clearly demonstrate the benefits of an enriched DWCNT material, the ultimate goal in DWCNT processing is to obtain material sorted by inner wall character on a large scale, as this would unlock the potential of DWCNTs to be used in devices in ways that SWCNTs and MWCNTs cannot be. For example inner wall sorting would allow for large-scale fabrication of S@S FETs with on/off ratios of 10^8 or higher, or even the formation of M@M FETs, an idea contrary to our fundamental knowledge of modern electronics because their electrical resistance is insensitive to gate voltage,[10,208] but which has been nevertheless been proposed based on the results of theoretical calculations.[209] The motivation behind such a study is that we are rapidly approaching the limit for the improvement of Si-based electronics, with all-metallic DWCNT FETs offering the ability to be scaled down to make smaller-sized structures with less energy consumption and improved performance at higher frequencies.[210] An alternative is to use telescoping DWCNTs, where the interaction between the inner and outer wall in the overlapped region plays a crucial role in the electrical transport properties. By using computational methods for a (5,5)@(10,10) DWCNTs, it is predicted that the sensitivity of all-metallic DWCNTs to gate voltage can be tuned by varying the amount of overlap between the inner and outer wall.[209] Furthermore, it has been determined that, through optimization of this overlap, on/off current ratios as high as 10^4 could be achieved, which approaches that of many semiconducting nanotube devices (typically ca. 10^6).[211,212] Clearly, the ability to further sort DWCNTs according to inner wall electronic character would allow for the fabrication of electronic devices, not to mention many other applications outlined in the next section, that are currently not possible.

In this respect, even DGU so far provides no specificity because, for any given diameter, the buoyant density of the nanotubes has no dependence on electronic character, although differences in polarizability due to electronic character do have an influence on surfactant encapsulation, which indirectly affects the buoyant density. It has thus been suggested that sorting by inner wall character could be achieved by DGU by exploiting such minute differences in surfactant encapsulation, coupled with shallower density gradients and longer centrifugation time.[35] However, inner wall sorting by DGU remains elusive, confirming that the task is not at all trivial. In theory, it is possible that other techniques that are sensitive to the polarizability of the nanotubes, such as polymer, DNA, and co-surfactant wrapping, could be developed to a level of refinement whereby the subtle differences in polarizability arising from the character of the inner wall can be exploited to provide the desired separation. A careful evaluation of the magnitude of such differences in polarizability, arising due to the character of the inner wall, compared to the magnitude of the differences that arise due to the character of the outer wall and to the binding energy of the wrapping agent would be helpful in this regard. The perfect technique would be capable of sorting DWCNTs not just by inner wall electronic character, but by inner wall chirality. It is a somewhat remote possibility that one of the wrapping techniques could be refined to the necessary degree of sensitivity, especially considering the recent reports of sorting by outer wall stereoisomerism using polymers, but this would depend on subtle factors such as the orientation

of the inner wall with respect to the outer wall. A more direct approach would be to use field effects to target specific chiralities. In this way, it could be possible to significantly alter the polarizability by, for example, irradiating the sample with light tuned to the S_{11} transition of an inner semiconducting nanotube. In conjunction with any of the techniques that are sensitive to polarizability, this could prove a powerful tool if the obvious practical challenges can be surmounted.

6. Devices and Applications

As processing techniques improve, DWCNTs are being employed in an increasing variety of devices and applications in which theory predicts they will offer benefits. These include FETs, which provide opportunities to investigate the intriguing effects of inter-wall coupling, and in various sensor and electronics applications. Such devices further demonstrate the need for DWCNT-sorting techniques, where DWCNTs of a specific type would provide ease of characterization and the ability to precisely tailor the electronic character for a specific function.

In many electronic applications it is desirable to use semiconducting nanotube species. While outer wall sorting greatly removes a large portion of metallic species, there are still come contaminant metallic inner walls present, which can result in electrical shorting. In such an instance, electrical breakdown can be used to remove any residual metallic species from a device in which nanotubes are integrated. The technique was first demonstrated by Collins et al., where application of a high bias voltage to an individual MWCNT resulted in wall-by-wall destruction.[154] The current distribution through a MWCNT favors the outermost wall, owing to its direct contact with the external electrode. Thus, upon application of a constant voltage across the nanotube, most of the current is carried through the outermost wall until enough power has been dissipated to induce Joule heating, resulting in the destruction of the individual nanotube. In the absence of significant defects or buckling, breaking normally occurs at the center[212] of the nanotube where the temperature is at a maximum,[213] resulting in a physical "cut" of the nanotube. The use of electrically induced breakdown for SWCNTs, enabling breakdown solely of the metallic elements, was also demonstrated.[154] This selectivity toward metallic nanotubes arises from the fact that gateable semiconducting nanotubes can be depleted of carriers so that the current is carried solely by the (non-gateable) metallic nanotube until enough power has been dissipated by them to cause significant heating and hence breakdown. Current-induced breakdown has since been used extensively for the removal of metallic nanotubes from FETs[214,215] and can produce highly purified networks of s-SWCNTs.[215]

Preserving all semiconducting walls is a much more difficult challenge for DWCNTs. In the case of DWCNTs, the situation is complicated by the possibility of either the inner or outer wall to be metallic, or both walls, or even special cases where two semiconducting walls become overall metallic in nature.[17,42] Thermal cross-talk between metallic and semiconducting walls is unavoidable, and heating of the metallic wall may lead to destruction of the semiconducting wall.[63] Hence, it is hard to design an experiment to selectively remove only metallic walls from an integrated film of mixed-wall DWCNTs. As an example, Wang and co-workers[63] deposited a film of semiconducting outer wall DWCNTs (purified using the DGU technique[35]) between two gold contacts, as shown in **Figure 14**b. Despite having 96% semiconducting outer wall purity, the presence of a small number of metallic outer walls and also metallic inner walls was evidenced in the transconductance measurements by a moderate on/off ratio of ca. 500 and on-state current of –700 nA. Electrical breakdown was performed by applying a source–drain bias of –100 V in cycles of 28 s, and three distinct regimes were identified with respect to the electronic properties of the devices. This process was followed by in situ monitoring of the off-state current during electrical breakdown as shown in Figure 14a. The first regime, after 1 cycle, corresponds to the removal of amorphous carbon and metallic percolation pathways, resulting in a 2-fold increase in on-state current (to –1.2 μA) and 4-fold increase in on/off current ratio (to 2×10^3). It is well known that the continued flow of current can result in annealing of carbon nanotubes, which may have also contributed to the observed improvement in on-state current.[216]

The second regime, consisting of two cycles, corresponds to the destruction of metallic nanotubes, and results in a decrease in both on- (–800 nA) and off-state current, with a significant increase in the on/off ratio (to 4.1×10^5). During the third regime, after a total of four cycles, no significant changes in the off-state current were seen, indicating the majority of metallic nanotubes have been removed. At this point the on-state current is reduced (–300 nA) due to destruction of some semiconducting pathways as a result of thermal cross-talk; however, the on/off ratio remains high at 1.4×10^4. Figure 14c shows a highlighted portion of the second regime wherein a stepwise decrease in the off-state current is observed, with each step corresponding to the destruction of a metallic pathway. Raman analysis was subsequently used in conjunction with diazonium chemistry to confirm that only DWCNTs with inner and outer semiconducting nanotubes were immune to electrical breakdown; however, whether the broken metallic outer walls remain around the semiconducting inner walls is not addressed.

In the case of few- or single-nanotube devices, more-controlled experiments are possible, and electrical breakdown has been used to selectively remove outer wall metallic nanotubes from DWCNTs. For example, Liu et al. demonstrated that the metallic outer wall of a (28,24)@(45,15) DWCNT can be "broken" by a high current.[10] While the device exhibited metallic behavior prior to electrical breakdown, afterwards, it became semiconducting with a low on/off current ratio of 20 – an order of magnitude lower that that observed for pure semiconducting SWCNTs of similar diameter. This suggests that the rest of the broken metallic outer wall remains in place, confounding the effect of the gate on the inner wall.[217] Wang et al. also demonstrated electrical breakdown of single-DWCNT devices, wherein the metallic inner wall of a M@S DWCNT was broken, significantly improving the on/off ratio.[217] Although such an approach essentially results in an SWCNT device, conflicting reports make it unclear if current-induced electrical breakdown leads to complete removal of the outer wall[154] or if the DWCNT remains mostly intact with only a small break in the outer wall.[217] The latter case would be of some interest to the carbon nanotube transistor community, as it could represent

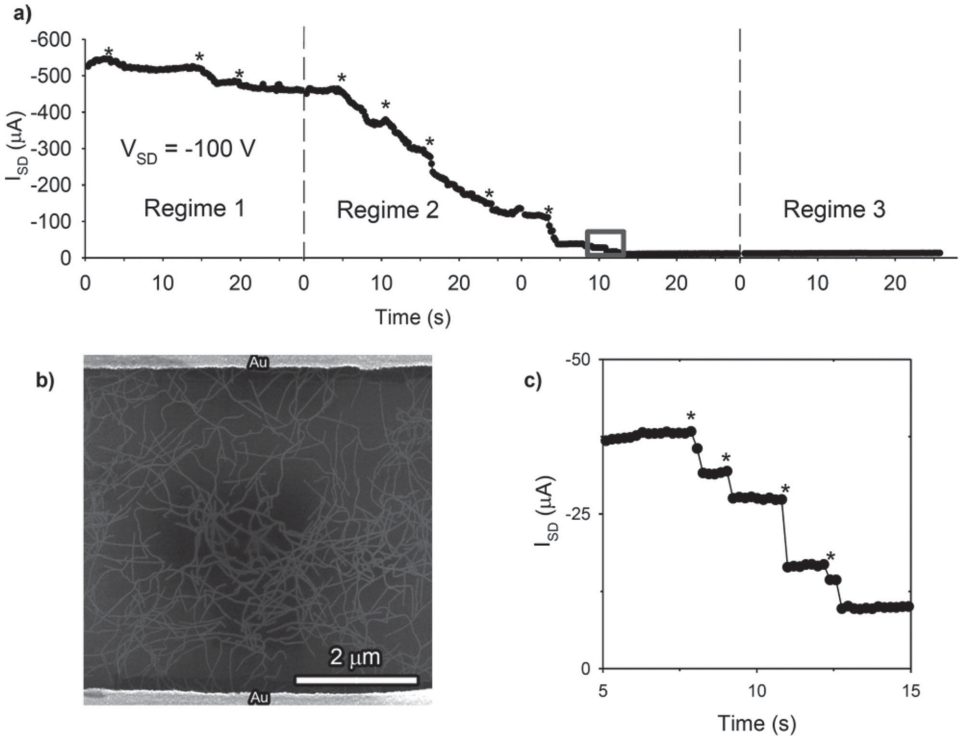

Figure 14. Enrichment of semiconducting DWCNTs by electrical breakdown of metallic percolation pathways. a) In situ current vs time measurement during electrical breakdown at a fixed source–drain bias (V_{SD} = –100 V) for the three regimes. Electrical breakdown events are characterized by sharp decreases in source–drain current (marked by the asterisks). b) Percolated DWCNT networks characterized by SEM before electrical breakdown. c) Enlargement of the boxed region in (a). Reproduced with permission.[63] Copyright 2014, Wiley-VCH.

a convenient method to provide a degree of shielding of an SWCNT from its surrounding environment.

In the work of Liu et al.,[10] DWCNTs were grown directly into an FET with narrow microfabricated slits for TEM analysis. This structure allowed the chirality of the inner and outer walls to be determined via electron diffraction and then directly correlated to in situ transconductance measurements. Although the inner@outer-wall combination was not controlled during growth, each of the four different types of DWCNTs could be located, and this allowed for comparison with theoretical calculations. As expected, the M@M (34,13)@(48,6) and S@M (19, 12)@(22,19) DWCNTs were found to be metallic in nature and showed no current modulation with varied gate voltages. However, the M@S and S@S DWCNTs were found to exhibit semiconducting character, albeit with very different on/off ratios. For the M@S (33,6)@(30,23) DWCNT, the on/off ratio was on the order of ca. 20. This is in stark contrast to the S@S (23,13)@(38,6) DWCNT with an on/off current ratio of ca. 10^4. Although metallic behavior was not observed for an S@S DWCNT in that study, Wang and co-workers[7] explain that this is still in accordance with the DFT predictions discussed previously in Section 2,[17,42] since the study employed large-diameter, incommensurate DWCNTs.

Similarly, Moore et al. characterized individual DWCNT FETs; however, in that case nanotube material of defined outer wall electronic type was used.[37] In that work, DWCNTs were gel-sorted by metallic or semiconducting outer wall and deposited onto lithographically-defined FET devices via dielectrophoretic deposition. Transconductance measurements revealed two sub-populations of behavior within each respective DWCNT outer wall type, which are shown in **Figure 15**. The first case corresponds to an M@M DWCNT with an on/off current ratio of unity at a source–drain voltage (V_{SD}) of 1 V, and no current modulation was observed with varying gate voltage. The second case, corresponding to S@M DWCNTs, exhibited an on/off ratio close to unity; however, a slight modulation with gate voltage was observed, revealing a semiconducting inner wall and differentiating it from the M@M case. The third case corresponds to S@S DWCNTs where typical p-type behavior was observed together with an on/off ratio of ca. 10^8. As the inter-wall distance is relatively low (0.380 ± 0.009 nm), the authors concluded that the behavior observed was from incommensurate DWCNTs. The last case corresponds to the M@S DWCNTs with a slight modulation observed and an on/off ratio of 1.4.

Bouilly et al. integrated DWCNTs of unknown chirality into FETs and used chemical functionalization to indirectly identify the four different DWCNT combinations.[218] This was done by assembling individual DWCNT FET devices (referred to as "pristine state") and covalently functionalizing them using an outer-wall-selective, reversible aryldiazonium reaction (then referred to as "functionalized state"). This introduced phenyl groups onto the outer wall carbon lattice which inhibited current flow due to an increase in backscattering from defect-induced quasibound states.[219] The devices were then annealed at 500 °C, removing the phenyl groups and returning

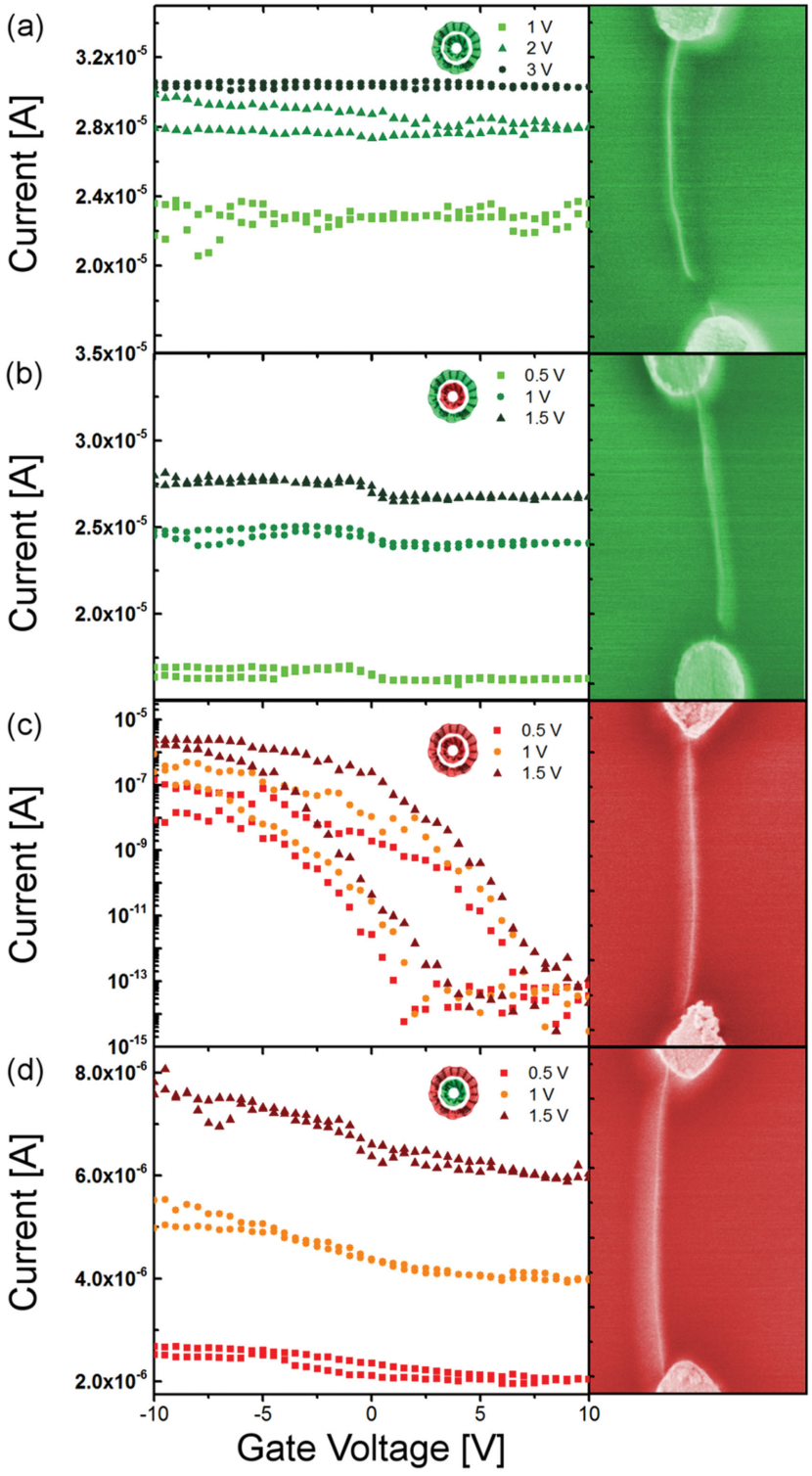

Figure 15. FETs comprising individual, electronically defined DWCNTs. Transconductance measurements at various source–drain voltages and corresponding false-color SEM images are shown and correspond to the four possible types of DWCNT FET: a) M@M, b) S@M, c) S@S, and d) M@S. Adapted with permission.[37] Copyright 2015, American Chemical Society.

the DWCNTs to their original ("defunctionalized") state. Transconductance measurements were made on DWCNTs in the pristine, functionalized, and defunctionalized states and they observed three distinct behaviors for the four inner@outer-wall combinations as shown in **Figure 16**.

The first was attributed to S@S DWCNTs, which, once again, were found not to be metallic, in contrast with the apparent predictions.[17,42] Indeed, this highlights the relative unlikelihood of inadvertently coming across an S@S DWCNT in the laboratory situation, which just happens to fit the strict requirements used in theoretical calculations, such that metallic behavior is observed. S@S DWCNTs were found to have an on/off ratio of ca. 10^4 in the pristine state, which remained high following functionalization. Consequently, the inner wall must also be semiconducting. The second behavior was attributed to S@M DWCNTs because an on/off ratio of ca. 10^2 was seen in the functionalized state, but in the pristine or defunctionalized states it was reduced to less than one order of magnitude. The authors attribute this lack of modulation in the pristine state to shorting of the device by the metallic outer wall. The third and last behavior was that attributable to either the M@S or M@M DWCNTs, in which no current modulation was observed in any of the pristine, functionalized or defunctionalized states. Owing to the constant current flowing through the metallic inner wall, the identity of the outer wall as being either metallic or semiconducting could not be determined.

The application of electronically defined DWCNTs in sensors for the detection of NH_3 was reported by Wang and co-workers.[220] In that work, DWCNTs with semiconducting outer walls[35] were first incorporated into thin-film FETs and then covalently functionalized using diazonium chemistry, resulting in the introduction of –COOH groups onto the outer wall. Upon exposure to NH_3, a change in transconductance behavior occurs and concentrations as low as 60×10^{-9} M (ca. 1 ppb) could be detected. Furthermore, the device exhibited 6000-times-higher sensitivity to amine-containing analytes (NH_3 and NH_2PhNH_2), compared with other small molecules. While this demonstrates a high sensitivity and selectivity, significant advances could stem from control over the inner wall. The high on-state current and on/off ratio of semiconducting nanotubes provide optimum performance in FETs and, coupled with the improved sensitivity of semiconducting nanotubes toward chemical or electrochemical changes in their environment,[221] this means that S@S DWCNTs would presumably provide both significantly higher on/off ratios and greatly improved sensitivity.[220]

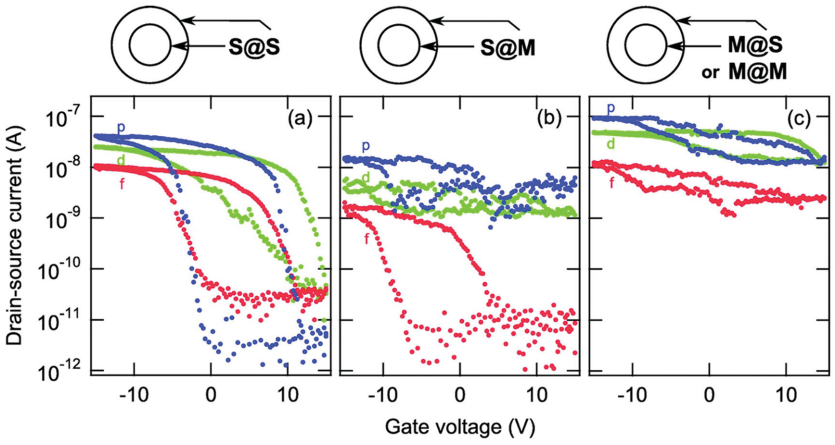

Figure 16. Transconductance measurements of individual DWCNT devices in the pristine (p – blue), functionalized (f – red), and defunctionalized (d – green) states as a function of gate voltage. The source-drain voltage is 10 mV. Three electrical signatures are distinguishable and assigned to the following electrical combinations: a) S@S, b) S@M, and c) M@S/M@M. Reproduced with permission.[218] Copyright 2011, American Chemical Society.

There is a variety of work directed to the implementation of DWCNTs in bioapplications (such as biosensors, drug carriers, or biocatalysts). An example is that conducted by Jung et al., who produced water-soluble, biologically and optically active protein-coated DWCNTs.[222] By employing a protein (specifically the mussel protein 3,4-dihydroxy-L-phenylalanin) as a biofunctionalization and individualization agent, the inherent insolubility in water and the low degree of biocompatibility of the DWCNTs was overcome. DWCNTs offer the most-appropriate material in such an instance because attachment of the protein requires covalent functionalization, which would render SWCNTs optically inactive.[223] Heavy covalent functionalization with carboxyl moieties, followed by attachment of the mussel protein through peptide bonds and subsequent ultracentrifugation yielded a uniform, transparent, protein-coated-DWCNT suspension. PL was used to characterize the suspension, and the authors concluded that several nanotube walls remained optically active, namely (6,4), (9,1), (8,3), (6,5), and (7,5), which the authors attribute to the inner walls. This is not in agreement with the work discussed previously by Yang et al.,[207] who determined that very few inner walls exhibit fluorescence, due to quenching. Jung et al. argue that the strongly oxidizing treatment of hydrogen peroxide would render the SWCNTs (which the authors estimate make up 5% of the pristine material) optically inactive; therefore, the PL could only originate from the inner walls.[222] Notwithstanding contemporary issues regarding the origin of the observed photoluminescence, it was determined that the protein-coated DWCNTs, when cast into thin films, remained conducting with an electrical conductivity of 5.31×10^3 S cm^{-1}.[222] Thus, protein coating may prove to be an effective means to realize the potential of DWCNTs in bioapplications because it can preserve the optical and Raman activity of the inner walls as well as the electronic functionality, providing two potential strategies for signaling.

The extra range of optical absorption provided by the inner wall of S@S DWCNTs could also be advantageous in respect to nanotube-based solar cells. Detailed modelling of the absorption properties of the first 70 semiconducting walls, spanning almost the entire useful region of the terrestrial solar spectrum, concluded that high-efficiency solar cells could only be obtained by using more than one type of nanotube absorber.[224] DWCNTs could thus provide the equivalent absorption range of a two-junction tandem nanotube solar cell in one single junction device. In several cases, DWCNTs have also been shown to be superior to their single- or multi-walled counterparts as transparent, conducting electrode materials in a variety of other photovoltaic architectures, including dye-sensitized[225] and carbon nanotube–silicon solar cells.[226]

The use of DWCNTs as electrochemical nanopores and nanochannels is currently being investigated, wherein they can mimic natural protein channels embedded within a biological system.[227] In this instance, nanotubes are incorporated into an epoxy membrane, resulting in a porous structure. By covalently functionalizing the protruding nanotube ends with chemical moieties, "gate molecules" capable of changing their physical orientation in response to external signals such as voltage, temperature, or light, can then be tethered to the nanotube, creating a gateable pore opening. Upon application of appropriate external stimuli, the gate molecules change their orientation, thus opening or closing the gate, and enabling or preventing ions and/or molecules to pass through the membrane. DWCNTs are an advantageous material for such a purpose because the smooth graphitic interior of the nanotubes provides faster fluid velocities than conventional membranes,[228] and because they provide adequate pore sizes and the outer wall enables a high density of functional groups at the nanotube ends. Zhan et al. recently used a one-step electro-oxidation process to attach an anodic dye (which acts as the gate molecule) to DWCNT/epoxy membranes.[227] The negative charge on the dye allows switching between an open and closed state through application of an external bias. When a negative bias is applied across the membrane, the anodic dye molecules are repelled away from the nanotube entrance and the pore is open. In this state, potassium ions are able to flow through the opening resulting in a measurable current. Conversely, when a positive bias is applied, the anionic dye molecules are dragged into the pore entrance, blocking or greatly reducing the flow of ionic current. While rectification of smaller molecules such as KCl was not observed due to the relatively large pore size (ca. 2 nm), a number of larger molecules, such as ferricyanide and sodium benzenesulphonate, were able to be rectified.

Field emission is another application where the properties of DWCNTs could be advantageous. In general, the geometry and chemical properties of nanotubes are ideal for field emission and owing to their low threshold voltage (the minimum gate-to-source voltage required to induce conduction between the source and the drain) and long lifetimes,[229] they could provide superior performance in applications such as field-emission displays[230] and miniature X-ray sources.[231] The high

aspect ratios of the SWCNTs creates excellent point sources of field emission; however, molecules such as O_2 and H_2O affect the structure of the tip, leading to fluctuations in current[232] and the nanotubes are readily degraded at high emission currents.[233] MWCNTs offer increased stability; however, their smaller aspect ratios result in reduced emission performance compared with SWCNTs.[232] DWCNTs are an effective compromise, offering comparably high aspect ratios to SWCNTs with the added stability of an extra wall.[232,234] As such, there have been many reports on DWCNTs for field emission, with particular emphasis on enhancement through doping,[115,235] annealing,[116] growth,[114,236] and assembly[81,237] techniques.

DWCNTs present unique opportunities for nanoelectromechanical systems, in which wear and friction are the main causes of mechanical energy dissipation and component failure.[238] Cumings and Zettl observed ultra-low friction between sliding nanotube surfaces in experiments, leading to the suggestion that MWCNTs could be used as 0.1–1 GHz oscillators.[239] Rivera et al. investigated the oscillatory motion of DWCNTs resulting from displacing the inner wall by varying lengths and then releasing it.[240] Both commensurate and incommensurate DWCNTs were investigated, with the latter showing significantly lower frictional resistance. In each case, the oscillation was somewhat damped, suggesting that DWCNTs could potentially be harnessed as nanoscale shock-absorbers. Work by Ruoff and co-workers investigated the use of DWCNTs as rotational bearings.[241] Motivation for the investigation is that one of the major limitations of microbearings is that high friction-induced wear results in rapid disintegration. It was therefore hypothesized that atomically precise bearings, such as defect-free DWCNTs, could overcome this problem. Indeed, through molecular mechanical modeling, Ruoff and co-workers determined that the small interlayer friction between the inner and outer walls suggests that wear may not occur for typical rotational frequencies, leading to wearless rotational bearings. Recently, Zhang et al. demonstrated superlubricity on the macroscale and in ambient conditions using centimeters-long DWCNTs.[238] Superlubricity is a phenomenon where friction almost vanishes between two incommensurate surfaces, since the structural incompatibility between the concentric walls allows them to easily move relative to one another along their common axis.[242] This low friction arises because the lateral forces between the constituent walls are cancelled and this means that DWCNTs could be used as moving components in machines and electromechanical devices, with huge savings in energy, resource consumption, and maintenance.[243] Prior to this study, superlubricity had only been observed on the nanoscale, under high vacuum conditions;[242,244] thus, the work of Zhang et al.[238] poses a significant advance toward many practical applications, such as ultrasensitive sensors, fine-positioning devices, gyroscopes, and fast switches. By growing ultra-long, structurally perfect DWCNTs (important because the presence of any structural defects or adsorbed impurities on the surface would lead to an increase in friction), measurements of the length-independent inter-wall friction as low as 1 nN were obtained.

Lastly, DWCNTs have been employed as nanoscale mass sensors.[245] In this case, the DWCNT acts as a nanomechanical resonator and can be used for precision mass spectrometry because its resonant frequency, which is related to its mass and is exquisitely sensitive to the presence of any material on its surface. Carbon nanotubes are of great interest for such applications because of their low mass (typically four orders of magnitude lower than state-of-the-art micromachined resonators[246] and high elastic modulus,[247] which means that they can sustain high resonance frequencies. Despite SWCNTs possessing the smaller mass, DWCNTs provide a superior option for nanoscale mass spectrometers owing to their increased rigidity, which allows for even higher resonant frequencies, and their more-uniform electronic properties (ca. 5/9 of DWCNTs possess a metallic wall, whereas only ca. 1/3 of SWCNTs are metallic). Metallicity is important as it enables detection of the resonant frequency by broadcasting radio signals to the nanotube and listening for the vibrations. By using a single DWCNT attached to one electrode and in close proximity to a counter electrode, Jensen et al. were able to measure "mass noise" of just 0.4 Au atoms $Hz^{-1/2}$, which correlates to atomic sensitivity.[245] Besides the obvious advantages of sensitivity, the use of nanotubes as mass sensors does not require ionization of the test sample, and is therefore suitable for large biomolecules. A nanotube mass sensor is also sensitive at higher mass ranges and is vastly smaller than any current alternative, potentially allowing for lab-on-a-chip measurements.

7. Summary and Outlook

Whilst on the surface it may at first appear that the DWCNTs are merely an extension of the SWCNT field, it is now clear that pivotal, yet often subtle, differences exist in terms of their processing requirements, challenges, and outcomes, and in their potential for a host of useful applications and devices. The reports of DWCNT processing methods discussed in this review have made considerable progress toward the realization of high-purity DWCNT material for electronic, nanoelectromechanical, and sensor applications, and more, yet many avenues remain unexplored in this emerging field. Just as the more mature field of SWCNT separation has achieved chiral and isomeric specificity via a number of techniques in a relatively short period of time, it seems likely that significant advances will be made in the field of DWCNT processing through extension of established and evolving SWCNT sorting methodologies and continued research addressing the four fundamental challenges of targeted growth, controlled purification, sorting by outer wall electronic character and chirality, and the ultimate goal of sorting by inner wall electronic character and chirality. There are, of course, future issues of scale up that must be resolved to allow for production of far more than the spectroscopic quantities of material currently possible, yet overall, despite the significant difficulties involved in dealing with all of these challenges, they do not seem insurmountable and with the variety of potential applications continually growing, the outlook for the DWCNT field is indeed bright.

Acknowledgements

All the authors contributed equally to this work. K.E.M. appreciatively acknowledges and thanks the Karlsruhe House of Young Scientists, the

Playford Memorial Trust, and scholarship support from Professor Michael Brunger of the Flinders University of South Australia. B.S.F. gratefully acknowledges support from the Deutsche Forschungsgemeinschaft's Emmy Noether Program under grant number FL 834/1-1.
Note: In the originally published Review, the arrows relating to the "*m*" index in Figure 1a were misleading and the incorrect chirality was named in the caption. The Figure and caption were corrected herein on May 20, 2015.

Received: December 12, 2014
Revised: February 27, 2015
Published online: April 20, 2015

[1] M. S. Dresselhaus, G. Dresselhaus, R. Saito, *Carbon* **1995**, *33*, 883.
[2] a) T. W. Odom, J.-L. Huang, P. Kim, C. M. Lieber, *Nature* **1998**, *391*, 62; b) T. W. Odom, J.-L. Huang, P. Kim, C. M. Lieber, *J. Phys. Chem. B* **2000**, *104*, 2794; c) M. S. Dresselhaus, G. Dresselhaus, A. Jorio, *Annu. Rev. Mater. Res.* **2004**, *34*, 247.
[3] T. W. Ebbesen, P. M. Ajayan, *Nature* **1992**, *358*, 220.
[4] C. D. Spataru, S. Ismail-Beigi, L. X. Benedict, S. G. Louie, *Phys. Rev. Lett.* **2004**, *92*, 077402.
[5] S. M. Bachilo, M. S. Strano, C. Kittrell, R. H. Hauge, R. E. Smalley, R. B. Weisman, *Science* **2002**, *298*, 2361.
[6] R. Pfeiffer, T. Pichler, Y. A. Kim, H. Kuzmany, in *Carbon Nanotubes*, (Eds: A. Jorio, G. Dresselhaus, M. S. Dresselhaus), Springer, Berlin/Heidelberg, Germany **2008**, p. 495.
[7] C. Shen, A. H. Brozena, Y. Wang, *Nanoscale* **2011**, *3*, 503.
[8] Y. A. Kim, K.-S. Yang, H. Muramatsu, T. Hayashi, M. Endo, M. Terrones, M. S. Dresselhaus, *Carbon Lett.* **2014**, *15*, 77.
[9] T. Shimada, T. Sugai, Y. Ohno, S. Kishimoto, T. Mizutani, H. Yoshida, T. Okazaki, H. Shinohara, *Appl. Phys. Lett.* **2004**, *84*, 2412.
[10] K. Liu, W. Wang, Z. Xu, X. Bai, E. Wang, Y. Yao, J. Zhang, Z. Liu, *J. Am. Chem. Soc.* **2008**, *131*, 62.
[11] a) Y. A. Kim, H. Muramatsu, T. Hayashi, M. Endo, M. Terrones, M. S. Dresselhaus, *Chem. Phys. Lett.* **2004**, *398*, 87; b) Y. F. Li, R. Hatakeyama, T. Kaneko, T. Izumida, T. Okada, T. Kato, *Applied Physics Letters* **2006**, *89*, 093110; c) S. Kuwahara, S. Akita, M. Shirakihara, T. Sugai, Y. Nakayama, H. Shinohara, *Chem. Phys. Lett.* **2006**, *429*, 581.
[12] R. Saito, G. Dresselhaus, M. S. Dresselhaus, *Physical Properties of Carbon Nanotubes*, Vol. *4*, Imperial College Press, London **1998**.
[13] a) M. Kociak, K. Suenaga, K. Hirahara, Y. Saito, T. Nakahira, S. Iijima, *Phys. Rev. Lett.* **2002**, *89*, 155501; b) F. Villalpando-Paez, H. Son, D. Nezich, Y. P. Hsieh, J. Kong, Y. A. Kim, D. Shimamoto, H. Muramatsu, T. Hayashi, M. Endo, M. Terrones, M. S. Dresselhaus, *Nano Lett.* **2008**, *8*, 3879.
[14] S. D. Liang, *Phys. B (Amsterdam, Neth.)* **2004**, *352*, 305.
[15] S. Wang, M. Grifoni, *Phys. Rev. Lett.* **2005**, *95*, 266802.
[16] T. Okazaki, S. Bandow, G. Tamura, Y. Fujita, K. Iakoubovskii, S. Kazaoui, N. Minami, T. Saito, K. Suenaga, S. Iijima, *Phys. Rev. B: Condens. Matter Mater. Phys.* **2006**, *74*, 153404.
[17] R. Moradian, S. Azadi, H. Refii-tabar, *J. Phys.: Condens. Matter* **2007**, *19*, 176209.
[18] K. Liu, C. Jin, X. Hong, J. Kim, A. Zettl, E. Wang, F. Wang, *Nat. Phys.* **2014**, *10*, 737.
[19] S. Uryu, T. Ando, *Phys. Rev. B: Condens. Matter Mater. Phys.* **2005**, *72*, 245403.
[20] A. H. Brozena, J. Moskowitz, B. Shao, S. Deng, H. Liao, K. J. Gaskell, Y. Wang, *J. Am. Chem. Soc.* **2010**, *132*, 3932.
[21] Y. Piao, C.-F. Chen, A. A. Green, H. Kwon, M. C. Hersam, C. S. Lee, G. C. Schatz, Y. Wang, *J. Phys. Chem. Lett.* **2011**, *2*, 1577.
[22] a) E. T. Mickelson, C. B. Huffman, A. G. Rinzler, R. E. Smalley, R. H. Hauge, J. L. Margrave, *Chem. Phys. Lett.* **1998**, *296*, 188; b) J. Zhao, H. Park, J. Han, J. P. Lu, *J. Phys. Chem. B* **2004**, *108*, 4227.
[23] J. L. Hutchison, N. A. Kiselev, E. P. Krinichnaya, A. V. Krestinin, R. O. Loutfy, A. P. Morawsky, V. E. Muradyan, E. D. Obraztsova, J. Sloan, S. V. Terekhov, D. N. Zakharov, *Carbon* **2001**, *39*, 761.
[24] T. Sugai, H. Yoshida, T. Shimada, T. Okazaki, H. Shinohara, S. Bandow, *Nano Lett.* **2003**, *3*, 769.
[25] H. Qiu, Z. Shi, L. Guan, L. You, M. Gao, S. Zhang, J. Qiu, Z. Gu, *Carbon* **2006**, *44*, 516.
[26] B. W. Smith, D. E. Luzzi, *Chem. Phys. Lett.* **2000**, *321*, 169.
[27] M. Kalbáć, L. Kavan, L. Juha, S. Civiš, M. Zukalová, M. Bittner, P. Kubát, V. Vorlíćek, L. Dunsch, *Carbon* **2005**, *43*, 1610.
[28] a) H. Dai, A. G. Rinzler, P. Nikolaev, A. Thess, D. T. Colbert, R. E. Smalley, *Chem. Phys. Lett.* **1996**, *260*, 471; b) J. Wei, L. Ci, B. Jiang, Y. Li, X. Zhang, H. Zhu, C. Xu, D. Wu, *J. Mater. Chem.* **2003**, *13*, 1340; c) A. Grüneis, M. H. Rümmeli, C. Kramberger, A. Barreiro, T. Pichler, R. Pfeiffer, H. Kuzmany, T. Gemming, B. Büchner, *Carbon* **2006**, *44*, 3177.
[29] Y. Saito, T. Nakahira, S. Uemura, *J. Phys. Chem. B* **2003**, *107*, 931.
[30] H. Yoshida, T. Sugai, H. Shinohara, *J. Phys. Chem. C* **2008**, *112*, 19908.
[31] S. Deng, A. H. Brozena, Y. Zhang, Y. Piao, Y. Wang, *Chem. Commun.* **2011**, *47*, 758.
[32] H. Nie, H. Wang, A. Cao, Z. Shi, S.-T. Yang, Y. Yuan, Y. Liu, *Nanoscale* **2011**, *3*, 970.
[33] G. Liu, Y. Saito, D. Nishio-Hamane, A. K. Bauri, E. Flahaut, T. Kimura, N. Komatsu, *J. Mater. Chem. A* **2014**, *2*, 19067.
[34] A. A. Green, M. C. Hersam, *Nat. Nanotechnol.* **2009**, *4*, 64.
[35] A. A. Green, M. C. Hersam, *ACS Nano* **2011**, *5*, 1459.
[36] K. E. Moore, M. Pfohl, F. Hennrich, V. S. Chakradhanula, C. Kuebel, M. M. Kappes, J. G. Shapter, R. Krupke, B. S. Flavel, *ACS Nano* **2014**, *8*, 6756.
[37] K. E. Moore, M. Pfohl, D. D. Tune, F. Hennrich, S. Dehm, V. S. K. Chakradhanula, C. Kuebel, R. Krupke, B. S. Flavel, *ACS Nano*; DOI: 10.1021/nn506869h.
[38] W. Gomulya, G. D. Costanzo, E. J. F. de Carvalho, S. Z. Bisri, V. Derenskyi, M. Fritsch, N. Frohlich, S. Allard, P. Gordiichuk, A. Herrmann, S. J. Marrink, M. C. dos Santos, U. Scherf, M. A. Loi, *Adv. Mater.* **2013**, *25*, 2948.
[39] S. K. Samanta, M. Fritsch, U. Scherf, W. Gomulya, S. Z. Bisri, M. A. Loi, *Acc. Chem. Res.* **2014**, *47*, 2446.
[40] C. Y. Khripin, J. A. Fagan, M. Zheng, *J. Am. Chem. Soc.* **2013**, *135*, 6822.
[41] N. K. Subbaiyan, S. Cambré, A. N. G. Parra-Vasquez, E. H. Hároz, S. K. Doorn, J. G. Duque, *ACS Nano* **2014**, *8*, 1619.
[42] S. Okada, A. Oshiyama, *Phys. Rev. Lett.* **2003**, *91*, 216801.
[43] V. Zólyomi, Á. Rusznyák, J. Kürti, Á. Gali, F. Simon, H. Kuzmany, Á. Szabados, P. Surján, *Phys. Status Solidi B* **2006**, *243*, 3476.
[44] W. Ren, F. Li, J. Chen, S. Bai, H.-M. Cheng, *Chem. Phys. Lett.* **2002**, *359*, 196.
[45] a) J. M. Zuo, I. Vartanyants, M. Gao, R. Zhang, L. A. Nagahara, *Science* **2003**, *300*, 1419; b) K. Hirahara, M. Kociak, S. Bandow, T. Nakahira, K. Itoh, Y. Saito, S. Iijima, *Phys. Rev. B: Condens. Matter Mater. Phys.* **2006**, *73*, 195420; c) K. Liu, Z. Xu, W. Wang, P. Gao, W. Fu, X. Bai, E. Wang, *J. Phys. D: Appl. Phys.* **2009**, *42*, 125412.
[46] Z. M. Li, Z. K. Tang, H. J. Liu, N. Wang, C. T. Chan, R. Saito, S. Okada, G. D. Li, J. S. Chen, N. Nagasawa, S. Tsuda, *Phys. Rev. Lett.* **2001**, *87*, 127401.
[47] a) K. H. Ahn, Y.-H. Kim, J. Wiersig, K. J. Chang, *Phys. Rev. Lett.* **2003**, *90*, 026601; b) J. Chen, L. Yang, H. Yang, J. Dong, *Chem. Phys. Lett.* **2004**, *400*, 384.
[48] S. Uryu, *Phys. Rev. B: Condens. Matter Mater. Phys.* **2004**, *69*, 075402.
[49] K.-H. Ahn, Y.-H. Kim, J. Wiersig, K. J. Chang, *Phys. E (Amsterdam, Neth.)* **2004**, *22*, 666.
[50] J. Chen, L. Yang, *J. Phys.: Condens. Matter* **2005**, *17*, 957.
[51] M. Kalbac, A. A. Green, M. C. Hersam, L. Kavan, *Chem. Eur. J.* **2011**, *17*, 9806.

[52] a) M. Kalbac, L. Kavan, L. Dunsch, *J. Phys. Chem. C* **2008**, *112*, 16759; b) M. Kalbac, H. Farhat, L. Kavan, J. Kong, K.-i. Sasaki, R. Saito, M. S. Dresselhaus, *ACS Nano* **2009**, *3*, 2320.
[53] J. Cambedouzou, J. L. Sauvajol, A. Rahmani, E. Flahaut, A. Peigney, C. Laurent, *Phys. Rev. B: Condens. Matter Mater. Phys.* **2004**, *69*, 235422.
[54] K. Liu, J. Deslippe, F. Xiao, R. B. Capaz, X. Hong, S. Aloni, A. Zettl, W. Wang, X. Bai, S. G. Louie, E. Wang, F. Wang, *Nat. Nanotechnol.* **2012**, *7*, 325.
[55] a) J. Lefebvre, J. M. Fraser, Y. Homma, P. Finnie, *Appl. Phys. A* **2004**, *78*, 1107; b) J. H. Choi, M. S. Strano, *Appl. Phys. Lett.* **2007**, *90*, 223114; c) M. Engel, K. E. Moore, A. Alam, S. Dehm, R. Krupke, B. S. Flavel, *ACS Nano* **2014**, *8*, 9324; d) K. Liu, X. Hong, Q. Zhou, C. Jin, J. Li, W. Zhou, J. Liu, E. Wang, A. Zettl, F. Wang, *Nat. Nanotechnol.* **2013**, *8*, 917; e) R. M. Jain, R. Howden, K. Tvrdy, S. Shimizu, A. J. Hilmer, T. P. McNicholas, K. K. Gleason, M. S. Strano, *Adv. Mater.* **2012**, *24*, 4436.
[56] A. M. Rao, E. Richter, S. Bandow, B. Chase, P. C. Eklund, K. A. Williams, S. Fang, K. R. Subbaswamy, M. Menon, A. Thess, R. E. Smalley, G. Dresselhaus, M. S. Dresselhaus, *Science* **1997**, *275*, 187.
[57] a) M. S. Dresselhaus, G. Dresselhaus, A. Jorio, A. G. Souza Filho, R. Saito, *Carbon* **2002**, *40*, 2043; b) P. T. Araujo, P. B. C. Pesce, M. S. Dresselhaus, K. Sato, R. Saito, A. Jorio, *Phys. E (Amsterdam, Neth.)* **2010**, *42*, 1251.
[58] M. S. Arnold, S. I. Stupp, M. C. Hersam, *Nano Lett.* **2005**, *5*, 713.
[59] K. Moshammer, F. Hennrich, M. Kappes, *Nano Res.* **2009**, *2*, 599.
[60] H. Liu, D. Nishide, T. Tanaka, H. Kataura, *Nat. Commun.* **2011**, *2*, 309.
[61] K. Tvrdy, R. M. Jain, R. Han, A. J. Hilmer, T. P. McNicholas, M. S. Strano, *ACS Nano* **2013**, *7*, 1779.
[62] B. S. Flavel, K. E. Moore, M. Pfohl, M. M. Kappes, F. Hennrich, *ACS Nano* **2014**, *82*, 1817.
[63] A. L. Ng, Y. Sun, L. Powell, C.-F. Sun, C.-F. Chen, C. S. Lee, Y. Wang, *Small* **2015**, *11*, 68.
[64] W. Wenseleers, I. I. Vlasov, E. Goovaerts, E. D. Obraztsova, A. S. Lobach, A. Bouwen, *Adv. Funct. Mater.* **2004**, *14*, 1105.
[65] a) T. Ando, *J. Phys.Soc. Jpn.* **1997**, *66*, 1066; b) M. Ichida, S. Mizuno, Y. Saito, H. Kataura, Y. Achiba, A. Nakamura, *Phys. Rev. B: Condens. Matter Mater. Phys.* **2002**, *65*, 241407; c) F. Wang, G. Dukovic, L. E. Brus, T. F. Heinz, *Science* **2005**, *308*, 838.
[66] M. Kalbac, A. A. Green, M. C. Hersam, L. Kavan, *ACS Nano* **2010**, *4*, 459.
[67] Y.-A. Kim, H. Muramatsu, M. Kojima, T. Hayashi, M. Endo, M. Terrones, M. S. Dresselhaus, *Chem. Phys. Lett.* **2006**, *420*, 377.
[68] A. Jorio, M. S. Dresselhaus, R. Saito, G. Dresselhaus, *Raman Spectroscopy in Graphene Related Systems*, John Wiley & Sons, New York **2010**.
[69] R. Pfeiffer, C. Kramberger, F. Simon, H. Kuzmany, V. N. Popov, H. Kataura, *Eur. Phys. J. B* **2004**, *42*, 345.
[70] R. Pfeiffer, H. Kuzmany, C. Kramberger, C. Schaman, T. Pichler, H. Kataura, Y. Achiba, J. Kürti, V. Zólyomi, *Phys. Rev. Lett.* **2003**, *90*, 225501.
[71] Z. Kominkova, V. Vales, M. C. Hersam, M. Kalbac, *Carbon* **2014**, *78*, 366.
[72] M. S. Dresselhaus, G. Dresselhaus, R. Saito, A. Jorio, *Phys. Rep.* **2005**, *409*, 47.
[73] M. A. Pimenta, A. Jorio, S. D. M. Brown, A. G. Souza Filho, G. Dresselhaus, J. H. Hafner, C. M. Lieber, R. Saito, M. S. Dresselhaus, *Phys. Rev. B: Condens. Matter Mater. Phys.* **2001**, *64*, 041401.
[74] M. H. Park, J. W. Jang, C. E. Lee, C. J. Lee, *Appl. Phys. Lett.* **2005**, *86*, 023110.
[75] Y. Sato, K. Yanagi, Y. Miyata, K. Suenaga, H. Kataura, S. Iijima, *Nano Lett.* **2008**, *8*, 3151.
[76] a) R. Bandyopadhyaya, E. Nativ-Roth, O. Regev, R. Yerushalmi-Rozen, *Nano Lett.* **2001**, *2*, 25; b) V. C. Moore, M. S. Strano, E. H. Haroz, R. H. Hauge, R. E. Smalley, J. Schmidt, Y. Talmon, *Nano Lett.* **2003**, *3*, 1379.
[77] S. Iijima, *Nature* **1991**, *354*, 56.
[78] E. G. Gamaly, T. W. Ebbessen, *Phys. Rev. B: Condens. Matter Mater. Phys.* **1995**, *52*, 2083.
[79] H. Huang, H. Kajiura, S. Tsutsui, Y. Murakami, M. Ata, *J. Phys. Chem. B* **2003**, *107*, 8794.
[80] T. Sugai, H. Omote, S. Bandow, N. Tanaka, H. Shinohara, *J. Chem. Phys.* **2000**, *112*, 6000.
[81] J. Zhao, Y. Su, Z. Yang, L. Wei, Y. Wang, Y. Zhang, *Carbon* **2013**, *58*, 92.
[82] L. Li, F. Li, C. Liu, H. M. Cheng, *Carbon* **2005**, *43*, 623.
[83] K. Xu, Y. Li, C. Xu, J. Gao, H. Liu, H. Yang, P. Richard, *Chem. Eng. J.* **2013**, *225*, 210.
[84] K. Xu, Y. Li, F. Yang, W. Yang, L. Zhang, C. Xu, T. Kaneko, R. Hatakeyama, *Carbon* **2014**, *68*, 511.
[85] R. H. Baughman, *Nat. Nanotechnol.* **2006**, *1*, 94.
[86] a) B. W. Smith, M. Monthioux, D. E. Luzzi, *Nature* **1998**, *396*, 323; B) B. W. Smith, M. Monthioux, D. E. Luzzi, *Chem. Phys. Lett.* **1999**, *315*, 31.
[87] T. Guo, P. Nikoleav, A. Thess, D. T. Colbert, R. E. Smalley, *Chem. Phys. Lett.* **1995**, *243*, 49.
[88] S. Bandow, M. Takizawa, K. Hirahara, M. Yudasaka, S. Iijima, *Chem. Phys. Lett.* **2001**, *337*, 48.
[89] a) L. Guan, Z. Shi, M. Li, Z. Gu, *Carbon* **2005**, *43*, 2780; b) L. Yongfeng, H. Rikizo, K. Toshiro, O. Takeru, *Jpn. J. Appl. Phys.* **2006**, *45*, L428; c) H. Shiozawa, T. Pichler, A. Grüneis, R. Pfeiffer, H. Kuzmany, Z. Liu, K. Suenaga, H. Kataura, *Adv. Mater.* **2008**, *20*, 1443.
[90] A. Barreiro, S. Hampel, M. H. Rümmeli, C. Kramberger, A. Grüneis, K. Biedermann, A. Leonhardt, T. Gemming, B. Büchner, A. Bachtold, T. Pichler, *J. Phys. Chem. B* **2006**, *110*, 20973.
[91] C. Kramberger, A. Waske, K. Biedermann, T. Pichler, T. Gemming, B. Büchner, H. Kataura, *Chem. Phys. Lett.* **2005**, *407*, 254.
[92] M. Berd, P. Puech, A. Righi, A. Benfdila, M. Monthioux, *Small* **2012**, *8*, 2045.
[93] M. Suzuki, T. Iida, K. Nasu, *Phys. Rev. B: Condens. Matter Mater. Phys.* **2000**, *61*, 2188.
[94] M. Melle-Franco, H. Kuzmany, F. Zerbetto, *J. Phys. Chem. B* **2003**, *107*, 6986.
[95] H. Kuzmany, W. Plank, R. Pfeiffer, F. Simon, *J. Raman Spectrosc.* **2008**, *39*, 134.
[96] A. Oberlin, M. Endo, T. Koyama, *J. Cryst. Growth* **1976**, *32*, 335.
[97] H. Dai, A. G. Rinzer, P. Nikolaev, A. Thess, D. T. Colbert, R. E. Smalley, *Chem. Phys. Lett.* **1996**, *260*, 471.
[98] C. L. Cheung, A. Kurtz, H. Park, C. M. Lieber, *J. Phys. Chem. B* **2002**, *106*, 2429.
[99] Y. Liu, W.-Z. Qian, Q. Zhang, G.-Q. Ning, Q. Wen, G.-H. Luo, F. Wei, *Carbon* **2008**, *46*, 1860.
[100] a) W. Z. Li, J. G. Wen, M. Sennett, Z. F. Ren, *Chem. Phys. Lett.* **2003**, *368*, 299; b) J. Wei, B. Jiang, D. Wu, B. Wei, *J. Phys. Chem. B* **2004**, *108*, 8844; c) G. Ning, F. Wei, Q. Wen, G. Luo, Y. Wang, Y. Jin, *J. Phys. Chem. B* **2005**, *110*, 1201; d) H. Qi, C. Qian, J. Liu, *Nano Lett.* **2007**, *7*, 2417; e) Q. Liu, W. Ren, F. Li, H. Cong, H.-M. Cheng, *J. Phys. Chem. C* **2007**, *111*, 5006.
[101] E. Flahaut, C. Laurent, A. Peigney, *Carbon* **2005**, *43*, 375.
[102] J. H. Hafner, M. J. Bronikowski, B. R. Azamian, P. Nikolaev, A. G. Rinzler, D. T. Colbert, K. A. Smith, R. E. Smalley, *Chem. Phys. Lett.* **1998**, *296*, 195.

[103] G. Xiong, Y. Suda, D. Wang, J. Huang, Z. Ren, *Nanotechnology* **2005**, *16*, 532.
[104] a) S. C. Lyu, B. C. Liu, C. J. Lee, H. K. Kang, C.-W. Yang, C. Y. Park, *Chem. Mater.* **2003**, *15*, 3951; b) S. C. Lyu, T. J. Lee, C. W. Yang, C. J. Lee, *Chem. Commun.* **2003**, *1404*; c) M. Hiramatsu, H. Nagao, M. Taniguchi, H. Amano, Y. Ando, M. Hori, *Jpn. J. Appl. Phys.* **2005**, *44*, L693; d) H. Ago, N. Uehara, N. Yoshihara, M. Tsuji, M. Yumura, N. Tomonaga, T. Setoguchi, *Carbon* **2006**, *44*, 2912; e) J. Huang, Q. Zhang, M. Zhao, F. Wei, *Nano Res.* **2009**, *2*, 872.
[105] a) J. Zhu, M. Yudasaka, S. Iijima, *Chem. Phys. Lett.* **2003**, *380*, 496; b) H. Ago, K. Nakamura, N. Uehara, M. Tsuji, *J. Phys. Chem. B* **2004**, *108*, 18908; c) G. Ning, Y. Liu, F. Wei, Q. Wen, G. Luo, *J. Phys. Chem. C* **2007**, *111*, 1969; d) Q. Zhang, M.-Q. Zhao, J.-Q. Huang, Y. Liu, Y. Wang, W.-Z. Qian, F. Wei, *Carbon* **2009**, *47*, 2600.
[106] T. Hiraoka, T. Yamada, K. Hata, D. N. Futaba, H. Kurachi, S. Uemura, M. Yumura, S. Iijima, *J. Am. Chem. Soc.* **2006**, *128*, 13338.
[107] S. B. Sinnott, R. Andrews, D. Qian, A. M. Rao, Z. Mao, E. C. Dickey, F. Derbyshire, *Chem. Phys. Lett.* **1999**, *315*, 25.
[108] E. Flahaut, R. Bacsa, A. Peigney, C. Laurent, *Chem. Commun.* **2003**, 1442.
[109] E. Flahaut, A. Peigney, C. Laurent, A. Rousset, *J. Mater. Chem.* **2000**, *10*, 249.
[110] L. Ci, Z. Rao, Z. Zhou, D. Tang, X. Yan, Y. Liang, D. Liu, H. Yuan, W. Zhou, G. Wang, W. Liu, S. Xie, *Chem. Phys. Lett.* **2002**, *359*, 63.
[111] a) H. M. Cheng, F. Li, G. Su, H. Y. Pan, L. L. He, X. Sun, M. S. Dresselhaus, *Appl. Phys. Lett.* **1998**, *72*, 3282; b) L. Ci, Y. Li, B. Wei, J. Liang, C. Xu, D. Wu, *Carbon* **2000**, *38*, 1933; c) Q. Liu, W. Ren, Z.-G. Chen, D.-W. Wang, B. Liu, B. Yu, F. Li, H. Cong, H.-M. Cheng, *ACS Nano* **2008**, *2*, 1722; d) H. M. Cheng, F. Li, X. Sun, S. D. M. Brown, M. A. Pimenta, A. Marucci, G. Dresselhaus, M. S. Dresselhaus, *Chem. Phys. Lett.* **1998**, *289*, 602; e) H. W. Zhu, C. L. Xu, D. H. Wu, B. Q. Wei, R. Vajtai, P. M. Ajayan, *Science* **2002**, *296*, 884.
[112] A. Modi, N. Koratkar, E. Lass, B. Wei, P. M. Ajayan, *Nature* **2003**, *424*, 171.
[113] S. C. Lim, Y. C. Choi, H. J. Jeong, Y. M. Shin, K. H. An, D. J. Bae, Y. H. Lee, N. S. Lee, J. M. Kim, *Adv. Mater.* **2001**, *13*, 1563.
[114] G. Chen, D. H. Shin, T. Iwasaki, H. Kawarada, C. J. Lee, *Nanotechnology* **2008**, *19*, 415703.
[115] K.-Y. Chun, H. S. Lee, C. J. Lee, *Carbon* **2009**, *47*, 169.
[116] S. I. Jung, S. H. Jo, H. S. Moon, J. M. Kim, D.-S. Zang, C. J. Lee, *J. Phys. Chem. C* **2007**, *111*, 4175.
[117] T. Yamada, T. Namai, K. Hata, D. N. Futaba, K. Mizuno, J. Fan, M. Yudasaka, M. Yumura, S. Iijima, *Nat. Nanotechnol.* **2006**, *1*, 131.
[118] L. Ci, R. Vajtai, P. M. Ajayan, *J. Phys. Chem. C* **2007**, *111*, 9077.
[119] H. Kim, J. Kang, Y. Kim, B. H. Hong, J. Choi, S. Iijima, *J. Nanosci. Nanotechnol.* **2011**, *11*, 470.
[120] T.-Y. Liu, L.-L. Zhang, W.-J. Yu, S.-S. Li, P.-X. Hou, H.-T. Cong, C. Liu, H.-M. Cheng, *Carbon* **2013**, *56*, 167.
[121] Y. Fu, S. Chen, J. Bielecki, A. Matic, T. Wang, L.-L. Ye, J. Liu, *Mater. Lett.* **2012**, *72*, 78.
[122] P. Nikolaev, D. Hooper, N. Perea-López, M. Terrones, B. Maruyama, *ACS Nano* **2014**, *8*, 10214.
[123] a) R. S. Ruoff, D. S. Tse, R. Malhotra, D. C. Lorents, *J. Phys. Chem.* **1993**, *97*, 3379; b) S. Bandow, S. Asaka, X. Zhao, Y. Ando, *Appl. Phys. A* **1998**, *67*, 23.
[124] a) J.-M. Moon, K. H. An, Y. H. Lee, Y. S. Park, D. J. Bae, G.-S. Park, *J. Phys. Chem. B* **2001**, *105*, 5677; b) M. T. Martinez, M. A. Callejas, A. M. Benito, M. Cochet, T. Seeger, A. Ansón, J. Schreiber, C. Gordon, C. Marhic, O. Chauvet, J. L. G. Fierro, W. K. Maser, *Carbon* **2003**, *41*, 2247; c) H. Hu, B. Zhao, M. E. Itkis, R. C. Haddon, *J. Phys. Chem. B* **2003**, *107*, 13838; d) J. Zhang, H. Zou, Q. Qing, Y. Yang, Q. Li, Z. Liu, X. Guo, Z. Du, *J. Phys. Chem. B* **2003**, *107*, 3712.
[125] Y. Miyata, Y. Maniwa, H. Kataura, *J. Phys. Chem. B* **2005**, *110*, 25.
[126] J. G. Wiltshire, A. N. Khlobystov, L. J. Li, S. G. Lyapin, G. A. D. Briggs, R. J. Nicholas, *Chem. Phys. Lett.* **2004**, *386*, 239.
[127] Y. Peng, H. Liu, *Ind. Eng. Chem. Res.* **2006**, *45*, 6483.
[128] Y. Feng, H. Zhang, Y. Hou, T. P. McNicholas, D. Yuan, S. Yang, L. Ding, W. Feng, J. Liu, *ACS Nano* **2008**, *2*, 1634.
[129] M. Zheng, A. Jagota, E. D. Semke, B. A. Diner, R. S. McLean, S. R. Lustig, R. E. Richardson, N. G. Tassi, *Nat. Mater.* **2003**, *2*, 338.
[130] S. Ghosh, S. M. Bachilo, R. B. Weisman, *Nat. Nanotechnol.* **2010**, *5*, 443.
[131] a) A. Nish, J.-Y. Hwang, J. Doig, R. J. Nicholas, *Nat. Nanotechnol.* **2007**, *2*, 640; b) F. Chen, B. Wang, Y. Chen, L.-J. Li, *Nano Lett.* **2007**, *7*, 3013; c) W. Gomulya, G. D. Costanzo, E. J. F. de Carvalho, S. Z. Bisri, V. Derenskyi, M. Fritsch, N. Fröhlich, S. Allard, P. Gordiichuk, A. Herrmann, S. J. Marrink, M. C. dos Santos, U. Scherf, M. A. Loi, *Adv. Mater.* **2013**, *25*, 2948; d) P. Gerstel, S. Klumpp, F. Hennrich, A. Poschlad, V. Meded, E. Blasco, W. Wenzel, M. M. Kappes, C. Barner-Kowollik, *ACS Macro Lett.* **2013**, *3*, 10; e) J. Ding, Z. Li, J. Lefebvre, F. Cheng, G. Dubey, S. Zou, P. Finnie, A. Hrdina, L. Scoles, G. P. Lopinski, *Nanoscale* **2014**, *6*, 2328.
[132] J. Y. Hwang, A. Nish, J. Doig, S. Douven, C. W. Chen, L. C. Chen, R. J. Nicholas, *J. Am. Chem. Soc.* **2008**, *130*, 3543.
[133] S. Deng, Y. Zhang, A. H. Brozena, M. L. Mayes, P. Banerjee, W.-A. Chiou, G. W. Rubloff, G. C. Schatz, Y. Wang, *Nat. Commun.* **2011**, *2*, 382.
[134] L. Vaisman, H. D. Wagner, G. Marom, *Adv. Colloid Interface Sci.* **2006**, *128–130*, 37.
[135] L. Cooper, H. Amano, M. Hiraide, S. Houkyou, I. Y. Jang, Y. J. Kim, H. Muramatsu, J. H. Kim, T. Hayashi, Y. A. Kim, M. Endo, M. S. Dresselhaus, *Appl. Phys. Lett.* **2009**, *95*, 233104.
[136] A. J. Blanch, C. E. Lenehan, J. S. Quinton, *J. Phys. Chem. B* **2010**, *114*, 9805.
[137] a) V. Georgakilas, N. Tagmatarchis, D. Pantarotto, A. Bianco, J.-P. Briand, M. Prato, *Chem. Commun.* **2002**, 3050; b) J. L. Hudson, M. J. Casavant, J. M. Tour, *J. Am. Chem. Soc.* **2004**, *126*, 11158; c) M. G. Ruther, F. Frehill, J. E. O'Brien, A. I. Minett, W. J. Blau, J. G. Vos, M. Panhuis, *J. Phys. Chem. B* **2004**, *108*, 9665; d) W.-J. Kim, N. Nair, C. Y. Lee, M. S. Strano, *J. Phys. Chem. C* **2008**, *112*, 7326.
[138] S. Banerjee, S. S. Wong, *Nano Lett.* **2004**, *4*, 1445.
[139] a) K. H. An, J. S. Park, C.-M. Yang, S. Y. Jeong, S. C. Lim, C. Kang, J.-H. Son, M. S. Jeong, Y. H. Lee, *J. Am. Chem. Soc.* **2005**, *127*, 5196; b) A. J. Blanch, C. E. Lenehan, J. S. Quinton, *J. Phys. Chem. C* **2011**, *116*, 1709.
[140] M. S. Arnold, A. A. Green, J. F. Hulvat, S. I. Stupp, M. C. Hersam, *Nat. Nanotechnol.* **2006**, *1*, 60.
[141] J. A. Fagan, M. L. Becker, J. Chun, P. Nie, B. J. Bauer, J. R. Simpson, A. Hight-Walker, E. K. Hobbie, *Langmuir* **2008**, *24*, 13880.
[142] F. Bonaccorso, T. Hasan, P. H. Tan, C. Sciascia, G. Privitera, G. Di Marco, P. G. Gucciardi, A. C. Ferrari, *J. Phys. Chem. C* **2010**, *114*, 17267.
[143] A. A. Green, M. C. Hersam, *Adv. Mater.* **2011**, *23*, 2185.
[144] M. Zheng, A. Jagota, M. S. Strano, A. P. Santos, P. Barone, S. G. Chou, B. A. Diner, M. S. Dresselhaus, R. S. Mclean, G. B. Onoa, G. G. Samsonidze, E. D. Semke, M. Usrey, D. J. Walls, *Science* **2003**, *302*, 1545.
[145] M. Zheng, E. D. Semke, *J. Am. Chem. Soc.* **2007**, *129*, 6084.
[146] X. Tu, S. Manohar, A. Jagota, M. Zheng, *Nature* **2009**, *460*, 250.

[147] A. Nish, J. Y. Hwang, J. Doig, R. J. Nicholas, *Nat. Nanotechnol.* **2007**, *2*, 640.
[148] F. M. Chen, B. Wang, Y. Chen, L. J. Li, *Nano Lett.* **2007**, *7*, 3013.
[149] M. F. Islam, E. Rojas, D. M. Bergey, A. T. Johnson, A. G. Yodh, *Nano Lett.* **2003**, *3*, 269.
[150] W. H. Duan, Q. Wang, F. Collins, *Chem. Sci.* **2011**, *2*, 1407.
[151] H. Liu, T. Tanaka, Y. Urabe, H. Kataura, *Nano Lett.* **2013**, *13*, 1996.
[152] A. J. Blanch, J. S. Quinton, J. G. Shapter, *Carbon* **2013**, *60*, 471.
[153] B. S. Flavel, M. M. Kappes, R. Krupke, F. Hennrich, *ACS Nano* **2013**, *7*, 3557.
[154] P. G. Collins, M. S. Arnold, P. Avouris, *Science* **2001**, *292*, 706.
[155] Z. Xu, X. Yang, Z. Yang, *Nano Lett.* **2010**, *10*, 985.
[156] N. R. Tummala, A. Striolo, *ACS Nano* **2009**, *3*, 595.
[157] T. J. McDonald, C. Engtrakul, M. Jones, G. Rumbles, M. J. Heben, *J. Phys. Chem. B* **2006**, *110*, 25339.
[158] M. C. Hersam, *Nat. Nanotechnol.* **2008**, *3*, 387.
[159] M. Zheng, A. Jagota, E. D. Semke, B. A. Diner, R. S. McLean, S. R. Lustig, R. E. Richardson, N. G. Tassi, *Nat. Mater.* **2003**, *2*, 338.
[160] J. H. Kim, M. Kataoka, Y. A. Kim, D. Shimamoto, H. Muramatsu, T. Hayashi, M. Endo, M. Terrones, M. S. Dresselhaus, *Appl. Phys. Lett.* **2008**, *93*, 223107.
[161] J. H. Kim, M. Kataoka, D. Shimamoto, H. Muramatsu, Y. C. Jung, T. Hayashi, Y. A. Kim, M. Endo, J. S. Park, R. Saito, M. Terrones, M. S. Dresselhaus, *ACS Nano* **2010**, *4*, 1060.
[162] D. Nepal, K. E. Geckeler, *Small* **2006**, *2*, 406.
[163] a) D. Nepal, K. E. Geckeler, *Small* **2007**, *3*, 1259; b) G. Raffaini, F. Ganazzoli, *J. Appl. Biomater. Biomech.* **2009**, *8*, 135.
[164] Q. Mu, W. Liu, Y. Xing, H. Zhou, Z. Li, Y. Zhang, L. Ji, F. Wang, Z. Si, B. Zhang, B. Yan, *J. Phys. Chem. C* **2008**, *112*, 3300.
[165] a) D. W. Horn, K. Tracy, C. J. Easley, V. A. Davis, *J. Phys. Chem. C* **2012**, *116*, 10341; b) M. Calvaresi, S. Hoefinger, F. Zerbetto, *Chem. Eur. J.* **2012**, *18*, 4308.
[166] a) Y. Li, T. Kaneko, R. Hatakeyama, *Small* **2010**, *6*, 729; b) C.-L. Cheng, G.-J. Zhao, *Nanoscale* **2012**, *4*, 2301.
[167] S. Deng, Y. Piao, A. H. Brozena, Y. Wang, *J. Mater. Chem.* **2011**, *21*, 18568.
[168] M. J. O'Connell, E. E. Eibergen, S. K. Doorn, *Nat. Mater.* **2005**, *4*, 412.
[169] a) M. Lundqvist, I. Sethson, B.-H. Jonsson, *Langmuir* **2004**, *20*, 10639; b) A. A. Vertegel, R. W. Siegel, J. S. Dordick, *Langmuir* **2004**, *20*, 6800.
[170] a) T. Dumitrică, C. M. Landis, B. I. Yakobson, *Chem. Phys. Lett.* **2002**, *360*, 182; b) H. G. Chae, T. V. Sreekumar, T. Uchida, S. Kumar, *Polymer* **2005**, *46*, 10925.
[171] X. Peng, N. Komatsu, S. Bhattacharya, T. Shimawaki, S. Aonuma, T. Kimura, A. Osuka, *Nat. Nanotechnol.* **2007**, *2*, 361.
[172] G. Liu, F. Wang, S. Chaunchaiyakul, Y. Saito, A. K. Bauri, T. Kimura, Y. Kuwahara, N. Komatsu, *J. Am. Chem. Soc.* **2013**, *135*, 4805.
[173] J. E. Hearst, J. Vinograd, *Proc. Natl. Acad. Sci. USA* **1961**, *47*, 999.
[174] R. Fleurier, J.-S. Lauret, E. Flahaut, A. Loiseau, *Phys. Status Solidi B* **2009**, *246*, 2675.
[175] S. Niyogi, C. G. Densmore, S. K. Doorn, *J. Am. Chem. Soc.* **2008**, *131*, 1144.
[176] J. G. Duque, C. G. Densmore, S. K. Doorn, *J. Am. Chem. Soc.* **2010**, *132*, 16165.
[177] J. A. Fagan, M. L. Becker, J. Chun, E. K. Hobbie, *Adv. Mater.* **2008**, *20*, 1609.
[178] J. Y. Huh, A. R. H. Walker, H. W. Ro, J. Obrzut, E. Mansfield, R. Geiss, J. A. Fagan, *J. Phys. Chem. C* **2010**, *114*, 11343.
[179] H. Liu, T. Tanaka, H. Kataura, *Nano Lett.* **2014**, *14*, 6237.
[180] B. S. Flavel, K. E. Moore, M. Pfohl, M. M. Kappes, F. Hennrich, *ACS Nano* **2014**, *8*, 1817.
[181] Y. Miyata, K. Shiozawa, Y. Asada, Y. Ohno, R. Kitaura, T. Mizutani, H. Shinohara, *Nano Res.* **2011**, *4*, 963.
[182] J. Wu, L. Xie, G. Hong, H. Lim, B. Thendie, Y. Miyata, H. Shinohara, H. Dai, *Nano Res.* **2012**, *5*, 388.
[183] J. Zhang, H. Gui, B. Liu, J. Liu, C. Zhou, *Nano Res.* **2013**, *6*, 906.
[184] K. S. Mistry, B. A. Larsen, J. L. Blackburn, *ACS Nano* **2013**, *7*, 2231.
[185] J. Han, Q. Ji, S. Qiu, H. Li, S. Zhang, H. Jin, Q. Li, *Chem. Commun.* **2015**, *51*, 4712.
[186] M. J. Shea, R. D. Mehlenbacher, M. T. Zanni, M. S. Arnold, *J. Phys. Chem. Lett.* **2014**, *5*, 3742.
[187] N. Berton, F. Lemasson, A. Poschlad, V. Meded, F. Tristram, W. Wenzel, F. Hennrich, M. M. Kappes, M. Mayor, *Small* **2014**, *10*, 360.
[188] N. Berton, F. Lemasson, J. Tittmann, N. Sturzl, F. Hennrich, M. M. Kappes, M. Mayor, *Chem. Mater.* **2011**, *23*, 2237.
[189] a) F. Lemasson, N. Berton, J. Tittmann, F. Hennrich, M. M. Kappes, M. Mayor, *Macromolecules* **2012**, *45*, 713; b) H. Wang, Y. Li, G. Jiménez-Osés, P. Liu, Y. Fang, J. Zhang, Y.-C. Lai, S. Park, L. Chen, K. N. Houk, Z. Bao, *Adv. Funct. Mater.* **2015**, *25*, 1837; c) H. L. Wang, G. I. Koleilat, P. Liu, G. Jimenez-Oses, Y. C. Lai, M. Vosgueritchian, Y. Fang, S. Park, K. N. Houk, Z. N. Bao, *ACS Nano* **2014**, *8*, 2609; d) H. Ozawa, T. Fujigaya, Y. Niidome, N. Hotta, M. Fujiki, N. Nakashima, *J. Am. Chem. Soc.* **2011**, *133*, 2651; e) H. Ozawa, T. Fujigaya, S. Song, H. Suh, N. Nakashima, *Chem. Lett.* **2011**, *40*, 470.
[190] K. Mulla, S. Liang, H. Shaik, E. A. Younes, A. Adronov, Y. Zhao, *Chem. Commun.* **2015**, *51*, 149.
[191] F. A. Lemasson, T. Strunk, P. Gerstel, F. Hennrich, S. Lebedkin, C. Barner-Kowollik, W. Wenzel, M. M. Kappes, M. Mayor, *J. Am. Chem. Soc.* **2011**, *133*, 652.
[192] H. W. Lee, Y. Yoon, S. Park, J. H. Oh, S. Hong, L. S. Liyanage, H. L. Wang, S. Morishita, N. Patil, Y. J. Park, J. J. Park, A. Spakowitz, G. Galli, F. Gygi, P. H. S. Wong, J. B. H. Tok, J. M. Kim, Z. A. Bao, *Nat. Commun.* **2011**, *2*, 541.
[193] P. Gerstel, S. Klumpp, F. Hennrich, O. Altintas, T. R. Eaton, M. Mayor, C. Barner-Kowollik, M. M. Kappes, *Polym. Chem.* **2012**, *3*, 1966.
[194] K. Akazaki, F. Toshimitsu, H. Ozawa, T. Fujigaya, N. Nakashima, *J. Am. Chem. Soc.* **2012**, *134*, 12700.
[195] N. Sturzl, F. Hennrich, S. Lebedkin, M. M. Kappes, *J. Phys. Chem. C* **2009**, *113*, 14628.
[196] H. L. Wang, B. Hsieh, G. Jimenez-Oses, P. Liu, C. J. Tassone, Y. Diao, T. Lei, K. N. Houk, Z. N. Bao, *Small* **2015**, *11*, 126.
[197] H. L. Wang, J. G. Mei, P. Liu, K. Schmidt, G. Jimenez-Oses, S. Osuna, L. Fang, C. J. Tassone, A. P. Zoombelt, A. N. Sokolov, K. N. Houk, M. F. Toney, Z. A. Bao, *ACS Nano* **2013**, *7*, 2659.
[198] a) S. Khasminskaya, F. Pyatkov, B. S. Flavel, W. H. Pernice, R. Krupke, *Adv. Mater.* **2014**, *26*, 3465; b) T. Hasan, Z. P. Sun, F. Q. Wang, F. Bonaccorso, P. H. Tan, A. G. Rozhin, A. C. Ferrari, *Adv. Mater.* **2009**, *21*, 3874.
[199] a) S. P. Schiessl, N. Fröhlich, M. Held, F. Gannott, M. Schweiger, M. Forster, U. Scherf, J. Zaumseil, *Appl. Mater. Interfaces* **2014**, *7*, 682; b) G. J. Brady, Y. Joo, M. Y. Wu, M. J. Shea, P. Gopalan, M. S. Arnold, *ACS Nano* **2014**, *8*, 11614; c) V. Derenskyi, W. Gomulya, J. M. S. Rios, M. Fritsch, N. Frohlich, S. Jung, S. Allard, S. Z. Bisri, P. Gordiichuk, A. Herrmann, U. Scherf, M. A. Loi, *Adv. Mater.* **2014**, *26*, 5969; d) S. Z. Bisri, J. Gao, V. Derenskyi, W. Gomulya, I. Iezhokin, P. Gordiichuk, A. Herrmann, M. A. Loi, *Adv. Mater.* **2012**, *24*, 6147.
[200] J. Gao, M. A. Loi, E. J. F. de Carvalho, M. C. dos Santos, *ACS Nano* **2011**, *5*, 3993.
[201] M. Tange, T. Okazaki, S. Iijima, *J. Am. Chem. Soc.* **2011**, *133*, 11908.
[202] J. A. Fagan, C. Y. Khripin, C. A. Silvera Batista, J. R. Simpson, E. H. Hároz, A. R. Hight Walker, M. Zheng, *Adv. Mater.* **2014**, *26*, 2800.

[203] G. Ao, C. Y. Khripin, M. Zheng, *J. Am. Chem. Soc.* **2014**, *136*, 10383.
[204] M. Zhang, C. Y. Khripin, J. A. Fagan, P. McPhie, Y. Ito, M. Zheng, *Anal. Chem.* **2014**, *86*, 3980.
[205] D. A. Tsyboulski, Y. Hou, N. Fakhri, S. Ghosh, R. Zhang, S. M. Bachilo, M. Pasquali, L. Chen, J. Liu, R. B. Weisman, *Nano Lett.* **2009**, *9*, 3282.
[206] a) T. Hertel, A. Hagen, V. Talalaev, K. Arnold, F. Hennrich, M. Kappes, S. Rosenthal, J. McBride, H. Ulbricht, E. Flahaut, *Nano Lett.* **2005**, *5*, 511; b) N. Kishi, S. Kikuchi, P. Ramesh, T. Sugai, Y. Watanabe, H. Shinohara, *J. Phys. Chem. B* **2006**, *110*, 24816; c) K. Iakoubovskii, N. Minami, S. Kazaoui, T. Ueno, Y. Miyata, K. Yanagi, H. Kataura, S. Ohshima, T. Saito, *J. Phys. Chem. B* **2006**, *110*, 17420; d) T. Hayashi, D. Shimamoto, Y. A. Kim, H. Muramatsu, F. Okino, H. Touhara, T. Shimada, Y. Miyauchi, S. Maruyama, M. Terrones, M. S. Dresselhaus, M. Endo, *ACS Nano* **2008**, *2*, 485.
[207] S. Yang, A. N. Parks, S. A. Saba, P. L. Ferguson, J. Liu, *Nano Lett.* **2011**, *11*, 4405.
[208] a) P. L. McEuen, M. Bockrath, D. H. Cobden, Y.-G. Yoon, S. G. Louie, *Phys. Rev. Lett.* **1999**, *83*, 5098; b) Y. Li, S. V. Rotkin, U. Ravaioli, *Nano Lett.* **2003**, *3*, 183.
[209] Q. Liu, L. Yu, H. Li, R. Qin, Z. Jing, J. Zheng, Z. Gao, J. Lu, *J. Phys. Chem. C* **2011**, *115*, 6933.
[210] S. V. Rotkin, K. Hess, *Appl. Phys. Lett.* **2004**, *84*, 3139.
[211] a) A. Bachtold, P. Hadley, T. Nakanishi, C. Dekker, *Science* **2001**, *294*, 1317; b) A. Javey, J. Guo, Q. Wang, M. Lundstrom, H. Dai, *Nature* **2003**, *424*, 654.
[212] A. Javey, J. Guo, M. Paulsson, Q. Wang, D. Mann, M. Lundstrom, H. Dai, *Phys. Rev. Lett.* **2004**, *92*, 106804.
[213] E. Pop, *Nanotechnology* **2008**, *19*, 295202.
[214] a) Y. Zhou, A. Gaur, S.-H. Hur, C. Kocabas, M. A. Meitl, M. Shim, J. A. Rogers, *Nano Lett.* **2004**, *4*, 2031; b) S. J. Kang, C. Kocabas, T. Ozel, M. Shim, N. Pimparkar, M. A. Alam, S. V. Rotkin, J. A. Rogers, *Nat. Nanotechnol.* **2007**, *2*, 230; c) S. Fujii, T. Tanaka, Y. Miyata, H. Suga, Y. Naitoh, T. Minari, T. Miyadera, K. Tsukagoshi, H. Kataura, *Appl. Phys. Express* **2009**, *2*, 071601.
[215] M. M. Shulaker, G. Hills, N. Patil, H. Wei, H.-Y. Chen, H. S. P. Wong, S. Mitra, *Nature* **2013**, *501*, 526.
[216] a) V. Derycke, R. Martel, J. Appenzeller, P. Avouris, *Appl. Phys. Lett.* **2002**, *80*, 2773; b) M. S. Wang, J. Y. Wang, Q. Chen, L. M. Peng, *Adv. Funct. Mater.* **2005**, *15*, 1825; c) Y. Woo, G. S. Duesberg, S. Roth, *Nanotechnology* **2007**, *18*, 095203; d) C. W. Marquardt, S. Dehm, A. Vijayaraghavan, S. Blatt, F. Hennrich, R. Krupke, *Nano Lett.* **2008**, *8*, 2767.
[217] S. Wang, X. L. Liang, Q. Chen, K. Yao, L. M. Peng, *Carbon* **2007**, *45*, 760.
[218] D. Bouilly, J. Cabana, F. Meunier, M. Desjardins-Carrière, F. Lapointe, P. Gagnon, F. L. Larouche, E. Adam, M. Paillet, R. Martel, *ACS Nano* **2011**, *5*, 4927.
[219] H. J. Choi, J. Ihm, S. G. Louie, M. L. Cohen, *Phys. Rev. Lett.* **2000**, *84*, 2917.
[220] J. Huang, A. L. Ng, Y. Piao, C.-F. Chen, A. A. Green, C.-F. Sun, M. C. Hersam, C. S. Lee, Y. Wang, *J. Am. Chem. Soc.* **2013**, *135*, 2306.
[221] M. E. Roberts, M. C. LeMieux, Z. Bao, *ACS Nano* **2009**, *3*, 3287.
[222] Y. C. Jung, H. Muramatsu, K. Fujisawa, J. H. Kim, T. Hayashi, Y. A. Kim, M. Endo, M. Terrones, M. S. Dresselhaus, *Small* **2011**, *7*, 3292.
[223] a) M. S. Strano, C. A. Dyke, M. L. Usrey, P. W. Barone, M. J. Allen, H. Shan, C. Kittrell, R. H. Hauge, J. M. Tour, R. E. Smalley, *Science* **2003**, *301*, 1519; b) H. Park, J. Zhao, J. P. Lu, *Nano Lett.* **2006**, *6*, 916.
[224] D. D. Tune, J. G. Shapter, *Energy Environ. Sci.* **2013**, *6*, 2572.
[225] a) S. Hwang, M. Batmunkh, M. J. Nine, H. Chung, H. Jeong, *ChemPhysChem* **2015**, *16*, 53; b) D. Zhang, X. Li, S. Chen, Z. Sun, X. Jiang Yin, S. Huang, *Microchim. Acta* **2011**, *174*, 73.
[226] a) D. D. Tune, B. S. Flavel, R. Krupke, J. G. Shapter, *Adv. Energy Mater.* **2012**, *2*, 1043; b) J. Wei, Y. Jia, Q. Shu, Z. Gu, K. Wang, D. Zhuang, G. Zhang, Z. Wang, J. Luo, A. Cao, D. Wu, *Nano Lett.* **2007**, *7*, 2317.
[227] X. Zhan, J. Wu, Z. Chen, B. J. Hinds, *Nanoscale Res. Lett.* **2013**, *8*, 1.
[228] M. Majumder, N. Chopra, R. Andrews, B. J. Hinds, *Nature* **2005**, *438*, 44.
[229] J.-M. Bonard, H. Kind, T. Stöckli, L.-O. Nilsson, *Solid-State Electron.* **2001**, *45*, 893.
[230] a) W. B. Choi, D. S. Chung, J. H. Kang, H. Y. Kim, Y. W. Jin, I. T. Han, Y. H. Lee, J. E. Jung, N. S. Lee, G. S. Park, J. M. Kim, *Appl. Phys. Lett.* **1999**, *75*, 3129; b) N. S. Lee, D. S. Chung, J. H. Kang, H. Y. Kim, S. H. Park, Y. W. Jin, Y. S. Choi, I. T. Han, N. S. Park, M. J. Yun, *Jpn. J. Appl. Phys.* **2000**, *39*, 7154.
[231] G. Z. Yue, Q. Qiu, B. Gao, Y. Cheng, J. Zhang, H. Shimoda, S. Chang, J. P. Lu, O. Zhou, *Appl. Phys. Lett.* **2002**, *81*, 355.
[232] Y.-W. Son, S. Oh, J. Ihm, S. Han, *Nanotechnology* **2005**, *16*, 125.
[233] J. M. Bonard, J.-P. Salvetat, T. Stockli, W. A. de Heer, L. Forró, A. Châtelain, *Appl. Phys. Lett.* **1998**, *73*, 918.
[234] K. Seko, J.-i. Kinoshita, Y. Saito, *Jpn. J. Appl. Phys.* **2005**, *44*, L743.
[235] C. Liu, K. S. Kim, J. Baek, Y. Cho, S. Han, S.-W. Kim, N.-K. Min, Y. Choi, J.-U. Kim, C. J. Lee, *Carbon* **2009**, *47*, 1158.
[236] T. Hiraoka, T. Yamada, K. Hata, D. N. Futaba, H. Kurachi, S. Uemura, M. Yumura, S. Iijima, *J. Am. Chem. Soc.* **2006**, *128*, 13338.
[237] J. Xu, T. Feng, Y. Chen, Z. Sun, *J. Nanomaterials* **2013**, *2013*, 1.
[238] R. Zhang, Z. Ning, Y. Zhang, Q. Zheng, Q. Chen, H. Xie, Q. Zhang, W. Qian, F. Wei, *Nat. Nanotechnol.* **2013**, *8*, 912.
[239] J. Cumings, A. Zettl, *Science* **2000**, *289*, 602.
[240] J. L. Rivera, C. McCabe, P. T. Cummings, *Nano Lett.* **2003**, *3*, 1001.
[241] S. Zhang, W. K. Liu, R. S. Ruoff, *Nano Lett.* **2004**, *4*, 293.
[242] M. Dienwiebel, G. S. Verhoeven, N. Pradeep, J. W. Frenken, J. A. Heimberg, H. W. Zandbergen, *Phys. Rev. Lett.* **2004**, *92*, 126101.
[243] M. Urbakh, *Nat. Nanotechnol.* **2013**, *8*, 893.
[244] a) J. M. Martin, C. Donnet, T. Le Mogne, T. Epicier, *Phys. Rev. B: Condens. Matter Mater. Phys.* **1993**, *48*, 10583; b) M. Hirano, K. Shinjo, *Phys. Rev. B: Condens. Matter Mater. Phys.* **1990**, *41*, 11837.
[245] K. Jensen, K. Kim, A. Zettl, *Nat. Nanotechnol.* **2008**, *3*, 533.
[246] Y. T. Yang, C. Callegari, X. L. Feng, K. L. Ekinci, M. L. Roukes, *Nano Lett.* **2006**, *6*, 583.
[247] M. M. J. Treacy, T. W. Ebbesen, J. M. Gibson, *Nature* **1996**, *381*, 678.